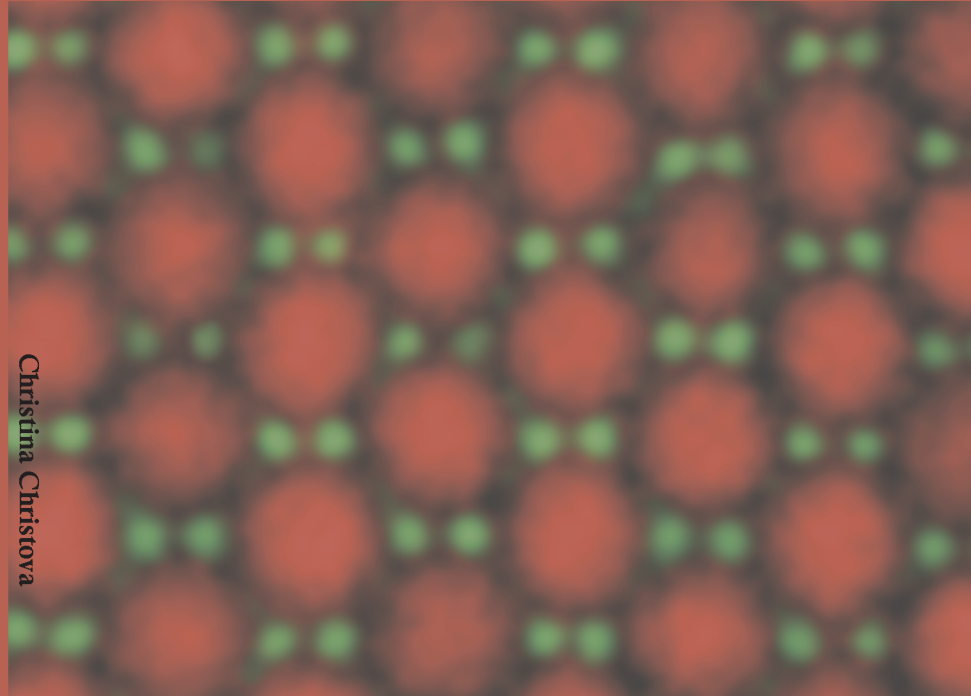


# Binary colloidal crystals

Binary colloidal crystals



Christina Christova

2005

Christina Christova

## Uitnodiging

voor het bijwonen van  
de openbare verdediging  
van mijn proefschrift

## Binary colloidal crystals

op maandag 12 december 2005  
om 16.15 uur

in het Academiegebouw  
Domplein 29 Utrecht

Receptie na afloop  
van de promotie

**Christina  
Christova-Zdravkova**

Boschdijk 207B  
5612 HC Eindhoven  
c.g.christova@phys.uu.nl  
040-2370415

paranimfen:  
**Denka Hristova**  
d.hristova@tue.nl  
**Arjen Bogaerds**  
arjen.bogaerds@dsm.com

# **Binary colloidal crystals**



# **Binary colloidal crystals**

Binare colloïdale kristallen

(Met een samenvatting in het Nederlands)

Proefschrift ter verkrijging van de graad van doctor aan de Universiteit Utrecht op gezag van de Rector Magnificus, Prof. dr. W.H. Gispen, ingevolge het besluit van het College voor Promoties in het openbaar te verdedigen op maandag 12 december 2005 des namiddags te 16.15 uur.

door

**Christina Georgieva Christova-Zdravkova**

geboren op 30 augustus 1973, te Sliven, Bulgarije



**Universiteit Utrecht**

Promotor: **Prof. dr. Alfons van Blaaderen**

Faculteit Natuur- en Sterrenkunde, Universiteit Utrecht

ISBN 90-393-4120-6

Digital version: <http://www.colloid.nl>

*to my son Maximilian and my husband Alex*



## CONTENTS

Chapter 1. Introduction	1
1.1. First binary crystals	1
1.2. Small size ratios ( $0 < \gamma < 0.3$ )	2
1.3. Large size ratios ( $\gamma \approx 1$ )	3
1.4. Intermediate size ratios ( $\gamma = 0.3 - 0.7$ )	3
1.5. Interparticle interactions	5
1.6. Methods for growing binary crystals	5
1.7. Methods for characterizing binary structures	6
1.8. Outline of the thesis	6
Chapter 2. Spectroscopic characterization of fluorescently labeled PMMA particles	7
2.1. Introduction	8
2.2. Experimental part	9
2.3. Results and discussion	11
2.3.1. Fluorescent dyes	11
2.3.2. RITC-labeled PMMA particles	13
2.3.3. NBD-labeled PMMA particles	18
2.3.4. DiIC <sub>18</sub> -labeled PMMA particles	20
2.3.5. Coumarin-labeled PMMA particles	20
2.4. Conclusions	21
Acknowledgements	21
Chapter 3. Layer-by-layer growth of binary colloidal crystals	23
3.1. Introduction	24
3.2. Experimental part	24
3.3. Results and discussion	25
3.4. Conclusions	31
3.5. Update	31
Acknowledgements	35
Chapter 4. Binary colloidal crystals grown under an external electric field	37
4.1. Introduction	38
4.2. Experimental part	38
4.3. Theoretical background	41
4.4. Results	43
4.4.1. Low-strength electric field	43
4.4.2. High-strength electric field	46
4.5. Discussion and conclusions	48
Acknowledgements	50

Chapter 5. Ionic colloidal crystals of oppositely charged particles	51
5.1. Introduction	52
5.2. Experimental part	54
5.3. Results	55
5.3.1. Equal-sized spheres	55
5.3.2. Spheres with a size ratio of 0.31	59
5.3.3. Madelung energy calculations and computer simulations	60
5.4. Discussion and conclusions	62
Acknowledgements	63
Chapter 6. Binary crystal structures in mixtures of oppositely charged colloids with a size ratio of 0.31	65
6.1. Introduction	66
6.2. Experimental results	66
6.3. Theory and simulations	70
6.4. Conclusions	73
Acknowledgements	73
Chapter 7. Preliminary observations on crystallization in binary mixtures of oppositely charged PMMA particles	75
7.1. Introduction	76
7.2. Nucleation and growth of LS <sub>8</sub> -binary crystals	77
7.3. Coexistence of binary crystals with different stoichiometries	84
Acknowledgements	85
Color figures	86
References	89
Summary	101
Samenvatting	105
Резюме (summary in Bulgarian)	109
List of publications	113
Acknowledgements	115
Curriculum vitae	117

# 1

## Introduction

### *1.1. FIRST BINARY CRYSTALS*

Natural gem opals are precious stones that owe their beautiful colors to the 3D ordered arrays of silica particles they consist of. The play of colors originates from diffraction of light with different wavelengths depending on the size of the spheres in these arrays<sup>1</sup>. In some rare opals bands of arrays of particles with different sizes can be found. Even rarer, bands consisting of small and large spheres mixed together can exist, as was the case in a specimen from a gem opal found in Brazil and examined carefully by Sanders and Murray<sup>2</sup>. They observed long-ranged ordered binary arrays of large (L) and small (S) particles with different structures in this Brazilian opal. This was the first observation of binary colloidal crystals reported. A detailed study on the crystals in the Brazilian opal<sup>3</sup> revealed two binary structures, one with a stoichiometry of  $LS_2$  and the other with a stoichiometry of  $LS_{13}$  (the structures will be described below). The authors discussed two possible mechanisms leading to the formation of these structures. In the first one, the particles with two different sizes were supposed to grow at the same time and the interparticle forces (Van der Waals and double layer repulsion) between the small and the large species were considered to be responsible for the preference to form a mixed structure instead of separation into two phases consisting of individual species. However, examinations of banded opals (where in each band the particles have different sizes) revealed that most likely the spheres in the different bands formed separately during different eras<sup>4</sup>. Therefore, a more realistic picture for the formation of the binary structures in the natural opal was proposed in which the larger species had grown first and sedimented under the influence of the gravity. Several eras later the smaller spheres had formed and penetrated through the not yet compacted array of the larger particles thus creating a binary structure. Gravity was found to be the main driving force in this mechanism and therefore maximizing the packing density was considered to be the factor that determines the preference for a structure to form. Based on this idea a phase diagram for the size ratio of the particles in the Brazilian opal (0.58) was constructed showing the stability regions of different structures depending on the concentrations of the two components<sup>5</sup>.

Motivated by the observations of Sanders and Murray on the binary structure formation in Brazilian gem opals, Hachisu and Yoshimura created for the first time binary crystals under laboratory conditions<sup>6</sup>. These crystals were made from charge-stabilized latex particles dispersed in water and had stoichiometries of  $LS_5$  and  $LS_{13}$ . The authors

pointed out the analogy of these structures with certain metallic alloys ( $\text{CaCu}_5$  and  $\text{NaZn}_{13}$ , respectively) and found that the appearance of a certain binary structure depends on the size ratio of the particles  $\gamma = R_S / R_L$  (where  $R_S$  and  $R_L$  are the radii of the small and the large spheres, respectively), their number ratio, the total particle concentration and on the electrolyte concentration. The electrostatic repulsive forces between the charged spheres could not, according to the authors, explain the spontaneous ordering of the particles into binary crystals and the influence of entropy was pointed out as an important factor in binary structures formation. Later on more types of binary colloidal crystals, resembling the intermetallic compounds  $\text{AlB}_2$  and  $\text{MgCu}_2$ , and a structure with a stoichiometry of  $\text{LS}_4$  having no atomic analogue, were reported by these authors in the same system of electrostatically repelling particles with different size ratios<sup>7</sup>. The phase transition from a disordered phase to an ordered binary crystals was suggested by the authors to be considered as an ‘extension of the Kirkwood-Adler transition’ for monodisperse hard-spheres<sup>8</sup> in which an ordered phase with a density higher than that of the coexisting disordered phase appears upon increasing the particle concentration above a critical value<sup>9, 10</sup>.

We have to mention that before these first observations of binary colloidal crystals, there were both theoretical and experimental attempts to study mixtures of particles with two different sizes. Nowick and Mader in 1965 constructed a simple model to simulate formation of thin metal alloys film<sup>11</sup>. The atoms and the repulsion between them were represented by plastic hard balls and the attraction between the atoms was simulated by using a tilted surface on which the balls roll together and form 2D structures. In addition, vibration of the surface was used to observe the effect of low-temperature ‘annealing’. The size ratio of the balls was 0.75 and 0.87, and the two species were mixed in different proportions. Pseudo phase diagrams were constructed showing the compositions at which a crystalline or an amorphous layer was formed. The authors found that when the two types of particles do not differ much in size (size ratio 0.87) a small amount (‘impurity’) of one of the species can be incorporated randomly in the crystalline layer of the other species, while for a larger size difference the ‘impurity’ particles tend to accumulate on the grain boundaries in the crystal of the other type spheres.

A similar segregation phenomenon was observed by Hachisu et al.<sup>12</sup> in a system of latex particles with a non-uniform size distribution dispersed in water where the spheres with sizes deviating significantly from the size of the major population of particles were expelled from the ordered arrays formed by the particles from that major population.

The pioneering work of Sanders and Murray<sup>2</sup> opened a whole new field for both, experimentalists and theoreticians, to search for new or to explain existing binary structures. In the following we will address some of the widely discussed issues in the field of binary colloidal crystals.

### 1.2. SMALL SIZE RATIOS ( $0 < \gamma < 0.3$ )

Monodisperse systems of colloidal particles were found to freeze into an ordered phase when the particle concentration was above some critical value<sup>9, 13</sup>. The presence of a second type of particles with different size influences this fluid-solid transition. One of the

most fundamental problems studied in the field of binary mixtures is whether a mixture of colloidal particles with different sizes should be uniform or should separate into coexisting phases, and if it does, what the composition of these phases will be. In early work Lebowitz derived an exact solution of an approximate theory for the equation of state for a binary mixtures of hard-spheres with different sizes<sup>14</sup> and found that no phase separation of the components in the mixtures should occur. Much later on, the calculations of Biben and Hansen showed that a phase separation should actually happen in binary mixtures with size ratios smaller than 0.2 and comparable volume fractions of the small and the large spheres<sup>15</sup>. Since then numerous investigations were performed, both theoretically and experimentally, to verify this demixing transition. Experiments on hard-sphere-like mixtures and on mixtures of charged particles showed that a phase separation indeed occurs at small size ratios and above a certain particle concentration<sup>16-21</sup>. The observed coexisting phases were a randomly stacked close-packed crystal of the large spheres, in which the small spheres can be distributed in a fluid-like state, and a fluid consisting mostly of the small species. Excluded-volume interaction, termed depletion, was found by theoretical calculations<sup>22, 23</sup> and computer simulations<sup>24</sup> to be the main driving forces of the observed phase separations.

### 1.3. LARGE SIZE RATIOS ( $\gamma \sim 1$ )

It was found theoretically<sup>25-27</sup> and in computer simulations<sup>28</sup> that at size ratios close to 1 ( $\gamma > 0.85$ ) the stable phase in hard-sphere mixtures is a substitutionally disordered solid solution. As the size disparity between the two species increases the fluid-solid phase transition occurs at higher freezing densities and at size ratios of about 0.85 the disordered solid solution becomes less stable than the binary fluid and the crystals of single species.

Despite of the fact that no binary crystal was predicted to be stable in hard-sphere mixtures with size ratios close to 1, experiments of Underwood et al.<sup>29</sup> and of Schofield<sup>30</sup> demonstrated the formation of CsCl-type crystals, consisting of two interpenetrating simple-cubic lattices of the two species, at a size ratio of  $\sim 1$  and of 0.74, respectively. The stability of this type of binary structure was suggested to be influenced by a 'cross-attraction' between the two species<sup>29</sup> but it was not clear what the mechanism of this attraction was. Electrostatic attraction between oppositely charged particles with almost equal sizes was found recently to induce formation of CsCl- and NaCl-type binary crystals<sup>31</sup>.

### 1.4. INTERMEDIATE SIZE RATIOS ( $\gamma = 0.3-0.7$ )

As was described above, the first binary colloidal crystals observed in Brazil opals<sup>3</sup> had a stoichiometry of LS<sub>2</sub> and LS<sub>13</sub>. Later on they were found to form in laboratory conditions as well<sup>6, 7, 32-34</sup> in mixtures containing an excess of the small species and having size ratios 0.35 - 0.58 for the LS<sub>2</sub> crystals and 0.43 - 0.58 for the LS<sub>13</sub> crystals. The structures of these crystals resembled that of the intermetallic alloys AlB<sub>2</sub> and NaZn<sub>13</sub>, respectively. In the AlB<sub>2</sub>-type structure the large spheres are ordered in a simple hexagonal lattice (hexagonal

close-packed layer stacked on top of each other) and the small particles fill the hexagonal interstices of this lattice forming honeycomb-like planes between the layers of the large spheres. The structure of the  $\text{NaZn}_{13}$ -type crystal is more complex. It consists of a simple cubic lattice of the large species and in the middle of each cube of the large spheres there is centered an icosahedron of the small spheres, which changes its orientation with 90 degrees when going from one cube to the next.

The stability of these structures within certain size ratio and mixtures composition ranges was confirmed by computer simulations<sup>35-38</sup> and cell theory calculations<sup>39</sup> on hard-sphere mixtures. The theoretical<sup>35, 39</sup> and the experimental<sup>33</sup> phase diagrams for a size ratio of 0.58 were in excellent agreement with each other. The results from the computer simulations showed that entropy alone is responsible for the formation of the complex binary structures observed<sup>35</sup>.

Several other binary colloidal structures were observed experimentally by different groups. A structure with stoichiometry of  $\text{LS}_5$ , resembling the alloy  $\text{CaCu}_5$ , was found in mixtures of charge-stabilized particles with a size ratio of 0.56 and 0.66 but it was not very stable and disappeared in a few days<sup>7</sup>. In the  $\text{CaCu}_5$ -type structure the large spheres are ordered in hexagonal layers and in these layers each large particle is surrounded by a ring of 6 small spheres occupying the trigonal interstices. These mixed planes of two species are stacked on top of each other but in between every 2 planes there is a plane of only small particles ordered in a kagomé-type arrangement. Another binary colloidal crystal with a stoichiometry  $\text{LS}_2$  but with the structure of the intermetallic compound  $\text{MgCu}_2$  was reported by Yoshimura and Hachisu<sup>7</sup> for size ratios in the range of 0.62-0.7, and by Ma et al.<sup>40</sup> for a size ratio of 0.73. The  $\text{MgCu}_2$  structure, known also as a Laves phase, is build up of a diamond-type lattice of the large spheres for which the interstices are occupied by four small particles forming a tetrahedron. Binary colloidal structure with a stoichiometry  $\text{LS}_4$ , having no atomic analogue found, was reported by Yoshimura and Hachisu<sup>7, 41</sup> for a size ratio of 0.48. The large spheres in this complex structure were arranged in planes consisting of trigonal clusters and the orientation of every two successive planes was different by 60 degrees. The small particles occupied the cavities obtained in the lattice of the large species – one small sphere filled the smaller holes while an icosahedron was formed in the larger holes<sup>7</sup>.

The stability of the structures of  $\text{CaCu}_5$ -,  $\text{MgCu}_2$ - and  $\text{LS}_4$ - type was not tested by computer simulations or theory so far and the mechanism underlying their formation is an open question.

For size ratios  $< 0.4$  it was suggested by Murray and Sanders<sup>5</sup>, based on packing arguments, that a  $\text{NaCl}$ -type crystal, consisting of two interpenetrating face-centered-cubic (fcc) lattices of the two species, should be stable. Theoretical calculations<sup>39</sup> and computer simulations<sup>42</sup> confirmed the stability of this type of crystal within a certain range of size ratios ( $\gamma < 0.42$ ) and mixture compositions (excess of small particles). Two possible binary crystal structures with a stoichiometry of  $\text{LS}$  have an equal packing density –  $\text{NaCl}$ - and  $\text{NiAs}$ -type. In both structures the small spheres occupy the octahedral interstices of the large-particles lattice, which in the case of  $\text{NaCl}$  is a face-centered cubic (fcc), while in the  $\text{NiAs}$ -type crystal it is hexagonal close-packed (hcp). Experimentally, crystals with a stoichiometry  $\text{LS}$  (the exact structure was not identified) were observed in hard-sphere

mixtures (size ratio of 0.39 and 0.43)<sup>34</sup>, and NaCl-type crystals were found in mixtures of silica and gold particles ( $\gamma = 0.15$ )<sup>43</sup> and in mixtures of attracting particles ( $\gamma = 0.43$ )<sup>40</sup>.

Binary crystals with different stoichiometries were observed also with nanoparticles made from different compounds. Because there are strong indications<sup>44-46</sup> that for the interactions between the nanoparticles other (dipolar, Van der Waals) than purely repulsive forces are important, these experiments were not discussed in the previous paragraphs. So far,  $\text{AlB}_2$ -,  $\text{CaCu}_5$ -,  $\text{NaZn}_{13}$ - and NaCl-type binary structures were found<sup>44, 45, 47-50</sup> in mixtures of nanoparticles and recently a new polymorph with a stoichiometry  $\text{LS}_{13}$  was observed<sup>46</sup>, in which the small particles are arranged in a cuboctahedron centered in the middle of the cube of the large spheres.

### 1.5. INTERPARTICLE INTERACTIONS

The most widely studied binary systems were those consisting of hard-sphere like particles<sup>30, 32-34</sup>. There, only entropy can be the driving force for the formation of the binary structures<sup>35-37</sup>. Charge-stabilized particles of different sizes were also found to crystallize into binary compounds with different structures<sup>6, 7, 41</sup> and the stability of the binary crystals was discussed in view of a mapping of the charged particles onto an effective hard-sphere system. Mixtures of charged and neutral species were considered as well both, experimentally<sup>51-53</sup> and theoretically<sup>54-56</sup>, but no binary crystals were reported so far for such systems. The presence of a weak attraction between the two components<sup>29, 31, 40</sup> was found to have an important effect on the stabilization of binary crystals and as we will show in Chapters 4-7 of this thesis it can facilitate extremely the formation of binary crystals.

### 1.6. METHODS FOR GROWING BINARY CRYSTALS

Most procedures to grow binary colloidal crystals do not exclude (some) gravitational sedimentation; usually, binary mixtures of certain compositions are prepared and left to form equilibrium structures<sup>21, 29, 30, 32-34, 40, 57</sup>. This way of growing binary crystals of hard-sphere like particles is time consuming; it takes typically several weeks before the first crystals are observed. Moreover, large differences in sedimentation result if the particles have different composition and/or a large size difference. Charged particles crystallize much faster but the structures obtained are not always stable in time<sup>7</sup> and it is much harder to use them in applications. A disadvantage of these methods, in which repulsive interactions only are used, is that there is not much control over the structures obtained, or in other words, a significant tuning of the mixtures compositions (and electrolyte concentration) is required to obtain a certain structure. In this thesis we present novel approaches to form binary crystals utilizing, amongst others, the advantages of having attractions between the particles, which gave us more freedom and control to create structures with different stoichiometries.

### 1.7. METHODS FOR CHARACTERIZING BINARY STRUCTURES

The structures in binary mixtures of colloidal particles were probed using a variety of experimental techniques. Indirect information was obtained using scattering methods – light<sup>18, 21, 29, 30, 32-34, 38, 58</sup>, X-ray<sup>44, 48, 59</sup>, neutron scattering<sup>18, 60-62</sup>. The measured intensities can be used to obtain the symmetry and the lattice spacing of the crystal structures. However, if the scattering strength of one of the components is much weaker than that of another component this method quickly fails. Direct visualization of the crystals was achieved with scanning<sup>30, 32, 33, 40, 57, 58</sup> and transmission<sup>40, 44-50</sup> electron microscopy, optical microscopy<sup>2, 3, 6, 7, 21</sup> and atomic force microscopy<sup>57</sup>. During the last 10 years confocal fluorescence microscopy turned out to be a powerful tool to study the crystal structures in the colloidal systems in real space and to obtain quantitative data on particle ordering<sup>63-74</sup> (for a review on the use of confocal microscopy in colloidal dispersions see Ref. [64,67]). The use of this technique with binary mixtures imposes certain requirements on the spectroscopic properties of the fluorescent particles<sup>63</sup> which we address in Chapter 2. Binary mixtures of fluorescent particles were for the first time visualized with confocal fluorescent microscopy by Verhaegh and Van Blaaderen<sup>63</sup> and later on qualitative observations were made with this technique on dense binary mixtures<sup>68</sup> and structures<sup>34, 64</sup>. We report in Chapter 4-7 the first direct visualization and quantitative characterization of both species in 3D binary crystals in real space using confocal laser scanning microscopy.

### 1.8. OUTLINE OF THE THESIS

In Chapter 2 we characterized the spectroscopic properties of fluorescent Polymethylmethacrylate (PMMA) particles we used for the experiments in the rest of the thesis and compared different labeled systems. Chapter 3 and 4 describe two novel methods we used to grow binary crystals of silica particles. A layer-by-layer approach reported in Chapter 3 in combination with controlled drying on a substrate allowed us to create binary structures of different stoichiometries (LS, LS<sub>2</sub>, LS<sub>3</sub>, the later one not seen before) and a non-close packed structure. In Chapter 4 we show how the influence of an external electric field can be used to fabricate large areas of NaCl-type crystals. Different mechanisms were involved in the formation of these crystals at relatively high and low electric field strength. Control over an other attractive interaction between PMMA particles was used in Chapters 5-7 to obtain binary crystals of oppositely charged spheres with different stoichiometries. Chapter 5 describes our novel approach and the crystal structures obtained: CsCl-, NaCl-, NiAs-, LS<sub>6</sub>-type (the last two never seen before with colloids) with particles of a size ratio of  $\approx 1$  and 0.3. More binary structures of oppositely charged PMMA particles (LS<sub>6</sub><sup>bcc</sup> and two LS<sub>8</sub>-type new structures) together with results from computer simulations are presented in Chapter 6. Some preliminary observations on the formation of the LS<sub>8</sub> structures and on the crystal-crystal transition between structures with stoichiometries LS and LS<sub>6</sub> are given in Chapter 7.

# 2

## Spectroscopic characterization of fluorescently labeled PMMA particles

The fluorescence of polymethylmethacrylate (PMMA) particles labeled with different dyes (RITC, NBD, DiIC<sub>18</sub>, and Coumarin) was characterized spectroscopically for use in confocal fluorescence microscopy. Absorption, excitation and emission spectra of the dyes before and after incorporation in the particles are presented, together with photodegradation ('bleaching') curves under continuous laser light illumination. A comparison between the different labeled systems is made. Interesting 'anti-bleaching' behavior was found for two of the RITC-labeled systems and possible reasons are discussed

## 2.1. INTRODUCTION

In the last twenty years colloidal particles have become an important system to study, not only because they exhibit similar phase behavior as atoms and molecules, but also because the number of possible applications of colloids continuously increases. Together with the enlarged variety of opportunities that these systems offer, the demands on their properties also expand. Colloidal particles labeled with fluorescent molecules (fluorophores) deserve special attention as these allow for a series of important experimental techniques such as (confocal) fluorescence microscopy, flow cytometry and fluorescence recovery after photobleaching, just to name a few, to be used. In previous work of our group we have shown how fluorescently labeled colloids are essential in combination with confocal microscopy to study quantitatively in real space different fundamental processes (as crystallization<sup>34, 63, 66, 73, 75, 76</sup>, nucleation<sup>71, 74, 77, 78</sup>, glass formation<sup>65, 69, 79</sup>). However, the use of fluorescent beads is not limited to techniques, but is also of importance for advanced applications such as photonic crystals<sup>66, 80-83</sup>.

Depending on the specific applications or experimental methods in which they are used, different spectroscopic properties of the fluorescently labeled particles are required. For instance, Verhaegh and van Blaaderen<sup>63</sup> and Imhof et al.<sup>84</sup> studied silica spheres having the fluorophores rhodamine and fluoresceine chemically incorporated in their volume and established optimal dye concentrations for certain applications. For example, for using the fluorescent colloids in confocal microscopy, photostable, highly fluorescent particles are needed, while for fluorescence recovery after photobleaching particles that are sensitive to irreversible photobleaching are more suitable.

In studies in which colloids are used as a model system polymer colloids, especially sterically stabilized PMMA particles, have attracted significant attention as they offer the possibility to simultaneously match both the refractive index and the density of the particles with those of the solvents in which they are dispersed<sup>68, 70, 71, 76, 85</sup> (for silica for example it is hard to do this). Besides, these systems allow precise control over the particle interactions which makes it possible to grow crystals with large variety of structures<sup>34, 70, 76, 86</sup> (see also Chapters 5 and 6). For binary mixtures of particles with different properties it is important that the two species are well distinguished under the fluorescence microscope. Therefore additional requirements on the particles are imposed that the fluorophores used for their labeling need to have well separated excitation and emission spectra.

Different fluorophores are reported in the literature as labeling agents for PMMA particles and different methods were used to incorporate them in the colloids. One of the most used dyes in the synthesis of fluorescent polymer particles is the fluorophore 4-amino-7-nitrobenzo-2-oxa-1,3-diazol (NBD) which can be coupled to specific groups or monomers depending on the synthesis procedures used to prepare the particles<sup>87-90</sup>. The fluorophore Rhodamine (and its derivatives) was also used either in pure form<sup>68, 91</sup> or coupled to monomers to label PMMA spheres<sup>87</sup>. In addition, other fluorophores have been incorporated, as alternatives for NBD and rhodamine, in PMMA particles among which the dye DiIC<sub>18</sub> (1,1'-dioctadecyl-3,3',3'-tetramethylindocarbocyanine perchlorate)<sup>92</sup> and two coumarin dyes<sup>83</sup>. In our work presented in this chapter, we used PMMA particles labeled with the above mentioned dyes (Rhodamine, NBD, DiIC<sub>18</sub>, coumarin) and

characterized their spectroscopic properties (excitation, emission, photostability) relevant for use with confocal fluorescence microscopy.

## 2.2. EXPERIMENTAL PART

### *Materials and Particles*

Four types of fluorophores were used in this research, three of which were coupled to monomers to be chemically incorporated into the PMMA particles. Rhodamine B isothiocyanate (RITC, Fluka, mixture of isomers) and 7-diethylaminocoumarin-3-carboxylic acid N,-succinimidyl ester (Coumarin, Molecular Probes) coupled to 4-aminostyrene (AS, Aldrich) as described in Ref. [87] and the fluorescent monomers obtained are referred to further in the text as RAS and CAS, respectively. 4-chloro-7-nitrobenzo-2-oxa-1,3-diazol (NBD-Cl, Acros Organics, 99%) was coupled to methylaminoethylmethacrylate (MAEM) following the procedure in Ref. [87] and the product is designated as NBD-MAEM. The dye 1,1'-dioctadecyl-3,3,3',3'-tetramethylindocarbocyanine perchlorate (DiIC<sub>18</sub>, Molecular Probes) was used as received. Different solvents were used as supplied: chloroform (Merck, analytical grade), cis-decahydronaphthalin (decalin, Aldrich, GC 99%) and petroleum ether (BUFA, B.V.). Cyclohexyl bromide (CHB, Fluka, GC >99%) was distilled prior to use as described by Royall et al<sup>70</sup>.

Polymethylmethacrylate (PMMA) particles were synthesized by dispersion polymerization following the methods of Bosma et al.<sup>87</sup>, and Campbell and Bartlett<sup>92</sup> for the DiIC<sub>18</sub> particles. All the particles were fluorescently labeled in their whole volume with different dyes. The fluorescent monomer RAS didn't dissolve well in the monomers used for the particle synthesis and was filtered prior adding it to the reactant mixture<sup>88</sup>. For some of the particles the steric stabilizer molecules, which consist of poly-12-hydroxystearic acid (PHS) grafted onto a PMMA backbone, were covalently linked to the particles through a crosslinking reaction with some monomers that are incorporated into the backbone of other pmma chains. This reaction step, in the rest of the chapter referred to as 'locking', required a heating step to 130°C for several hours<sup>87</sup>. The particles were cleaned from the reactant mixture into petroleum ether by repeated centrifugation and after that dried under nitrogen atmosphere at a room temperature. Dispersions with different particles concentrations were prepared by weighting a certain amount of dry particles and adding the desired amount of solvent (mixture).

The size and polydispersity of the particles was measured with static light scattering on dilute dispersions (volume fraction  $\sim 10^{-5}$ ) of particles in hexane using a home-build apparatus and a wavelength of the incident light 632.8 nm (He-Ne laser). The experimental scattering data were fitted using so-called 'Mie' theory for the particle form factor, taking polydispersity into account<sup>93</sup>.

### *Absorption measurements*

Absorbance was measured with an HP8452A Diode Array Spectrophotometer, using quartz cuvettes with a width of 1 cm. The wavelength range for scanning was from 190 to 820 nm, with a resolution of 2 nm.

Extinction coefficients of the fluorophores and of the fluorescent monomers used were determined by measuring absorption spectra of series of dye solutions with different known concentrations and plotting the absorbance at a wavelength close to the absorbance maximum as a function of dye concentration. Then from a linear fit of the data the decadic molar extinction coefficient  $\epsilon$  was obtained according to the Lambert's law:

$$\text{Absorbance} = \log \frac{I_0}{I} = c d \epsilon, \quad (1)$$

where  $I_0$  and  $I$  are the intensities of the light that comes into and that goes out of the sample, respectively,  $c$  is the fluorophore molar concentration and  $d$  is the thickness of the sample. In all cases good linear plots were obtained with correlation coefficients exceeding 0.999.

Dye concentration inside the particles was determined by dissolving a known amount of them into a mixture of chloroform and CHB (50/50 volume ratio) for the RAS-labeled PMMA and in chloroform for all the other particles. For the RAS-PMMA spheres a solvent mixture of CHB and chloroform was used to dissolve them because it was not possible to obtain an accurate value for the extinction coefficient of RITC (and RAS) in chloroform alone. Dissolving of the particles is here not to be taken as dispersing, as these solvent mixtures literally made the particles fall apart in the polymer subunits that made up these non-crosslinked particles. Then from the absorption spectra and the extinction coefficient, obtained as described above, the concentration of the fluorophore in the particles was calculated similar to a procedure used by Verhaegh and van Blaaderen<sup>63</sup> for silica particles.

#### *Fluorescence measurements*

Fluorescence excitation and emission spectra of diluted dispersions of the PMMA particles in CHB/decalin (80/20 volume ratio) were taken by using a Perkin Elmer Luminescence Spectrometer LS50B and quartz cuvettes with a sample holding volume  $1.5 \times 1.5 \times 5 \text{ mm}^3$ . For the excitation spectra the emission at 620 nm was recorded for the RITC and DiIC<sub>18</sub> -labeled particles, and at 560 nm for the NBD-PMMA. For the emission spectra excitation wavelength of 500 nm was used for the RITC and DiIC<sub>18</sub> spheres and 400 nm for the NBD-labeled particles. The scan speed of the spectrophotometer used was 500 nm/min and the slit width was 5 nm.

#### *Bleaching measurements*

Concentrated dispersions of the PMMA particles in CHB/decalin mixture (80/20 volume ratio) were filled in 0.05x1 mm glass capillaries (VitroCom) and densified by centrifugation for 30 min at 2500 rpm. In the dense sediment, where the particles were highly localized in a glassy or close-packed crystalline state and thus didn't perform any diffusive motion, measurements were performed with a confocal laser scanning microscope (Leica DM IRB with a confocal head Leica TCS SP2 attached) mounted on a Melles Grior air-pressure stabilized optical table using a 1.4 NA/100x oil-immersion objective and an immersion oil for fluorescence microscopy (Cargille Laboratories Inc., type DF). A 2D slice at about 12

$\mu\text{m}$  from the bottom wall was illuminated either with 488 nm (Ar-Kr laser) or with 543 nm (He-Ne laser) excitation wavelength. Unless stated otherwise, all scans were performed with a scan speed of 400 lines per second, the images format was 512x512 pixels and the area of illumination was  $75 \times 75 \mu\text{m}^2$  (sample area per pixel  $0.15 \times 0.15 \mu\text{m}^2$ ), thus giving a dwell time of the laser beam of  $4.9 \mu\text{s}$  per pixel. The change of the fluorescence intensity with the time was recorded by performing successive scans with a constant laser power of this area or scanning repeatedly a stack of three two-dimensional slices at a distance of about  $12 \mu\text{m}$  from the bottom wall separated by a small distance (from  $0.1$  to  $1 \mu\text{m}$ ). It was checked that the same spot in the sample was illuminated each time. No difference was found between the shapes of the bleaching curves measured for a 2D area or for a slice from a 3D stack. The average image intensity was calculated for each scan, normalized to the mean intensity of the first scan (at  $t = 0$ ) and plotted vs. illumination time per pixel. Several different spots in each sample were scanned with identical conditions for better statistics.

## 2.3. RESULTS AND DISCUSSION

### 2.3.1. Fluorescent dyes

The absorption spectra of solutions of the fluorescent monomers were found to be identical to those of the uncoupled dyes (RITC and Coumarin, respectively) but because they didn't dissolve as well as the pure dyes and the yield of fluorescent monomer after the coupling reaction varied from batch to batch we used solutions of the pure dyes (RITC and Coumarin) for a determination of the extinction coefficients. Figure 2.1 shows the normalized absorption spectra of RITC dissolved in CHB/chloroform (50:50 volume

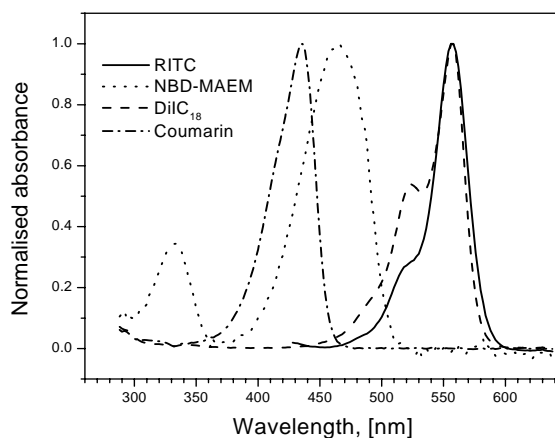


**Figure 2.1.**

*Normalized absorption spectra of the fluorescent dyes used dissolved in CHB/chloroform (RITC) or in chloroform (all the other dyes).*

Dye	Solvent	$\lambda_{abs}$ [nm]	Molar decadic extinction coefficient $\epsilon$ , [M <sup>-1</sup> m <sup>-1</sup> ]
RITC	CHB:Chl (1:1 volume ratio)	558	$8.8 * 10^6$
DiIC <sub>18</sub>	Chloroform	558	$15.4 * 10^6$
NBD-MAEM	Chloroform	466	$1.4 * 10^6$
Coumarin	Chloroform	436	$7.6 * 10^6$

**Table 2.1.**

*Absorption maxima ( $\lambda_{abs}$ ) and molar decadic extinction coefficients ( $\epsilon$ ) of the fluorescent dyes used.*

ratio) and of NBD-MAEM, Coumarin and DiIC<sub>18</sub> dissolved in chloroform. As the graph shows, the dyes Coumarin and NBD-MAEM absorb in the blue part of the spectrum, while the fluorophores RITC and DiIC<sub>18</sub> have in practice an identical absorption maximums at 558 nm in these solvents. The wavelengths of maximum absorption together with the extinction coefficients obtained for the four dyes at these wavelengths are summarized in Table 2.1. The data in Table 2.1 show that the fluorophore DiIC<sub>18</sub> had the highest extinction coefficient of the dyes used and that the extinction coefficient of NBD-MAEM was about a factor of 10 lower.

The absorption spectra of RITC and DiIC<sub>18</sub> fluorophores exhibit a shoulder on the left side of the main peak. The position of this shoulder was not found to depend on the dye concentration for both dyes. The ratio between the height of the main peak and the shoulder however decreased to 84% when the concentration of RITC increased from 1 to 15  $\mu$ M which suggests that dimmers or trimmers formed in the excited state of the RITC

RITC-PMMA particles	R <sub>SLS</sub> [ $\mu$ m]	C [ mM ]	$\lambda_{exc}$ [nm]	$\lambda_{emis}$ [nm]
LaR2, locked	1.16	0.01	552	562
LaR2, unlocked	1.16	0.10	558	568
cd29, unlocked	0.285	0.26	558	571
LaR1, unlocked	0.270	0.31	558	570
D35, unlocked	0.75	0.37	558	572

**Table 2.2.**

*Properties of the RITC-PMMA particles used. R<sub>SLS</sub> is their radius determined by static light scattering, c is the dye concentration inside the particles (in milimoles per liter PMMA),  $\lambda_{exc}$  and  $\lambda_{em}$  are the excitation and emission maxima in CHB/decalin.*

molecule<sup>94</sup>. For the DiIC<sub>18</sub> fluorophore the peak-to-shoulder ratio did not depend on the dye concentration indicating that this is likely due to absorption to a higher vibrational state or states<sup>94</sup>.

Two peaks were found also in the absorption spectrum of NBD-MAEM - one at 334 nm and the other at 466 nm. The positions of these peaks as well as their relative height did not depend on the dye concentration.

### 2.3.2. RITC-labeled PMMA particles

To determine the concentration of dye molecules in the PMMA particles we dissolved them and recorded the absorption spectra of the obtained solutions which were similar in shape and location of the absorption maximum to the absorption spectrum of RITC shown in Fig. 2.1. The concentrations of the dye molecules in the RITC-PMMA particles, presented in Table 2.2., are in the range of several hundreds micromoles per liter PMMA, which is much smaller than the concentration of RITC in silica particles<sup>63</sup>.

The effect of 'locking' the stabilizer molecules to the PMMA particles on their

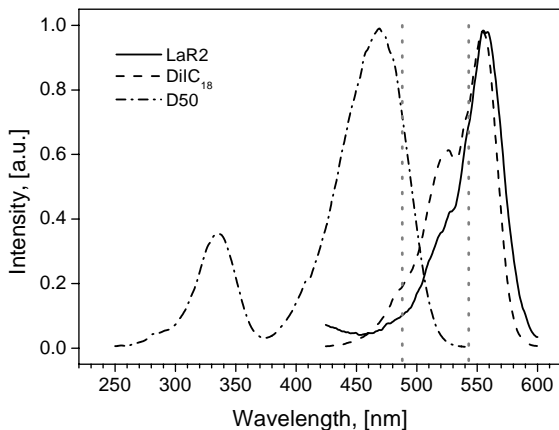


**Figure 2.2.**

Normalized excitation spectra of RITC-PMMA (LaR2), DiIC<sub>18</sub> and NBD-PMMA (D50) particles in CHB/decalin. The emission was detected at 620 nm for the first two systems and at 560 nm for the NBD-labeled spheres. The dotted vertical lines correspond to the excitation wavelengths used in the confocal fluorescence microscopy of these systems.

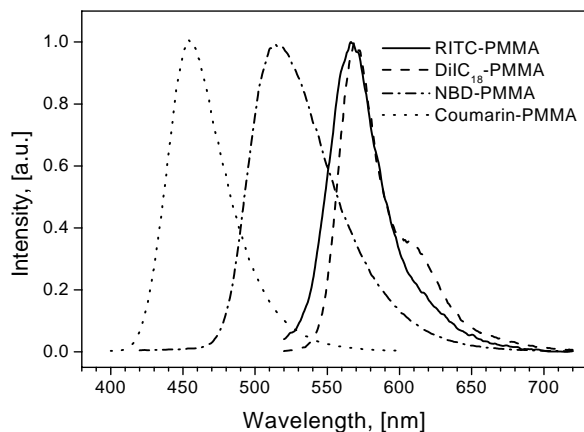


**Figure 2.3.**

Normalized emission spectra of RITC- (LaR2), DiIC<sub>18</sub>- ,NBD- (D50) and Coumarin-labeled PMMA particles in CHB/decalin. Excitation wavelength was 500 nm for the first two systems, 400 nm for NBD-PMMA and 380 nm for the Coumarin-spheres.

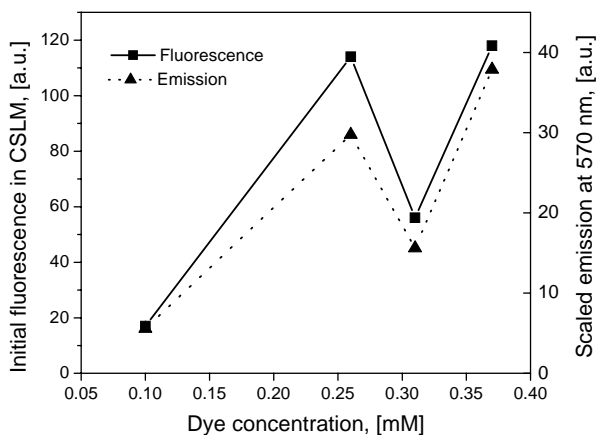


**Figure 2.4.**

*Initial fluorescence measured with confocal microscope (on the left axis) and the emission at 570 nm (at excitation wavelength of 500 nm) scaled to the particle volume fractions (on the right axis) as a function of RITC concentration in the particles.*

spectroscopic properties was verified with one of the systems – LaR2. It was observed that after locking the absorption maximum of the dye shifts to smaller wavelengths and the concentration of dye molecules as determined from their absorption drastically decreases with an order of magnitude. A possible reason for this decrease might be that during the procedure of locking, performed at relatively high temperature of 120 °C<sup>87</sup>, a significant part of the dye molecules is destroyed by the heat (only 10% of the dye molecules remained fluorescent after the locking procedure).

Representative excitation and emission spectra of RITC-labeled PMMA particles are plotted in Figures 2.2 and 2.3, respectively, and the wavelengths of maximum excitation and emission are listed in Table 2.2. The emission intensity as a function of the dye concentration in the particles dependence was not monotonic (Fig. 2.4). The same trend was found in the initial fluorescence intensity as it was measured with the confocal microscope (Fig. 2.4). The data in Table 2.2 indicate that the excitation maxima of all the systems are the same (558 nm) and equal to that of the RITC dissolved in CHB/chloroform, which suggests that the environment of the dye inside the PMMA matrix is probably similar to the not very polar environment of the CHB/chloroform mixture. The emission wavelength of the RITC-PMMA particles ( $570 \pm 2$  nm) was found to be independent on the dye concentrations within the accuracy of the measurement and to be shifted with about 13-15 nm towards higher wavelengths compared to the excitation maximum (Stokes' shift) which is a commonly seen feature of emission spectra of many fluorophores. Possible reasons for this Stokes' shift can be a rapid decay to the lowest vibrational level of the excited state, decay to a higher vibrational state of the ground state, excited state reactions, energy transfer. No significant dependence of the emission spectra on the excitation wavelength was observed (Kasha's rule). Locking of the particles had an effect on the spectroscopic properties of the particles – the excitation maximum of the

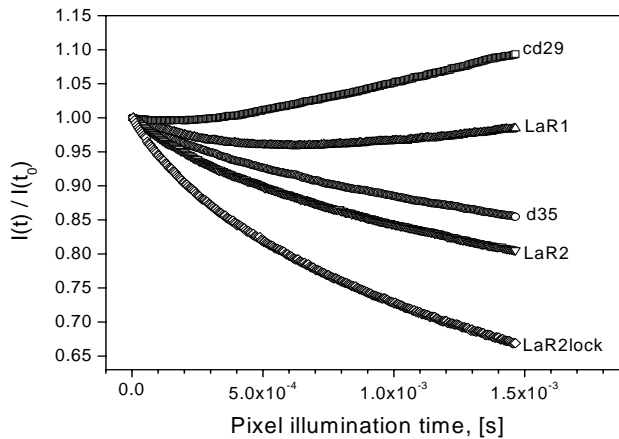


**Figure 2.5.**

*Bleaching curves of RITC-PMMA particles with different dye concentrations in CHB/dec at excitation wavelength 543 nm and laser power 25  $\mu$ W.*

system LaR2 was shifted with 6 nm towards lower wavelengths and the Stokes' shift was 10 nm.

The photostability of the PMMA particles was accessed by measuring the change in the fluorescence during continuous illumination with a laser beam. Either a 2D area was scanned repeatedly or a 3D stack of three images but no significant change in the obtained bleaching curves was observed for the two scanning modes. Figure 2.5 shows the photostability curves for the Rhodamine-labeled PMMA particles illuminated with excitation wavelength 543 nm. The systems with the lowest (LaR2) and with the highest (d35) dye concentration were found to exhibit a decrease of their fluorescence with increase of the illumination time. The other two systems with intermediate concentrations behaved quite surprisingly – their fluorescence initially decreased but very soon after that

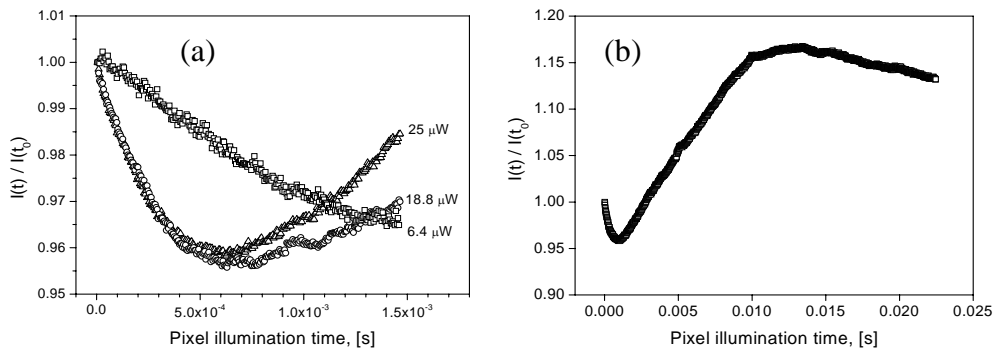


**Figure 2.6.**

*Bleaching curves of the RITC-labeled system LaR1 (dye concentration 0.31 mM) in CHB/decalin at excitation wavelength of 543 nm. (a) dependence on the excitation laser power; (b) evolution of the intensity over a large number of scans (2300), scanning speed 200 lines per second, excitation laser power of 25  $\mu$ W.*

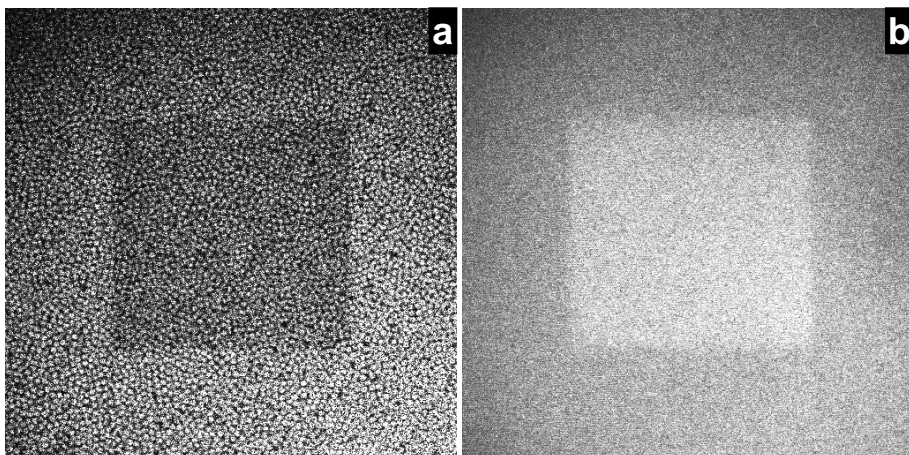


**Figure 2.7.** Confocal images showing the illuminated area of a system with: (a) normal bleaching behavior (LaR2, dye concentration 0.1mM) and (b) with anti-bleaching behavior (cd29 dye concentration 0.26mM). The dark and the bright squares correspond to the area that was illuminated and that was bleached (a) or anti-bleached (b).

started to increase. This anti-bleaching behavior was sensitive to the excitation power. On Fig. 2.6a are plotted the photostability curves for the system LaR1 (dye concentration 0.31mM) for three different laser powers and as it can be seen the higher the excitation power, the stronger is the anti-bleaching effect. The increase of the intensity with time was found to saturate after a certain number of scans (over 1500) and then the fluorescence started slowly to decrease, as shown on Fig. 2.6b for the system LaR1. Figure 2.7 shows fluorescence images of the illuminated area of a system with normal bleaching behavior (a) and with anti-bleaching behavior (b). The dark and the bright squares correspond to the area that was illuminated and that was bleached (a) or anti-bleached (b). The bleaching curves with a monotonous decreasing trend were not fitted well with a single-exponential law but rather with a double exponential which is often the case for fluorophores in solid materials<sup>63, 84</sup>.

We do not have yet a clear explanation of the observed initial increase of fluorescence with illumination for two of the systems and we couldn't find a similar phenomenon reported in the literature. The possibility of multiple photon excitation was ruled out by measuring the initial fluorescence as a function of the laser power for the system LaR1 (dye concentration 0.31mM). This dependence is plotted on Fig. 2.8 together with a linear fit through the data. For an  $n$ -photons excitation process the fluorescence intensity depends on the excitation power  $P$  as  $P^n$ . Then in the case of a single-photon absorption process the fluorescence should increase linearly with the excitation power, which is the case in our systems as seen from the good quality of the linear fit in Fig. 2.8 (correlation coefficient 0.99959).

An other possibility to explain the anomalous bleaching behavior of two of the systems is connected with the occurrence of energy transfer between neighboring excited dye molecules (acceptor and donor) leading to quenching of the fluorescence. The

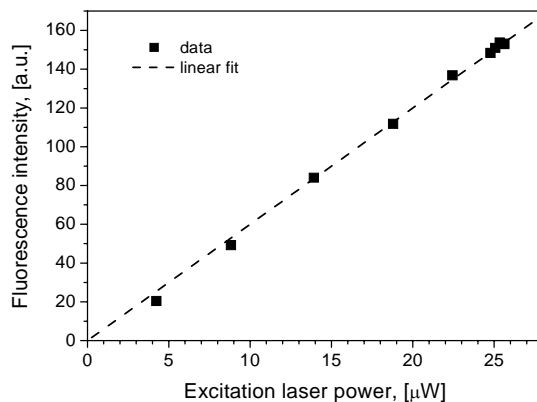


**Figure 2.8.**

*Initial fluorescence intensity vs illumination laser power for the RITC-PMMA particles with dye concentration 0.31 mM (LaR1) at excitation wavelength 543 nm. The line shows a linear fit through the data.*

probability to have such energy transfer depends on the distance between the molecules and is characterized by a critical Förster distance at which the efficiency of energy transfer is 50%. In our case the donor and the acceptor molecules are identical and this is called a self-quenching process. If we assume a homogeneous distribution of the dye molecules in the particles, then the average distance  $r$  between two molecules can be estimated from the number concentration of the dye molecules inside the PMMA particles  $c_n$ :

$$r = c_n^{-1/3}$$

For the RITC-PMMA used this distance is about 15 nm, which is larger than the critical Förster distance for rhodamine dyes (about 5-7 nm). It is possible however, that the dye molecules are not distributed homogeneously inside the particles but form clusters instead with an average intermolecular distance smaller than the critical Förster distance. Then energy migration from the excited state of a fluorophore to some other state of a neighboring fluorophore (for example a triplet state), from which no radiation decay occurs, might happen and the fluorescence is quenched. Dye molecules that are not able to emit photons via a radiation process can be considered as bleached. But such molecules can act also as less effective quenchers of fluorescence for their neighboring molecules. In this way, if initially a reduction of fluorescence is observed due to photodegradation of some of the molecules, then an increase of intensity can happen as the bleached molecules do not quench anymore the fluorescence of their neighbors by energy transfer. Such a hypothesis of increased photostability at higher dye concentrations was suggested to be possible by Imhof et al. for silica particles labeled with fluorescein<sup>84</sup>. In view of this explanation it is likely that the two systems, cd29 (dye concentration 0.26mM) and LaR1 (dye concentration 0.31mM), might have a more inhomogeneous distribution of the dye molecules inside, leading to large number of molecules at small distances from each other, and the described above effect of self-quenching and decrease of the quenchers during

illumination is more pronounced. Measurements of the fluorescence lifetime may shed additional light on the mechanism of photodegradation and the role of quenching in the systems studied as quenching is often accompanied by a decrease in the life time.

### 2.3.3. NBD-labeled PMMA particles

The absorption spectra of NBD-labeled PMMA particles dissolved in CHB/chloroform looked similar to that of the fluorescent monomer NBD-MAEM presented in Fig. 2.1. The two maxima observed in the spectra of the NBD-MAEM solutions were present here as well. From the absorption at 466 nm and the extinction coefficient of the dye determined at this wavelength the concentration of the fluorophore in the particles was calculated and presented in Table 2.3. Comparing the dye concentration of the NBD-PMMA particles to that of RITC-PMMA we see that the NBD levels are about an order higher. The average intermolecular distance of the fluorophores in the particles (assuming a homogeneous dye distribution) was on the order of 6 nm – close to the critical Förster distance for energy transfer, suggesting that self-quenching of the fluorescence is likely to occur for these particles. Locking of the stabilizer to the NBD-labeled PMMA particles was found to have no significant effect on the dye molecules, as the absorptions of the fluorophores before and after locking of the system d26 were identical. This is in contrast to RITC-labeled spheres where locking was found to decrease the amount of dye molecules significantly.

Typical excitation and emission spectra of the NBD-labeled-particles are plotted on Fig 2.2 and 2.3, respectively, and their emission and excitation maxima are listed in Table 2.3. The maximum excitation wavelength slightly increased (with 4 nm) after incorporation of the dye inside the particles and the Stokes' shift for these colloids was 46 nm - higher than that of the RITC-PMMA spheres. The possible reasons for this large difference between the excitation and the emission maxima were discussed above. The positions of the maximum excitation and emission wavelengths were found to be independent on the dye concentration.

NBD-PMMA particles	$R_{SLS}$ [ $\mu\text{m}$ ]	C [mM]	$\lambda_{exc}$ [nm]	$\lambda_{emis}$ [nm]
D26, <i>locked</i>	0.36	5.5	470	516
D26, <i>unlocked</i>	0.36	5.6	470	516
D49, <i>unlocked</i>	polydisperse	7.3	470	516
D51, <i>unlocked</i>	1.20	8.2	470	516
D50, <i>unlocked</i>	0.55	8.4	470	516
D47, <i>unlocked</i>	polydisperse	9.3	470	516

**Table 2.3.**

*Properties of the NBD-PMMA particles used.  $R_{SLS}$  is their radius determined by static light scattering,  $c$  is the dye concentration inside the particles (in millimoles per liter PMMA),  $\lambda_{exc}$  and  $\lambda_{em}$  are the excitation and emission maxima in CHB/decalin.*

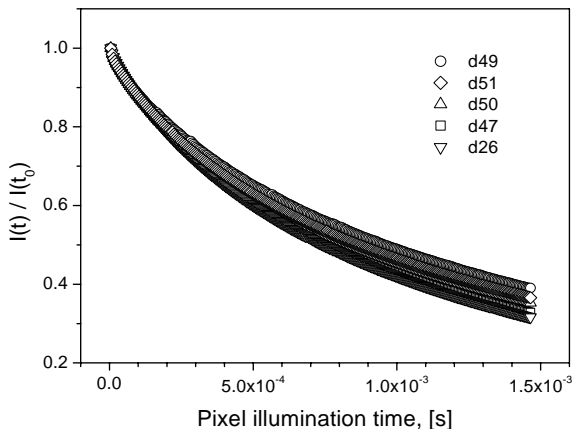


**Figure 2.9.**

Bleaching curves of NBD-PMMA particles with different dye concentration in CHB/dec at excitation wavelength of 488 nm and laser power of 15.4  $\mu\text{W}$ .

Photostability curves of these particles are shown in Fig. 2.9 for an excitation wavelength of 488 nm and a laser power of 15  $\mu\text{W}$ . As is visible in the graph, all systems had similar bleaching behavior under continuous laser illumination. There was a weak trend to a higher bleaching rate as the dye concentration is increased. Illuminating the particles with a higher excitation laser power led to a decreased photostability (faster bleaching) as shown in Fig. 2.10a for the system d51 (8.2 mM) but when the decrease of the fluorescence was plotted as a function of the dosage energy (Fig. 2.10 b) the curves fell on top of each other. This is an indication that no saturation of the dye excitation occurs at the excitation powers we used and that the decrease of the fluorescence intensity is linearly proportional to the excitation power. It was not possible to fit good the fluorescence decay curves with a single or a double-exponential law, which indicates that

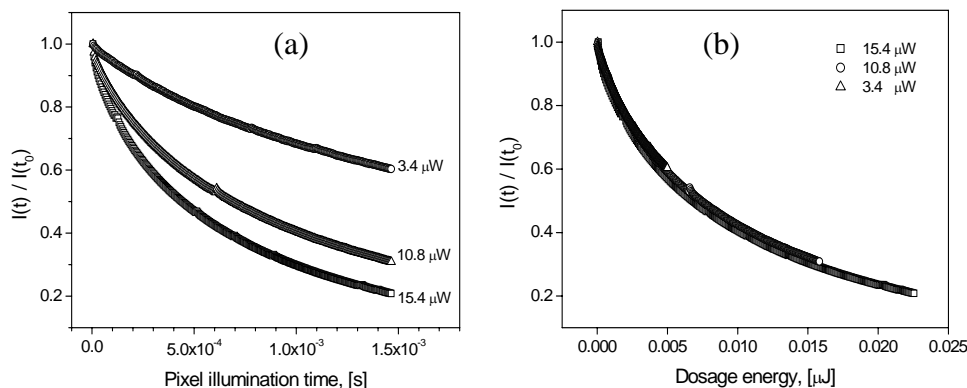


**Figure 2.10.**

Normalized fluorescence intensity of the NBD-PMMA particles D51 (dye concentration 8.2 mM) in CHB/decalin as a function of the pixel illumination time (a) and the dosage energy (b) for different excitation laser power and excitation wavelength 488 nm.

the bleaching mechanism is not a simple first or second order process. Again the possibility of multiphoton absorption was excluded by the obtained linear dependence of the fluorescence intensity of these particles on the excitation laser power (results not shown, the correlation coefficient of the linear fit was 0.9995). Comparing the photostability curves of RITC- and NBD-labeled PMMA particles we can see that the later bleach much faster under the illumination conditions used. It can be argued that the dye concentration is about one order of magnitude higher than that of the RITC particles (translating into a smaller distance between the fluorophore molecules) and the chance of fluorescence quenching by energy transfer (or some excited state reactions) is therefore higher. However, in the case of 'over-labeling' with rhodamine and fluorescein in silica it was found that the self-quenching that occurred actually made bleaching less likely by decreasing the fluorescence life time significantly<sup>63, 84</sup>. Fluorescence life time measurements would be useful to check if these were not decreased in the present case.

#### 2.3.4. DiIC<sub>18</sub>-labeled PMMA particles

As an alternative for RITC another dye, DiIC<sub>18</sub>, was incorporated in PMMA. The absorption spectra of the DiIC<sub>18</sub>-labeled particles in chloroform looked similar as that of the fluorophore DiIC<sub>18</sub> shown in Fig. 2.1. The amount of dye determined (2.2 mM) is much higher than that of the RITC-labeled spheres but the effect of locking the colloids was similar – the dye concentration after the locking step was determined to be 0.13 mM – about 20 times smaller than that before locking.

Typical normalized excitation and emission spectra of the DiIC<sub>18</sub> particles measured in CHB/decalin are plotted in Fig. 2.2 and 2.3, respectively. The maximum excitation was found to occur at a wavelength of 554 nm – slightly lower than the absorption maximum of the dye dissolved in chloroform. The emission maximum was observed at 570 nm, thus giving a Stokes' shift of about 15 nm. It is quite remarkable that no significant difference of the fluorescence intensity between unlocked and locked DiIC<sub>18</sub> particles was found; this result points to a high level of self-quenching present in the unlocked particles having a much higher dye concentration. A similar trend was found in the preliminary results on the bleaching behavior of these systems, showing that the photostability of the particles before and after locking is similar and higher than that of the RITC-labeled spheres studied (results not shown).

#### 2.3.5. Coumarin-labeled PMMA particles

The last dye we used to label PMMA particles was a coumarin-dye. By measuring the absorbance of a solution of this system in chloroform we determined the concentration of the fluorophore in the particles to be 2.7 mM which is high but still lower than that of the NBD-particles. The maximum emission wavelength of this system in CHB/decalin (Fig. 2.3) was found to be 456 nm – about 60 nm lower than that of the NBD-particles. Preliminary measurements of the photostability of the coumarin labeled PMMA particles indicate that they are much more stable against photobleaching than the NBD-labeled spheres but more systematic and detailed measurements are needed to establish the spectroscopic properties of this system.

## 2.4. CONCLUSIONS

The spectroscopic properties of PMMA particles labeled with four different fluorophores, two with emission in the red part of the visible light spectrum and two in the blue-green part, were investigated. The particles with the highest number of fluorophores incorporated were those labeled with NBD, followed by the coumarin- and DiIC<sub>18</sub>-labeled spheres, while the RITC-particles had the smallest dye concentration. All the systems studied showed no substantial dependence of the excitation and absorption maxima on the dye concentration. A difference between the excitation and emission maxima (Stokes' shift) was observed for all the systems, the highest shift was found for the NBD-labeled particles (46 nm), the smallest for the RITC-labeled colloids (about 13 nm). The DiIC<sub>18</sub> particles and some of the RITC labeled colloids were most stable to bleaching, while the NBD-particles bleached most. A more detailed study is necessary to investigate the mechanisms involved in the observed anomalous anti-bleaching behavior of two of the RITC labeled systems. For confocal measurements the requirements are to have as much photostable system as possible and with this respect the DiIC<sub>18</sub> particles are the best candidate. For imaging binary mixtures of particles with a fluorescence microscope, labeling of the particles with two fluorescent dyes having a large difference in the emission spectra is necessary, and from the results presented in this chapter it is clear that the combination of RITC or DiIC<sub>18</sub> with NBD or Coumarin is suitable enough. For the quantitative measurements described in Chapters 5, 6 and 7 on fluorescently labeled particles we used 488 excitation wavelength for NBD-PMMA and 543 nm wavelength to excite RITC-labeled spheres. As seen from the excitation spectra of these particles (Fig. 2.2), the chosen excitation wavelengths (the vertical dotted lines in Fig. 2.2) are close to the maximum excitation wavelengths of the dyes in the particles which makes them suitable for fluorescence microscopy.

## ACKNOWLEDGEMENTS

We thank Didi Derks for synthesis of the particles and helpful discussions, Roel Dullens for the synthesis of the NBD-dye, Dave van den Heuvel and Oleg Tovmachenko for help with the absorption, excitation and emission measurements, Arnout Imhof for assistance in measuring the laser power and Prof. dr. Hans Gerritsen for useful discussions.



# 3

## Layer-by-layer growth of binary colloidal crystals

Well-ordered single binary colloidal crystals with a stoichiometry of large (L) and small (S) particles of  $LS$ ,  $LS_2$  and  $LS_3$  are grown with control over the crystal orientation through a simple layer-by-layer technique. In addition, growth of a hexagonal non-close-packed colloidal crystal is demonstrated by using spheres of different composition and selectively removing one of the components. A review of recent results (since the publication of our method) in the field of colloidal crystals fabrication based on the work we initiated is given as well.

### 3.1. INTRODUCTION

A mixture of submicron or colloidal particles of two sizes can self-organize into two-(2D)<sup>47</sup> and three-dimensional (3D)<sup>33, 35, 95-97</sup> binary crystals, which can have different stoichiometries and crystal symmetries depending on the size ratio and concentration. Binary colloidal crystals of large (L) and small (S) particles were first observed in nature. Two types of structures, with stoichiometry  $LS_2$  (atomic analog  $AlB_2$ ) and  $LS_{13}$  (atomic analog  $NaZn_{13}$ ), were found in Brazilian opals.<sup>96</sup> Later, binary crystals were observed in suspensions of charge-stabilized polystyrene<sup>97</sup> and of hard-sphere like PMMA<sup>33</sup> particles. Formation of small 2D binary crystals was observed in a mixture of alkanethiol-derivatized gold nanoparticles although it is unclear if the formation of these crystals was determined by thermodynamics alone.<sup>47</sup> Colloidal crystals with lattice constants comparable to the wavelength of visible light are important for applications and processes as diverse as photonic crystals,<sup>98</sup> (including structures with small refractive index contrast as in optical filters and switches<sup>99</sup>), chemical sensors,<sup>100</sup> lithography,<sup>101</sup> surface enhanced Raman scattering,<sup>102</sup> and the creation of macroporous materials.<sup>103-106</sup> However, binary crystals have not been investigated experimentally as extensively as one-component colloidal crystals, mainly because it is harder to grow and characterize them.

Theoretically, it has been shown that entropy alone can lead to the formation of stable  $LS_2$  and  $LS_{13}$  binary crystals in bulk crystallization in a mixture of hard spheres of two sizes.<sup>35</sup> At higher particle concentrations packing arguments can be used to predict which crystal phase will form.<sup>95, 96</sup> In bulk crystallization there is not much control over the size and orientation of single crystals. That is why for single crystals of one size particles methods like colloidal epitaxy<sup>66, 107</sup> and a form of controlled drying on a substrate<sup>108-110</sup> have been developed. In this controlled drying technique, a colloidal crystal is formed at the drying front of an evaporating dispersion with a relatively low volume fraction of particles. Particles are transported to and concentrated at the drying edge by a fluid flow induced by the evaporation. The crystallization is not only driven by a lowering of the free energy but also under the influence of surface tension effects exerted on particles that are partially sticking through the drying meniscus<sup>110</sup> and the templating action of particles that are already deposited.<sup>66</sup> With this non-equilibrium process, it is possible to grow large single 2D<sup>111</sup> and 3D<sup>109</sup> colloidal crystals with precise control over the thickness through the particle volume fraction<sup>109, 112</sup>.

In this Chapter, we present the fabrication of binary (composite) colloidal crystals through layer-by-layer controlled drying as it was described several years ago<sup>113</sup>. In a short section "Unsuccessful attempts" we describe experiments that led us to develop the layer-by-layer growth method<sup>113</sup> and in a separate section "Update" we review what happened in this field after publication of our method.

### 3.2. EXPERIMENTAL PART

Silica particles (radius  $R = 101, 110$  and  $203$  nm) were prepared via a microemulsion method.<sup>114</sup> and a continuous-feed seeded-growth procedure<sup>115</sup>. The polystyrene particles ( $R = 97$  nm) were purchased from Duke Scientific. Glass substrates were cleaned with chromic acid prior to use. A clean glass substrate was vertically immersed in a scintillation

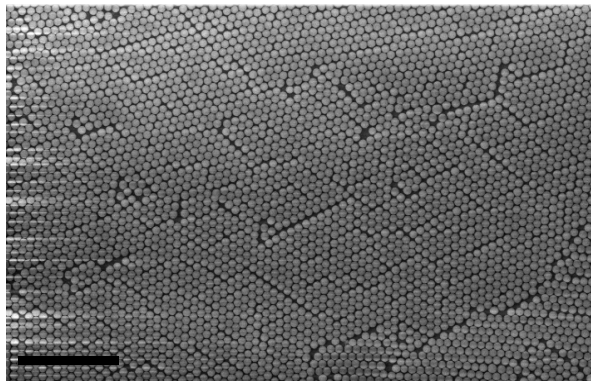


**Figure 3.1.**  
Scanning electron micrograph of a monolayer of silica particles with a radius of 203 nm.  
The scale bar is 5  $\mu\text{m}$ .

vial containing colloidal particles dispersed in ethanol, covered with a crystallization dish. The experiments were performed on an anti-vibration table in a room of constant temperature and humidity. The crystal growth rate was on the order of 1 – 2 mm per day. After each deposition of a layer of particles, the sample was dried for 24 hour at room temperature. Scanning electron microscopy (SEM) was carried out on a Philips XL30 FEG microscope. Polystyrene particles were burned away in an oven at 600°C for four hours under air.

### 3.3. RESULTS AND DISCUSSION

First, a 2D hexagonal close-packed (hcp) crystal of large (L) silica spheres ( $R_L = 203 \text{ nm}$ ) was grown on a clean glass substrate (Fig. 3.1). In the next, structure-determining step, the 2D crystal was used as a template on which small (S) silica or polystyrene particles were deposited. The small particles ( $R_S = 101, 110 \text{ nm}$  silica or 97 nm polystyrene) arranged themselves in regular structures depending on their volume fraction,  $\phi$ , and on the size ratio,  $\gamma = R_S / R_L$ . Subsequently, another layer of large particles was deposited. These steps can be successively repeated to grow a 3D structure of the desired thickness and composition. We studied a narrow range of size ratios,  $\gamma = 0.48 - 0.54$ , where we expected LS<sub>2</sub> structures to be stable based on experimental observations in bulk crystallisation<sup>33, 97</sup> and on packing arguments<sup>96</sup>.

First, we will present our results for the largest size ratio  $\gamma = 0.54$ . When depositing the second layer of small particles at relatively high volume fraction,  $\phi = 0.043 \%$  - sufficient to form a 2D close-packed crystal on a smooth substrate, a slightly corrugated but ‘complete’ close-packed layer of small particles on top of the large ones was observed (not shown). Decrease of the volume fraction to  $\phi = 0.021\%$  led to the formation of large ( $\sim 200 \mu\text{m}^2$ ) areas with a still hexagonal, but more open, packing<sup>116</sup> (Fig. 3.2a) where the small spheres filled all the hexagonally arranged interstices made by the first layer of larger spheres. The next layer of larger particles deposited themselves exactly on top of the first

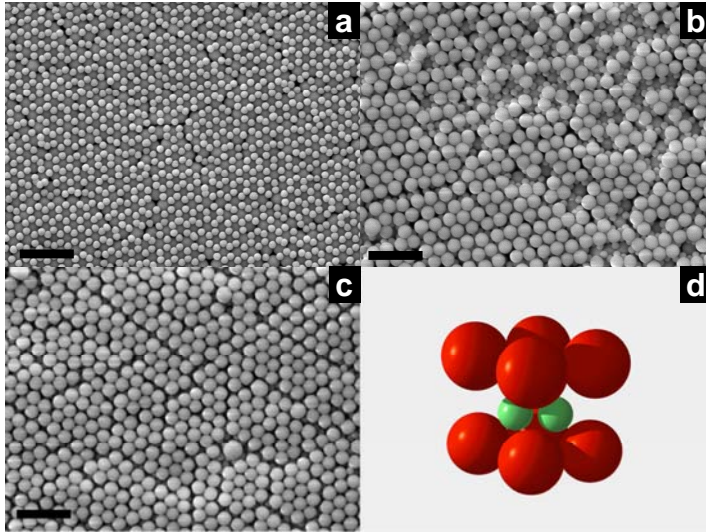


**Figure 3.2.**

SEM pictures showing binary colloidal crystals (size ratio,  $\gamma = 0.54$ ) with a stoichiometry  $LS_2$  (atomic analog  $AlB_2$ ). (a) Open packing with hexagonal symmetry where each small sphere has three neighbors on top of a 2D crystal of large spheres. (b) An incomplete third layer of large particles enabling a ‘look-through’. (c) Well-ordered complete third layer of large spheres. (d) Schematic presentation of the unit cell of an  $LS_2$  binary crystal. The scale bars are  $2 \mu m$ .

layer as expected (Fig. 3.2b, c), which leads to the formation of the well-known  $LS_2$  binary colloidal crystal (Fig. 3.2d). The preserved order of the small spheres can be seen through a patch in the crystal which had an incomplete top layer (Fig. 3.2b). Continuation in a layer-by-layer fashion will lead to an  $LS_2$  binary colloidal crystal of desired thickness with exactly the same  $AlB_2$ -type structure that is observed in bulk colloidal crystallization<sup>33</sup>. We created  $LS_2$ -type crystals consisting of three layers of large and three layers of small particles; it is worth to mention here that interesting photonic effects can already be achieved with only 1.5 unit cells of a photonic crystal<sup>17</sup>. Stacking faults in this structure during the layer-by-layer growth are not possible as the optimal positions of small and large particles are uniquely defined in each growing step.

Further decrease of the volume fraction led to the formation of another open structure with hexagonal symmetry. This structure, with stoichiometry  $LS$ , is similar to  $LS_2$ , but instead of six small particles around each large one there are now three. Fig. 3.3a shows a large region formed by polystyrene particles ( $\phi = 0.011\%$ ,  $\gamma = 0.48$ ) on a 2D crystal of large silica particles. It is quite interesting that the small particles retain a long-range hexagonal order even when they are not touching as it can be seen from the Fourier transform in Fig. 3.3c. The next layer of larger particles can now stack in two positions: exactly on top of the first layer as for the  $LS_2$  structure (AA stacking) or in the non-occupied by the small particles interstices formed by the first hexagonal layer (AB stacking). Our results for  $\gamma = 0.48$  indicated that the next layer always grew as an AB sequence of the larger spheres (Fig. 3.3b). This configuration has a higher packing density,

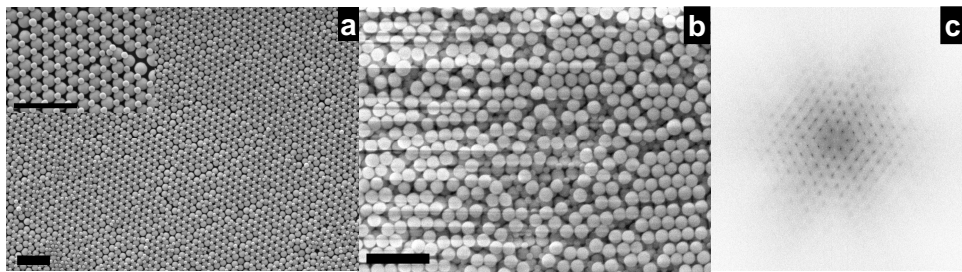


**Figure 3.3.**

SEM images (a and b) showing binary colloidal crystals ( $\gamma = 0.48$ ) with a stoichiometry  $LS$ . (a) Small spheres ordered in an open hexagonal lattice on top of a 2D crystal of large spheres. (b) An incomplete third layer of large particles shows that the large spheres deposit in the interstices not occupied by the small spheres. (c) Fourier transform of (a) after assigning the large and small particles similar gray values. The scale bars are  $2 \mu\text{m}$ .

although it could be that this preference for AB stacking of the large spheres is lost for large  $\gamma$ . For the fourth layer, formed from small particles, we did not expect any preferred orientation with respect to the second layer of small particles. This was indeed confirmed by observations and leads to ambiguity in the stacking of the resulting 3D structure. Therefore, only randomly stacked analogs of NaCl or NiAs can be grown by our layer-by-layer method. Although binary colloidal crystals of NaCl type have been predicted to be a stable phase in bulk crystallization,<sup>118</sup> only very recently small crystallites of binary crystal of stoichiometry  $LS$  were observed for the first time.<sup>34</sup> It was not clear for this structure whether it was a pure NaCl structure or whether it was a random-stacked crystal.

For size ratios  $\gamma = 0.48 - 0.5$ , a completely different arrangement of the small spheres, in addition to the already described  $LS$  and  $LS_2$  structures, was observed. Again, at a relatively high volume fraction ( $\phi = 0.041\%$ ,  $\gamma = 0.48$ ) of the small particles, a ‘complete’ coverage on the top of the big particles was found. At lower volume fraction ( $\phi = 0.021\%$ ) a kagomé-type arrangement of the small spheres on top of the 2D crystal of large spheres was observed in which each large sphere was surrounded by a hexagonal ring

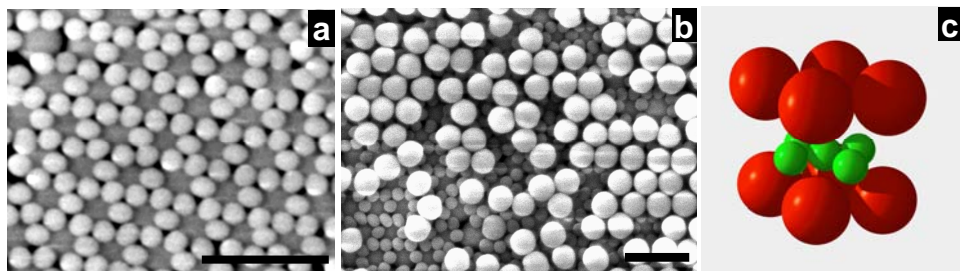


**Figure 3.4.**

Scanning electron micrographs (SEM) showing binary colloidal crystals with stoichiometry  $LS_3$  (no binary atomic analog was found). (a) A magnified region with a kagomé net of small spheres on top of a 2D crystal of large spheres ( $\gamma = 0.50$ ). (b) An incomplete third layer of large particles ( $\gamma = 0.48$ ). (c) Schematic presentation of the unit cell of an  $LS_3$  binary crystal. The scale bars are  $1 \mu\text{m}$ .

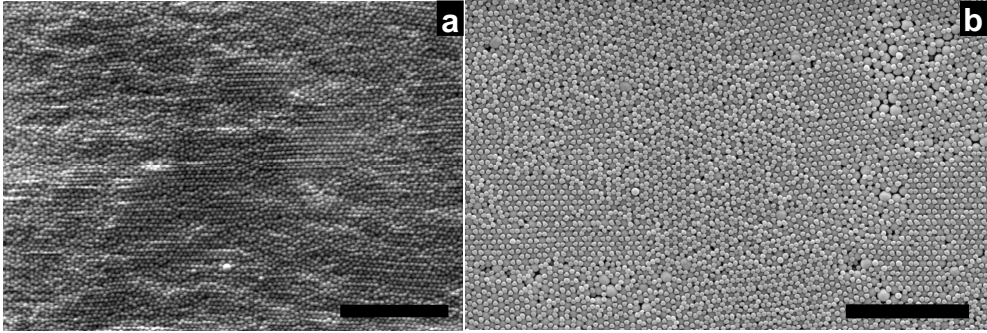


**Figure 3.5.**

Scanning electron micrographs (SEM) showing areas with a kagomé ( $LS_3$ ) net of small spheres on top of a 2D crystal of large spheres ( $\gamma = 0.48$ ), which co-exist with a ‘complete’ close-packed layer of small spheres (a) and an  $LS_2$  net of small spheres (b). The scale bars are  $5 \mu\text{m}$ .

of six small particles (similar to  $LS_2$ ) rotated in such a way that three small particles can fit in every interstice in the form of a (planar) triangle (Fig. 3.4a) (in the  $LS_2$  crystal there is one small sphere per interstice). Mostly, this open structure was found to co-exist with the  $LS_2$  structure observed earlier or with a complete layer of small particles (Fig. 3.5). The second layer of big particles lay on top of the first one and an  $LS_3$  binary colloidal crystal was formed (Fig. 3.4b). Just as with the  $LS_2$  structure, degeneracy in stacking is not possible as the position of every next layer is unambiguously defined. A schematic presentation of the unit cell of the  $LS_3$  is shown in Fig. 3.4c. To our knowledge  $LS_3$  does not have a reported isostructural binary atomic analog. It is interesting to note that this structure has a higher packing fraction than  $LS_2$  for  $\gamma < 0.48$  (Fig. 3.6) and should therefore be the thermodynamically stable phase at high pressure. However, as far as we are aware, it has not been studied theoretically or ever suggested before as a possible binary colloidal crystal.

The complex self-organization of the small particles in the second layer is the result

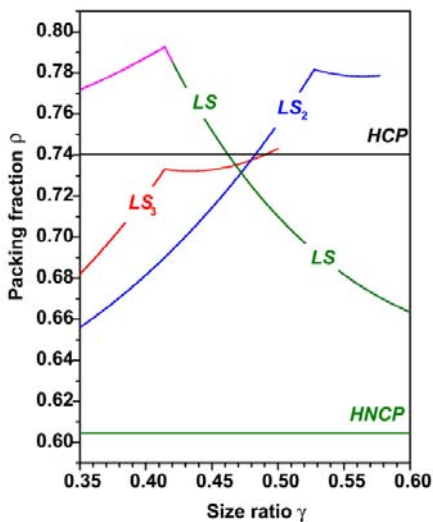


**Figure 3.6.**

Packing fraction diagram as a function of the size ratio  $\gamma$  for the  $LS$  (NaCl type),  $LS_2$  ( $AlB_2$  type), and  $LS_3$  binary colloidal crystals. The calculations are performed only for touching large spheres in the basal plane. The packing limits of hexagonal close-packed (hcp) (0.7405) and hexagonal non-close-packed (hncp) (0.6046) crystals of one-size spheres are shown by horizontal lines. Note that the new  $LS_3$  structure has a higher packing fraction than  $LS_2$  for  $\gamma < 0.48$

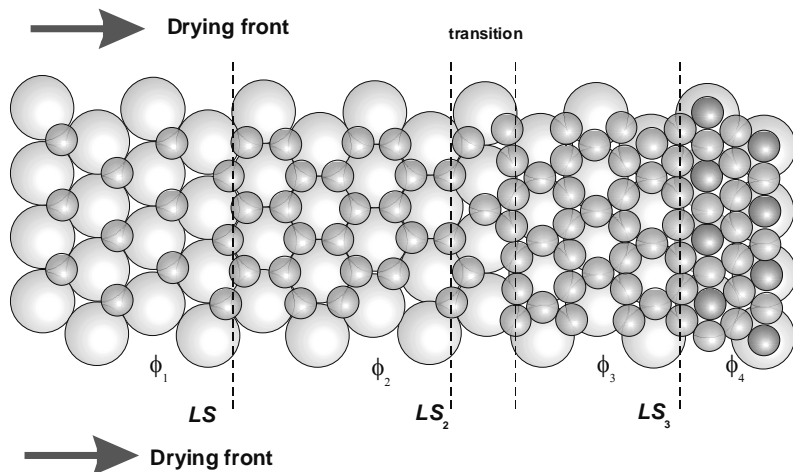


**Figure 3.7.**

*Schematic representation of the structures of small spheres with size ratio close to 0.5 that form onto a 2D hexagonal layer of larger spheres as function of the volume fraction. The symmetry of the structures can be understood as resulting from the templating effect of the first layer, and the forces resulting from the particle-liquid interfacial tension. Particles are lined up parallel to the drying front and go into those places that lie lowest on the 2D crystalline layer of the larger particles. The volume fraction,  $\phi$ , determines finally how many of the available low-lying sites can be occupied.*

of the interplay of geometrical packing arguments, minimization of the surface free energy of the drying liquid film, and surface forces due to the curved menisci. During the drying of the wetting film, particles partially immersed experience both the attractive capillary forces that tend to draw particles together<sup>11</sup> and the corrugated surface of the first layer of large particles. As the drying rate is constant, which (open) packing will be realized is determined by the local particle concentration and the symmetry and orientation of the already deposited layers. A schematic representation of the process, as we have inferred it by studying defects formed and by observations on the orientation of the crystal layers relatively to the drying front, is given in Fig. 3.7. At sufficiently high volume fraction the layer of smaller particles on top of the 2D hexagonally close packed layer of larger ones is also hexagonal with lines of touching particles parallel to the drying front (see Fig. 3.7,  $\phi_4$ ). This layer cannot be flat, e.g., the darker particles in the figure are elevated because they are exactly on top of the particles in the first layer but the size ratio close to 0.5 makes it

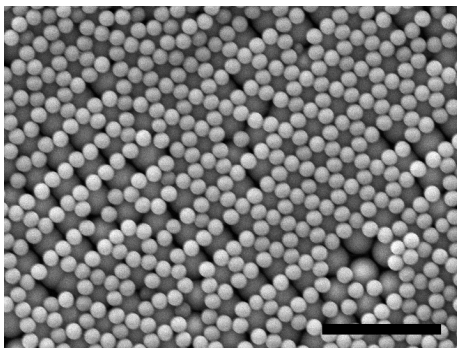


**Figure 3.8.**

*Scanning electron micrographs (SEM) showing areas with line-like defects in the kagome ( $LS_3$ ) net of small spheres on top of a 2D crystal of large spheres ( $R_L = 716$  nm,  $\gamma = 0.49$ ). The scale bars are 5  $\mu$ m.*

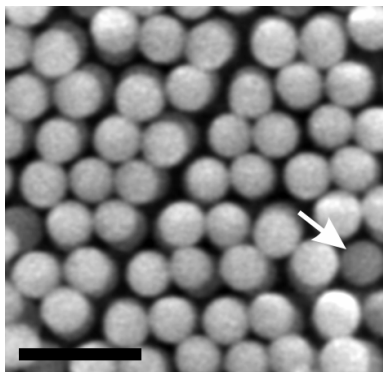


**Figure 3.9.**  
Scanning electron micrograph (SEM) of the top layer of a hexagonal non-close-packed (hncp) colloidal crystal. The arrow points to a particle from the bottom layer. The scale bars is 1  $\mu\text{m}$ .

geometrically possible for the second layer to become hexagonal as well. At slightly lower volume fraction,  $\phi_3$ , complete coverage by the second layer is not possible, thus the dark particles (see Fig. 3.7), which protrude from the drying film the most, are lost first. This leads to the kagomé net observed for the second layer in Fig. 3.5a. At yet lower volume fraction,  $\phi_2$ , the structures formed can be again explained by taking fewer particles in the drying front and placing them at the lowest points that become available. These are formed by the trigonal interstices of the hexagonally arranged first layer. This structure has the  $\text{LS}_2$  arrangement from Fig. 3.2a. Because the change in volume fraction from  $\phi_3$  to  $\phi_2$  is quite subtle, the  $\text{LS}_3$  structures are mostly seen in combination with the  $\text{LS}_2$  (Fig. 3.5a) and with defects (Fig. 3.8) seen in the transition region indicated in Fig. 3.7. At  $\phi_1$  there are even less particles in the drying front and now filling up lowest points in a line parallel to the drying film results in the  $\text{LS}$  structure from Fig. 3.3a.

In order to show how our method can be used to create non-close-packed crystals of single-sized particles, we first created a composite  $\text{LS}_2$  binary crystal of alternating layers of inorganic (silica) and organic (polystyrene) particles. Then, the organic layer was removed by heating in an oven in air. The resulting structure consists of hexagonal close packed layers stacked on top of each other, thus forming a non-close-packed crystal with a simple hexagonal stacking (AAAA, Fig. 3.9), which, to our knowledge has not been made before with colloids. This non-close-packed structure with a low packing fraction of  $\rho = 0.6046$  (Fig. 3.6) compared to close-packed (0.7405) is another example of how the layer-by-layer method can be used to create new crystal structures that cannot be grown in bulk.

#### *Unsuccessful attempts*

Motivated by the work of Kiely et al.<sup>47</sup> where 2D crystals of metal particles with two sizes were obtained by drying mixtures of them directly on a substrate, we also tried their procedure before resorting to a layer-by-layer approach.

The size ratio of the silica particles we used was  $\gamma=0.542$ , the ratio between the number of the large ( $N_L$ ) and the number of the small ( $N_S$ ) particles in the mixture was:  $N_L:N_S = 1:4, 1:3, 1:2, 1:1, 2:1, 3:1, 4:1$ . The total volume fraction of the particles was  $\sim 0.15\%$ . A small volume (10-20  $\mu\text{L}$ ) of the binary dispersion was put on a clean substrate which was tightly covered with a glass dish and the solvent was left to evaporate at constant temperature. The influence of the substrate position (vertical or horizontal) as

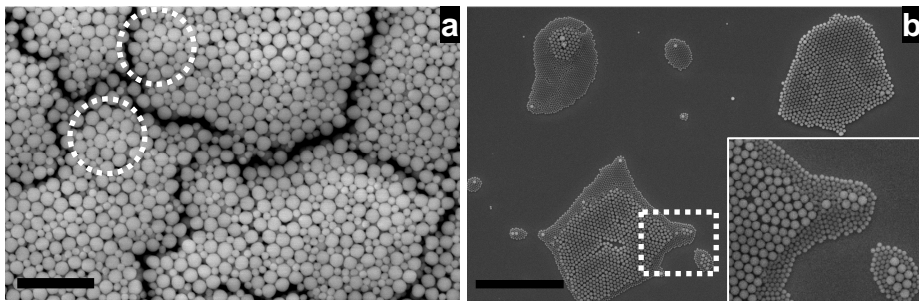


**Figure 3.10.**

Scanning electron micrographs (SEM) of structures formed after drying binary mixtures of large and small silica particles ( $\gamma = 0.542$ ) on a horizontal substrate. (a) mixed disordered layers with small areas of local order marked with circles; scale bar  $2 \mu\text{m}$ . (b) “islands” with monolayers of only large or small spheres and segregated monolayers; the inset shows enlarged view of the marked with a rectangle area. The scale bars are  $10 \mu\text{m}$ .

well as the solvent evaporation conditions (evaporating at solvent vapor rich or poor atmosphere) on the structures formed was found to be insignificant. For all the mixtures used no binary crystals were observed. Instead, areas with either mixed disordered mono- or multilayers with small areas of very local order (Fig. 3.10a), or “islands” of one-sized particles, or segregated “islands” were found (Fig. 3.10b). These observations are in accordance with the observed by Prevo et al.<sup>119</sup> and Yamaki et al.<sup>120</sup> local areas of size selective segregation and disordered mixed regions in mixtures with size ratios in the range  $0.4 - 0.65$ , and with the results of Kitaev and Ozin<sup>121</sup> who found (see below) a disordered binary layer for size ratios above  $0.3$ .

### 3.4. CONCLUSIONS

We have demonstrated the formation of large areas of  $LS$ ,  $LS_2$  and  $LS_3$  type binary colloidal crystals (the  $LS_3$  structure seen for first time) using a non-equilibrium layer-by-layer growth process. In the work presented here, we explored only a small region of size ratios and already found new structures. Clearly, other size ratios could be explored and using surface templates<sup>66</sup>, the method can be further extended by growing different crystal planes and new types of crystals with a well-defined crystal orientation<sup>122</sup>. For instance, the use of a template with square pattern will provide the possibility to grow  $CsCl$  type binary structures. Our method will substantially expand the stoichiometries, compositions, and symmetries achievable with crystals of colloidal particles.

### 3.5. UPDATE

Over the last few years there has been extensive ongoing research on creating new and/or improving the existing approaches for fabricating binary colloidal crystals. This section is

intended to review some of the recent results (since the publication of our method<sup>113</sup>) for making colloidal crystals related to the method described in this chapter.

In order to improve the quality of the growing crystal and to gain more control during the process of convective self-assembly, the effect of different parameters involved was studied by different groups. Wostyn et al.<sup>123</sup> have found that the meniscus of the drying film plays an important role as a template to direct the orientation of the hexagonal close-packed crystal layers and that this orientation is an intrinsic property of the convective self-assembly process. The observations made by the authors on the orientation of the hexagonal close-packed layers relative to the meniscus are different from what we suggested in our model (see Fig. 3.7) – the lines of touching particles in our model are parallel to the meniscus (the drying front) while in Ref. [123] they are perpendicular to it. The observations of Xia et al.<sup>124</sup>, on the other hand, seem to agree with the model in Fig. 3.7 as these authors found that particles confined in template holes orient upon drying of the solvent in such a way as to have one of the edges of the obtained clusters inside each hole parallel to the drying front. This configuration according to the authors is, under the experimental conditions they used, more stable than a configuration in which lines of touching particles are perpendicular to the drying front. Preliminary x - ray and electron microscopy measurements performed in our group<sup>125</sup> agree with the observations of Wostyn et al.<sup>123</sup> but a more detailed study is needed to resolve this issue.

The influence of the solvent flow during self-assembly was also discussed by Noris et al.<sup>126</sup> who put forward a hypothesis of flow-driven placement of spheres. Two types of flows were considered – one that is perpendicular to and the other that is along the crystal layers (the direction of the lateral flow was considered to be perpendicular to the lines of touching particles as it is in Fig. 3.7) and their effect on the occupation of preferred interstices in the crystal layers could explain the formation of crystals with specific structures. This hypothesis can also be used to understand the formation of the LS structure described in this chapter as only the interstices with preferred positions would be occupied by the small particles driven by the solvent flow thus producing a regular arrangement of the small species.

Another hypothesis for the formation of different structures in processes where solvent drying is important was brought forward to explain the experiments of Manoharan et al.<sup>127</sup> on the formation of clusters of particles with unique packings upon evaporation of liquid emulsion droplets containing different amount of particles. Recent theoretical work<sup>128</sup> confirmed the hypothesis of minimization of the total surface energy<sup>127, 129</sup> as responsible for the specific packing of particles into small well-defined clusters.

The position of the substrate relative to the gravity direction and the patterning of the substrate<sup>130</sup> as well as the temperature<sup>131</sup> are also very important factors that influences the symmetry and the structure of the growing crystal.

Kitaev and Ozin<sup>121</sup> utilized control over the rate of solvent evaporation and made it to be comparable with that of particles sedimentation to obtain reproducible 2D crystals on a large scale using convective vertical deposition technique. Using mixtures of particles with different sizes (size ratio  $\gamma = 0.11 \div 0.3$ ) and changing the concentration of the small particles, different binary structures were observed. The small particles settled in all the interstices of the hexagonal close packed monolayer of the large spheres forming triangles, tetrahedra, hexagons or more complex arrangements. Above some critical concentration

the small colloids couldn't make an ordered array. For size ratios above 0.3 only disordered mixed layers were observed. Thus, this method is limited to only small size ratios which makes it less universal than the layer-by-layer approach described in this chapter.

Another alternative method for growing binary colloidal crystals was proposed by Wang and Mohwald<sup>132</sup>. They used step-wise spin-coating of colloidal dispersions on a substrate to fabricate 2D binary crystals with stoichiometries  $LS_2$  and  $LS_3$  similar to the structures reported in this chapter. An additional parameter to control the structures formed in this case is the rotation speed. Advantages of this method are that it is fast and has high tolerance for particles polydispersity. It can also be further optimized to produce more complex structures by using patterned substrates. On the other hand, for successive spin-coatings the particles in the upper layer have to be strongly localized in their positions (not to be swept away by the centrifuge force) which imposes some limitations on the size ratios and the structures that can be generated (for example the  $LS$  crystals reported in the present chapter could not be created with the spin-coating method).

Kim and co-authors<sup>133</sup> used a 'confined convective assembly' technique in which by controlling the lift-up rate of a vertical substrate mono- and multilayers were obtained quickly. Performing a consecutive deposition of particles with different sizes (similar to the described in this Chapter layer-by-layer approach) binary 2D structures resembling the  $LS_2$  crystals reported in this Chapter were fabricated.

A binary mixture of nanocrystals with size ratio 0.42 was found to form  $LS$  crystals after a quick (few seconds) evaporation on a substrate<sup>45</sup>. Different crystal planes were observed (probably due to local fluctuations of the particles density and number ratio during drying) which revealed that the crystals had a NaCl-type structure. A crystallization mechanism was discussed according to which in places where the large nanocrystals are in excess a hexagonal close-packed layer of the large particles will form first on the substrate followed by occupying the interstices by the small particles. On the other hand, in areas with local excess of small spheres, the mixed (100) plane of the NaCl-type crystal could be favored as it will lead to a high packing density. It was suggested that interparticle attractions have a significant role in formation of these binary crystals.

In a recent work reported by Cong and Cao<sup>57</sup> binary structures were made during a slow (up to 10 days) convective deposition on an inclined substrate dept in a binary mixture of poly(styrene-MMA) particles with a size ratio of 0.5 in water. Square and hexagonal patterns were observed with a stoichiometry of  $LS$  and they were interpreted as coming from NaCl- and ZnS-type crystals (although more likely this patterns are the (100) and (111) plane of NaCl-type crystal because ZnS structure at this size ratio would be unstable if the interactions between the two species are hard-sphere like or can be mapped onto such). Areas with patterns similar to those of the  $LS_2$  crystals were observed as well and two isomeric arrangements with  $LS_3$  stoichiometry. One of them is the same as the  $LS_3$  structure reported in the present chapter while in the other the large spheres form a square-like layer and there are six small particles around each large one. The coexistence of different structures was explained by the different mobility of the large and the small particles causing local variation of the number ratio. It was not very clear what is the quality of the crystal structures and what the stacking is in the direction perpendicular to the substrate.

Another approach was developed by Schaak and co-workers.<sup>134</sup> They used dewetting from lithographically made templates to form mono- and bilayers of particles with different size. A two-dimensional LS<sub>2</sub>-crystal was created by first depositing a non-close packed hexagonal layer of large spheres on a template and then letting the small particles fill the interstices of that layer. It is possible with this method to create also open 2D structures of one-size particles with different patterns – kagome-type, square, linear, which can be further used as templates for binary crystals growth. Advantages of this method are that it is fast, versatile and it gives the opportunity to make on a single substrate many microarrays with different structure and composition.

Colloidal lithography is a method that offers the possibility to design a variety of crystal structures. It has been used by Choi et al.<sup>135</sup> to make binary arrays by applying reactive ion etching (RIE) technique to a preformed crystal with controlled thickness. With this technique the upper layers are etched more (or even completely) but the structure order is preserved. In this way, starting from a multilayer crystal of single-size spherical particles, it is possible to obtain arrays of particles with different size and shape. The structure of these arrays depends on the structure and thickness of the layers before the RIE and on the conditions of etching. The RIE technique can be used also to make templates for creating non-close packed 2D arrangements with patterns resembling the LS<sub>2</sub> and LS<sub>3</sub> structures presented in this chapter<sup>136</sup>.

Successive deposition of monolayers of particles with different size from an air/water interface on a solid substrate can lead to a formation of layered arrays of colloids<sup>137</sup>. This method is an alternative to the method of Colvin et al.<sup>138</sup> for making sandwich-like arrays but it provides more control over the thickness and the structure of the crystals at a single layer level. In contrast to the layer-by-layer approach reported in this chapter it is limited only to close-packed layers and it can not produce more open and complex structures.

More recently a modification of this procedure was described<sup>139</sup> where first multilayers were formed on a vertical substrate, then on top of them a single layer of larger particles was deposited from an air/water interface followed by a second multilayer vertical deposition. The presence of a layer of larger particles between multilayers of smaller spheres caused appearance of an impurity defect mode in a photonic stop band.

A method explored by Li and Marlow<sup>140</sup> uses capillary deposition to fabricate crystals consisting of alternating crystalline stripes of particles with different size. In contrast to the other reported methods to make sandwich-like arrays where the different crystal bands are changing in direction perpendicular to the substrate<sup>137, 139</sup>, here the stripes are alternating along the plane of the substrate. It is possible to make stripes with different curvature and to control the interface between them.

By using convective assembly mixtures of particles with size ratio  $\approx 0.55$  and relatively high polydispersity were found to form disordered mixed layer where the large and small particles are randomly arranged<sup>119</sup>. This layer, because of its non-close packed structure, can serve as an effective antireflective coating.

Binary colloidal crystals are very good candidates for photonic materials as they offer the possibilities to create non-close packed structures with different symmetries. Recently, new applications of the binary structures have been pointed out - as templates for macromolecular separation techniques<sup>141</sup> and as efficient antireflective coatings<sup>119</sup>. The method described in the present chapter has the advantages over the other mentioned

above methods that it provides high control on the structures formed, can generate non-close packed structures with complex arrangement and is tolerant for different particles composition and size ratios. It can be further improved by using patterned substrates to direct the crystal orientation and structure and by controlling more precisely the evaporation rate.

#### *ACKNOWLEDGEMENTS*

We thank Paul M. Chaikin, Arnout Imhof and Job Thijsen for helpful discussions.



# 4

## Binary colloidal crystals grown under an external electric field

We present a method to grow large binary colloidal crystals of NaCl-type from silica particles with a size ratio of 0.3 using an electric field oriented perpendicular to the direction of gravity. Different mechanisms are responsible for the formation of the binary crystals at low and at high dipolar interactions compared to  $k_B T$ . The observed areas and orientation of the binary crystals grown are promising for (photonic) applications and demonstrate that an external (electric) field can overcome problems in binary crystallization that are due to a large difference in sedimentation coefficients. We found strong indications that at high field strength the binary NaCl crystals are either thermodynamically stable or strongly metastable.

#### 4.1. INTRODUCTION

Binary crystals consisting of large (L) and small (S) particles have attracted significant attention in the past few years not only because they exhibit a much richer variety of crystal phases than one-component crystals (so far 10 different binary structures with stoichiometries LS, LS<sub>2</sub>, LS<sub>3</sub>, LS<sub>5</sub>, LS<sub>6</sub>, LS<sub>8</sub> and LS<sub>13</sub> have been observed)<sup>2, 5, 6, 34, 41, 45, 86, 113</sup> but also because of the possibility to use such systems in different applications, like templates for macromolecular separation techniques<sup>141</sup>, efficient antireflective coatings<sup>119</sup> and photonic materials<sup>82</sup>.

Crystals of silica spheres are of particular interest as these offer the opportunity to achieve materials with a large ‘inverse’ index contrast through chemical vapor deposition of silicon<sup>142</sup>. Growing large areas of such crystals with a good quality is a task that has initiated a lot of work trying to come up with effective methods. For binary crystals of silica particles with a large size difference it is even more difficult to achieve large crystal areas as the large difference in sizes translates into large difference in sedimentation rates and sedimentation is known to be an important obstacle against the formation of binary crystals<sup>143</sup>. In Chapter 3 and Ref. [113] we reported a method for fabricating binary crystals of silica particles based on self-assembly by capillary forces in a layer-by-layer fashion. This method gives good control over the crystal structure and orientation at a single layer level but it is time-consuming and gives rise to point defects.

In the current chapter we used a completely different approach to make binary crystals of silica spheres with a size ratio of 0.3. Previous research in our group<sup>80, 144, 145</sup> has shown that an external electric field can be used to induce a preferred crystal orientation. Large areas of single-domain crystals were prepared by using repeated sedimentation (turning the sample cell several times up-side-down) in an external electric field to anneal out defects and by manipulating the electric field strength. At relatively high field strengths the spheres form a body-centered tetragonal (bct) crystal which can be turned into a face-centered cubic crystal via a Martensitic transition<sup>144, 145</sup> by (slowly) decreasing the field strength. We based our approach on the idea to make a large oriented fcc crystal from the large spheres by using the procedure of Yethiraj et al.<sup>80</sup> and let the small particles fill the available holes in that crystal, thus generating a binary structure of NaCl-type. We used relatively low electric field strengths to assure that only the large particles interact with the field but as we will show in the results section of this chapter even at high field strength binary crystals can be formed. This study of our method of using an external electric field to grow binary crystals should be considered preliminary as we have only explored a size ratio of 0.3 and we have not made significant attempts to optimize the experimental procedure.

#### 4.2. EXPERIMENTAL PART

##### *Particles*

We used silica particles with two different sizes, synthesized via a modified Stöber-method<sup>63, 146</sup> and a continuous-feed seeded-growth procedure<sup>115</sup>. Both types of particles had a fluorescently labelled core and an unlabeled shell. The large silica spheres had the

dye fluorescein isothiocyanate (FITC) incorporated in a core with a radius of 192 nm, which was surrounded by a 500 nm thick silica shell, thus the total particle radius was  $R_L = 692$  nm and the polydispersity 2 % (measured by transmission electron microscopy (TEM))<sup>147</sup>. The smaller silica colloids were labelled with rhodamine isothiocyanate (RITC) in a core of radius 187 nm and had a total radius of  $R_S = 212$  nm (TEM) and a polydispersity of 7% (measured with static light scattering). The size ratio of the particles was  $\gamma = R_S / R_L = 0.30$ . The colloids were dispersed in a solvent mixture of dimethylsulfoxide (DMSO) and water (80/20 volume ratio), which had a refractive index matched to that of the silica spheres, thus minimising the Van der Waals attraction between them and allowing quantitative microscopy in the bulk of concentrated dispersions. Individual dispersions of the two species were prepared in the solvent mixture and binary mixtures with certain compositions were made by mixing.

### Set-up

The dispersions were filled in a cell made by two 50  $\mu\text{m}$  diameter parallel alumel wires (Goodfellow T2 Thermocouple Alloy Ni95/(Al+Mn+Si)5) placed at a distance of 1.5 mm apart between two glass slides<sup>80, 145</sup>. The cell was closed with wax (Microwax 863, Frank B. Ross Co. Inc.) along the long sides and with a two-component epoxy glue (Bison Epoxy Rapide) on the short sides, see Fig. 4.1. We used a function generator (Agilent 33120A) to apply an AC electric field between the wires perpendicular to gravity, with a frequency of 1 MHz, high enough to avoid polarization of the double layer and significant movement of the ions or colloids. A wide-band amplifier (Krohn-Hite 7602M), a home-made transformer and an oscilloscope (Tektronix TDS 3012B) were connected to the set-up to control and monitor the electric field.

If we assume infinitely long wires and neglect the influence of the glass slides on the electric field between the wires, the electric field is given by<sup>148</sup>:

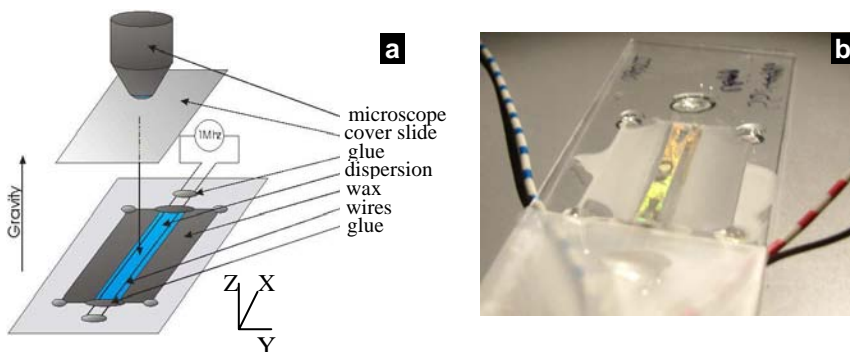
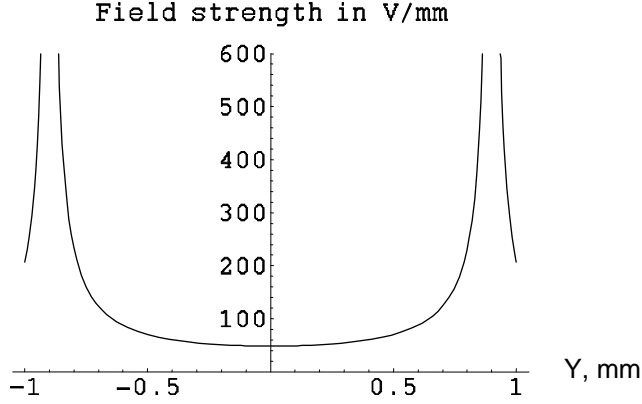


Figure 4.1.  
Schematic representation (a) and a photo (b) of the experimental cell used.



**Figure 4.2.**

Electric field strength inside the experimental cell at a voltage peak-to-peak difference between the wires of 100 V, a wire spacing of 1.8 mm, and a wire radius of 0.025 mm. An infinitely long cell is assumed and the glass slides are assumed to have no effect on the field in the cell. The plane  $y = 0$  corresponds to the middle of the cell.

$$E(y, z) = 2V_0 \sqrt{\frac{(d^2 - R^2) \cos^2(\omega t)}{((y^2 + R^2 - d^2)^2 + (d^2 - R^2 + y^2)z^2 + z^4) \operatorname{arccosh}^2(d/R)}}, \quad (1)$$

where  $V_0$  is the amplitude of the voltage applied,  $R$  is the radius of the wires,  $d$  is half the distance between the wires and  $\omega$  is the angular frequency of the electric field. Fig. 4.2 shows the electric field strength in the direction perpendicular to the wires and it can be seen that the field is quite uniform in the middle of the cell but rises steeply near the wires. Further in the text we shall refer to  $E_{\text{rms}}$  as to the root-mean-squared electric field strength in the middle of the cell (at  $y=0, z=0$ ).

We used confocal scanning fluorescent microscopy to observe the structures formed in the sample cells. Because the two types of silica colloids were core-shell particles and were labeled with fluorescent dyes having significantly different emission and excitation spectra, we were able to distinguish them well under the microscope. We extracted 3D-coordinates of the particles from the xyz-stacks<sup>65, 70</sup> which allowed quantitative characterization of the structures formed.

#### *Crystal growth procedure*

To prepare binary NaCl-type crystals we slightly modified the procedure described by Yethiraj et al<sup>80</sup>. A typical experimental protocol that we followed consists of the following steps. After filling the cell with a binary mixture and quickly connecting it to the electric set-up, we applied an electric field with a typical strength of  $E_{\text{rms}} = 40$  V/mm in the middle of the cell. Two hours later we turned the cell up-side-down for 15 minutes to anneal out defects<sup>80</sup>, then we turned it back and simultaneously lowered the electric field strength to  $E_{\text{rms}} = 35$  V/mm. We repeated this procedure 3 times and left the cell for

about 15 hours (overnight) with an electric field strength of  $E_{\text{rms}} = 20$  V/mm. Then the electric field strength was reduced to  $E_{\text{rms}} = 10$  V/mm and about 30 hours after sample preparation the electric field was switched off.

For observing the effect of a high-strength electric field we applied an electric field of  $E_{\text{rms}} = 230$  V/mm for a long period of time (up to 10 days).

### 4.3. THEORETICAL BACKGROUND

The larger silica spheres used in this study acquired a small charge when dispersed in the DMSO/water solvent mixture as judged from the mean interparticle distance in the crystal they formed ( $d \approx 1.07d_1$ ). Based on these results the smaller spheres were assumed to be also slightly charged.

When the dielectric silica colloids dispersed in the polar solvent medium of DMSO and water were brought under the influence of an external electric field, they polarized because of the difference between the dielectric constant of the particles and that of the solvent. The induced dipole moment  $p$  (under the reasonable assumption that no polarization effects of the double layer around the particles take place) is:

$$p = 4\pi\epsilon_m\epsilon_0 \left( \frac{\epsilon_p/\epsilon_m - 1}{\epsilon_p/\epsilon_m + 2} \right) R^3 E_0, \quad (2)$$

where  $E_0$  is the external electric field,  $\epsilon_0$  is the permittivity of free space,  $\epsilon_p$  is the relative dielectric constant of the particles ( $\epsilon_p = 4.5$  for silica),  $R$  is their radius and  $\epsilon_m$  the relative dielectric constant of the medium ( $\epsilon_m = 54$  for the DMSO/water mixture, determined assuming that the dielectric properties of the two liquids are additive). The energy of interaction between two dipoles is given by:

$$W_d(\vec{r}) = \frac{1}{4\pi\epsilon_m\epsilon_0} \frac{\vec{p} \cdot \vec{p} - 3(\vec{n} \cdot \vec{p})(\vec{n} \cdot \vec{p})}{|\vec{r}|^3}, \quad (3)$$

where  $\vec{r}$  is the vector connecting the two dipoles and  $\vec{n}$  is the normal unit vector in the direction of  $r$ . The dipole-dipole interaction energy can also be presented in polar coordinates:

$$W_d(r, \vartheta, \phi) = \frac{1}{4\pi\epsilon_m\epsilon_0} \frac{p^2(1 - 3\cos^2 \vartheta)}{r^3}, \quad (4)$$

where  $\theta$  is the angle between the external electric field and the vector  $\vec{r}$ . From this dependence it follows that the interaction energy is minimal for  $\theta = 0$ , i.e when the dipoles align in the direction of the electric field, and it is maximal when the dipoles align perpendicular to the electric field. This minimization of the dipole-dipole energy causes

the polarized colloidal particles in the presence of an external electric field to attract each other and form chains oriented parallel to the field direction.

The minimum strength of the electric field required for the strings to start forming,  $E_{str}$ , can be estimated by using the dipole-dipole energy in the direction of the electric field derived from eq. (4) at  $\theta = 0$  and  $r = R$  and the expression for the dipole moment (2):

$$W_d(R,0,0) \propto \frac{p^2}{R^3} \propto \frac{E_{str}^2 R^6}{R^3} = E_{str}^2 R^3. \quad (5)$$

If we assume that the particles are hard spheres without the field then the total energy of interaction between the two touching colloids in a string is equal to their dipole-dipole interaction energy from eq. (5). Assuming further that both, small and large particles, have the same kinetic energy driving them to leave the string, then balancing it with the dipole-dipole energy which is keeping the particles aligned we get:

$$E_{str}^2 R^3 = \text{const} \tan t \quad \Rightarrow \quad E_{str} \propto R^{3/2}. \quad (6)$$

This means that the smaller particles would require a higher electric field strength to start forming strings. For example, the small spheres in our system, approximately 3 times smaller than the larger ones, would start to form strings at an electric field strength 6 times higher than that needed for the larger ones.

We characterized the structures observed by calculating the two and three dimensional radial distribution functions  $g(r)$  which are determined by the probabilities to find a particle at a certain distance  $r$  from another particle:

$$g(r) = \frac{1}{\rho^2} \left\langle \sum_i \sum_{j \neq i} \delta(\vec{r}_i) \delta(\vec{r}_j - \vec{r}) \right\rangle, \quad (7)$$

where  $\rho$  is the average number density of the colloids,  $\vec{r}_{i/j}$  denote the particle centers,  $\delta$  is the Dirac delta function and the summation runs over all particles.

To determine the symmetry of the crystals found we used a two dimensional global bond order parameter<sup>149</sup> which for hexagonal symmetry is given by:

$$\Psi_6 = \frac{1}{N} \sum_{\text{colloids}} \frac{1}{N_b} \sum_{j=1}^{N_b} e^{i6\phi_j}. \quad (8)$$

Here a ‘‘bond’’ is defined as the vector from the center of a particle to the center of one of its nearest neighbors,  $N$  is the number of particles,  $N_b$  is the number of bonds and  $\phi$  is the angle between a bond and an arbitrary vector. This global bond order parameter has a value of 1 when the characterized plane has a perfect hexagonal symmetry and it is zero when there is no hexagonal order. We defined a bond by an interparticle distance cutoff, determined from the first minimum of the radial distribution function<sup>68,74</sup>.

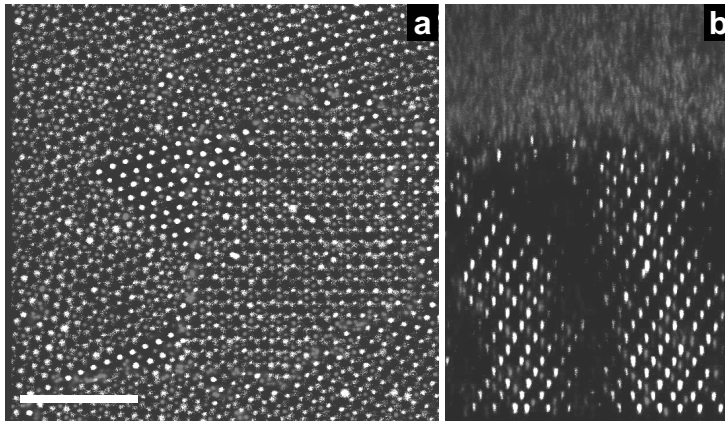


**Figure 4.3.**

*XY (a) and XZ (b) confocal images of a binary mixture of large and small silica spheres left to sediment without electric field present. Scale bar is 10  $\mu\text{m}$ .*

#### 4.4. RESULTS

##### 4.4.1. Low-strength electric field

We will focus our results on a binary mixture consisting of 15 volume percent of large (L) and 7 volume percent of small (S) silica particles, as with this system nice binary crystals were observed.

Without an electric field applied, the large spheres in the mixture formed upon sedimentation small domains with an fcc or rhcp arrangement (as in the case without small particles present). The small particles were sitting in some of the available holes (filling approximately 30 % of the holes) (Fig. 4.3a) but most of them were forming a fluid layer on top of the sediment (Fig. 4.3b). The red “blobs” visible in some of the images result

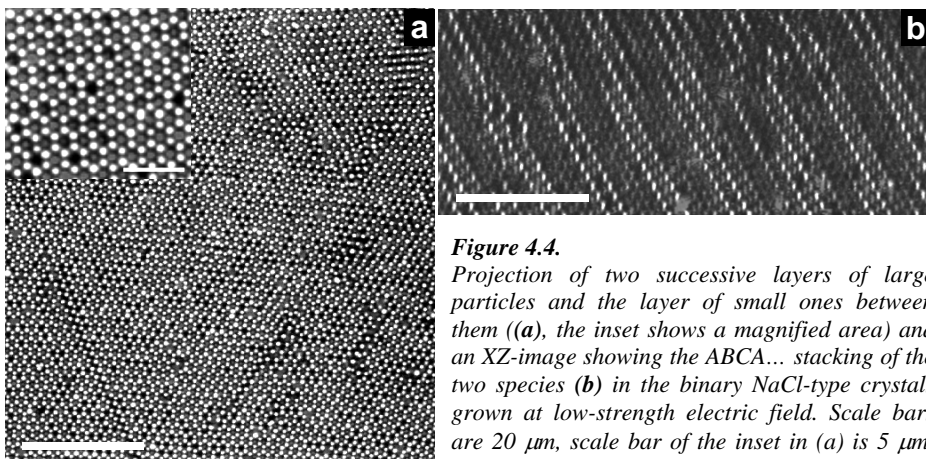


**Figure 4.4.**

*Projection of two successive layers of large particles and the layer of small ones between them ((a), the inset shows a magnified area) and an XZ-image showing the ABCA... stacking of the two species (b) in the binary NaCl-type crystals grown at low-strength electric field. Scale bars are 20  $\mu\text{m}$ , scale bar of the inset in (a) is 5  $\mu\text{m}$ . (See page 86 for color version)*

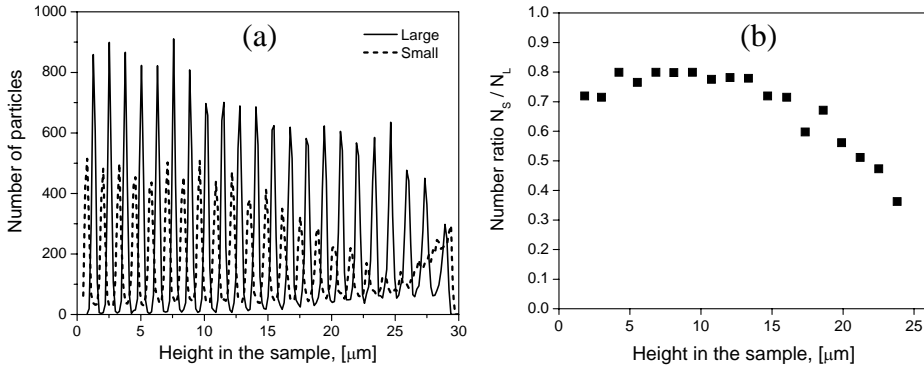


**Figure 4.5.**

Number density (a) and number ratio (b) of the small and the large silica particles in the binary crystals as a function of the height in the sample.

from the high mobility of the small particles ( $\sqrt{\langle x^2(t) \rangle} \approx 1 \mu\text{m}$  for the time  $t = 1\text{s}$  it takes to scan one image).

When the mixture was subjected to the influence of an external electric field as described in the experimental section and the field strength was lowered in several steps from  $E_{\text{rms}} \approx 40 \text{ V/mm}$  to  $E_{\text{rms}} \approx 10 \text{ V/mm}$ , large areas of binary crystals (single domain size  $\sim 70 \times 70 \times 30 \mu\text{m}^3$ ) were observed in the middle of the sample cell (Fig. 4.4). After the field was switched off, the crystal domains grew larger but their quality a few days later was slightly worse. We identified the structure of these binary crystals by looking at the ordering of both, large and small spheres. Fig. 4.5a shows the number of particles in a  $\approx 25 \mu\text{m}$  thick binary crystal as a function of the height ( $z$ ) in the sample, from where is clear that both species exhibit a high level of layering in the vertical direction. The layers of small spheres are situated exactly between the layers of large spheres and the distance between two layers of either large or small particles was found to be  $1.28 \pm 0.03 \mu\text{m}$ . The graph in Fig. 4.5b shows the change of the number ratio between the small and large spheres in the binary crystal with the height in the sample. For the bottom 10 layers it is

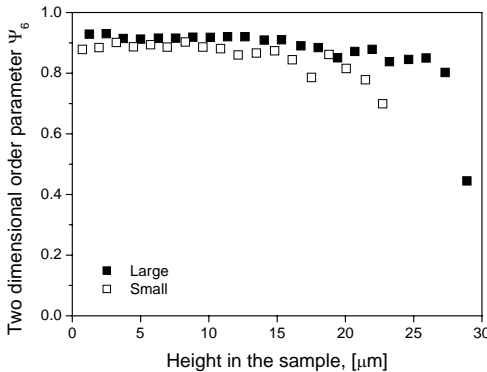


**Figure 4.6.**

The two-dimensional order parameter  $\Psi_6$  for the different layers of large and small particles in a binary crystal.

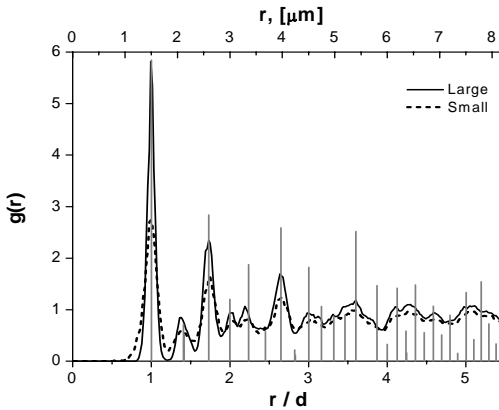


**Figure 4.7.**

The three dimensional radial distribution functions of the large and small spheres in the binary crystal. The vertical lines correspond to the calculated peak positions for a perfect fcc lattice.

close to 0.8 which indicates that only about 20% of the available holes in the crystal of the large spheres are not filled by the small particles.

In these layers both types of colloids were ordered in a hexagonal arrangement as can be seen from the image in Fig. 4.4a. The quality of this hexagonal order was determined by using the two-dimensional order parameter  $\Psi_6$ , see eq (8), which is plotted as a function of the height in the sample in Fig. 4.6. We can see that for the bottom 12 layers  $\Psi_6$  is above 0.9 for the large spheres and above 0.85 for the small particles, which indicates a very high hexagonal symmetry of the layers of both species. From the two dimensional radial distribution function (eq. (7)) calculated separately for both type of spheres an average in-plane nearest neighbors distance of  $1.51 \mu\text{m}$  was determined. Using this value the calculated distance between the close packed hexagonal layers of either large or small spheres is  $1.23 \mu\text{m}$ , which is slightly smaller than the measured one ( $1.28 \mu\text{m}$ ), probably due to the presence of planes of small particles between the layers of large ones.

The stacking of the hexagonal layers of both large and small particles in the vertical direction was determined by projecting images of successive layers and by making XZ-cuts through planes perpendicular to the hexagonal layers. As it can be seen from Fig. 4.4a the small spheres occupy the octahedral interstices between two layers of the large ones. Furthermore, Fig. 4.4b shows that the hexagonal planes of both species are stacked in ABC-fashion on top of each other, which means that both types of particles are arranged in separate face-centered cubic (fcc) lattices. This kind of order was confirmed by plotting the 3D radial distribution functions for the individual components and comparing them with the calculated peak positions for a perfect fcc lattice – Fig. 4.7. The mean distance in 3D between nearest neighbors of single species is found to be  $1.51 \mu\text{m}$ , as

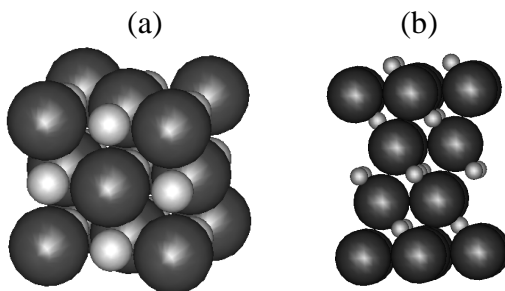


**Figure 4.8.**

A cubic (a) and a hexagonal (b) representation of the unit cell of a NaCl-type binary crystal.

judged from the position of the first peak in the 3D  $g(r)$  and is in accordance with the 2D measurements.

Thus, the structure of the binary crystals observed was determined to be of NaCl-type (Fig. 4.8), where the small spheres occupy all the octahedral interstices in the fcc lattice of the large ones, in this way generating a second, interpenetrating fcc lattice. The size of the cubic unit cell of this structure was found to be  $2.13 \mu\text{m}$ , which gives a packing fraction of both large and small particles in the crystal of 0.64 (the large spheres occupy 60% of the volume in the binary crystals which is in accordance with close packing of spheres of diameter  $1.51 \mu\text{m}$ ).

The presence of the small particles did not affect the lattice parameter of the large spheres in the close packed planes. If the two species can be considered as almost hard-spheres, this observation is expected as the size of the small particles is smaller than the maximum size that can fit in the octahedral holes of the lattice of the large spheres without disturbing their packing even at close packing.

#### 4.4.2. High-strength electric field

We also investigated the effect of an electric field with a higher strength ( $E_{\text{rms}} \approx 210 \text{ V/mm}$ ) on the binary mixtures of large and small silica particles. Immediately after the field was switched on, the large spheres formed strings which started to sediment. The small particles polarized to such an extent in the presence of such a high field that they formed small strings among themselves as well; these were most pronounced close to the wires. This observation is in agreement with the fact that at a field strength 6 times (or more) higher than the one needed for the large spheres to form strings (which is  $E_{\text{rms}} \approx 25 \text{ V/mm}$ ), the small particles should start to polarize and align in chains as well, according to eq (6). The induced dipoles of the two species interacted also with each other and formed binary strings and structures as is shown in Fig. 4.9. The structure of these strings was identified by taking time series and observing the motion of the particles in these movies. It was found that between every two almost touching large spheres in a string there were several (3 to 4) small particles rotating in the plane perpendicular to the string (Fig. 4.9b).

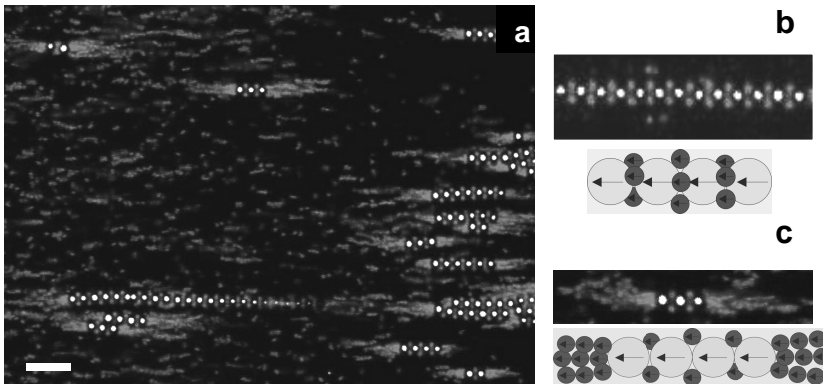


**Figure 4.9.**

(a) Binary strings of large and small particles forming in the presence of an electric field with a strength  $E_{\text{rms}} = 230 \text{ V/mm}$ . (b),(c) Close-ups of the small particles along (b) and at the ends (c) of the binary strings together with schematic representations. Scale bar is  $6 \mu\text{m}$ .

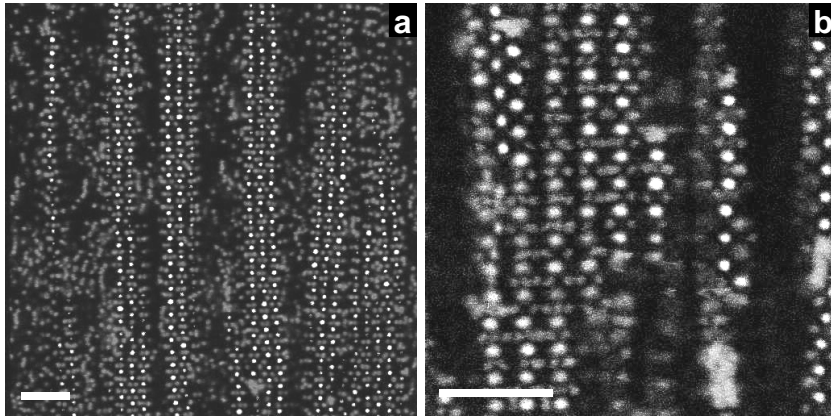


**Figure 4.10.**

*Two-dimensional structures formed by the binary strings with a hexagonal (a) and a rectangular (b) arrangements of the large spheres. Scale bars 6  $\mu\text{m}$ .*

Furthermore, at the ends of the strings there were clusters of chains of only the small particles aligned along the electric field (Fig. 4.9c). This tendency of the small spheres to stay either in between the large spheres or at the ends of their strings can be understood by recalling that the dipole-dipole energy favors the alignment of the colloids along the field. As this favorable configuration, chains along the field, is already adapted by the large particles first, the smaller spheres minimize their dipole-dipole energy by staying either between two large spheres, or at the ends of the strings of the large spheres forming small strings by themselves. Similar chain configurations were suggested by Wang and Holm<sup>150</sup> who performed computer simulations on mixtures of large and small magnetic particles with a permanent dipole moment.

When the binary strings meet each other, they arrange in two-dimensional sheets in such a way that the large spheres form either a hexagonal (Fig. 4.10a) or a rectangular (Fig. 4.10b) pattern. Because of the larger mobility of the small spheres, it is not exactly known what their average positions in these structures are.

After keeping the samples for several days in a high-strength electric field of  $E_{\text{rms}} \approx 230 \text{ V/mm}$ , binary crystal structures were observed as those shown in Fig. 4.11. By looking carefully at the particle positions we found that the structure was most likely that of a NaCl-crystal – both types of particles were ordered in interpenetrating fcc lattices, although they were slightly compressed in the vertical direction (the measured size of the cubic unit cell in the vertical direction was with about 5 % smaller than the one in the xy-plane). Different planes of the NaCl-type crystal were identified, among which the most often occurring parallel to the bottom wall were the (100) and (110) planes (Fig. 4.11a and 11b, respectively). The areas of single binary crystals were rather small and had much more defects, compared to the crystals obtained with a lower electric field strength. The lattice parameter of the cubic unit cell of these binary crystals was  $\approx 2.1 \mu\text{m}$ , similar to what was found for the low-field binary NaCl-type crystals.

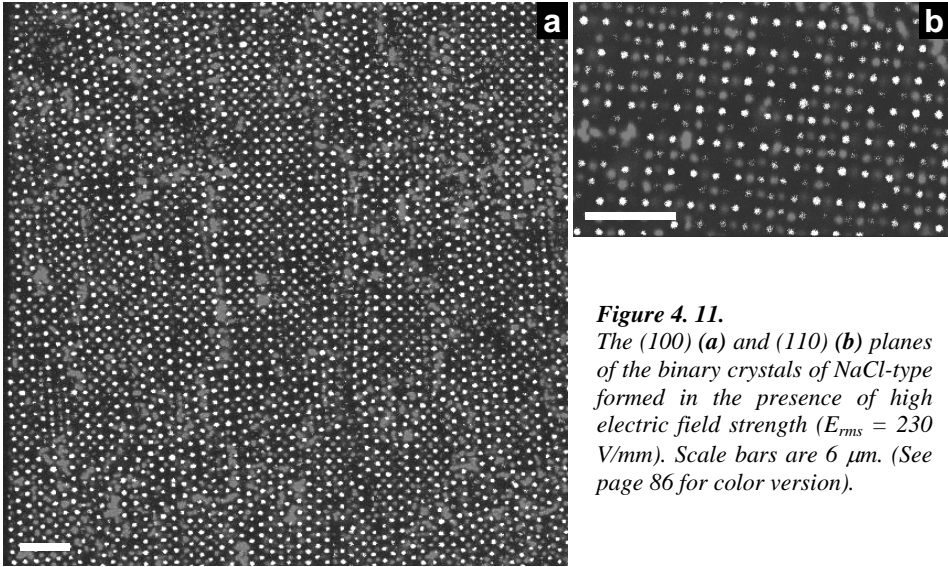


**Figure 4.11.**  
 The (100) (a) and (110) (b) planes of the binary crystals of NaCl-type formed in the presence of high electric field strength ( $E_{rms} = 230$  V/mm). Scale bars are  $6 \mu\text{m}$ . (See page 86 for color version).

#### 4.5. DISCUSSION AND CONCLUSIONS

We observed binary NaCl-type crystals from silica particles with a size ratio of 0.3 by applying an external electric field perpendicular to the direction of gravity with low and high strength resulting in dipolar interactions that were either small or large compared to  $k_B T$ . The size, quality and orientation of the crystal areas were found to be different in the two cases. At low electric field strength, the domains exhibited (111) planes parallel to the bottom of the sample, the single-domain sizes were much larger and had less defects than in the case of high strength, where mostly the (100) and (110) planes were found parallel to the bottom and the size and quality of the crystals was much worse. We speculate that these differences in the binary crystals are due to different mechanisms involved in their formation. At low electric field strength, only the large particles polarize and form strings, while the small ones are not affected by the field. The strings of large spheres form sheets and sediment to the bottom. By turning the sample several times up-side-down while continuously decreasing the field strength, we assure that enough small particles will be ‘trapped’ between the sedimented sheets of large colloids and will occupy the holes formed by the transformation from a bct to an fcc crystal of the large particles, thus giving a NaCl-type structure. We should remark that although our conditions (volume fraction and size ratio) are such that for hard spheres NaCl-type crystals are predicted to be stable<sup>39</sup>, we do not know if this is still the case when there are dipolar interactions of a few  $k_B T$  between the larger spheres. These interactions are not strong enough to drive a crystal of only the large spheres to a bct structure, but will certainly change the free energy of the binary NaCl-type crystal. However, for applications it is not important if the structures formed have the lowest free energy, as long as the crystals are large and have low amounts of defects.

In the case of high-strength electric field, both species polarize and interact significantly compared to  $k_B T$  with the field and with each other. Therefore, the structures they form are a result of dipole-dipole interactions not only between the large spheres but also between the small ones and between the large and the small. The preference for the (100) and (110) planes to be displayed parallel to the bottom in this case is likely due to this fact. It is very significant that in this parameter space, where separate bcc crystals of both the larger and the smaller spheres could have formed, the end result was a binary crystal. The way this binary crystal formed makes it likely that the binary crystal was either the minimum free energy structure or represents a deep metastable intermediate. Free energy calculations need to resolve this issue. However, it was only very recently, by researchers from our group<sup>151</sup>, that the free energy of the single species structure, bcc, was determined by computer simulations. If the structure we found is the equilibrium structure, this implies not only new ways to grow NaCl-type colloidal crystals, but also that electrorheological fluids can be made stronger by using binary mixtures of particles.

The advantages of using the low-field mechanism to make binary NaCl-type crystals are that it results in large areas of single domain crystals with a good quality and controlled orientation. The high-field method, on the other hand, offers a different approach which deserves more detailed study as it can lead to some other structures at different conditions. For example, a binary crystal with a bcc structure of the large ones is likely to be obtained by varying the experimental conditions. Such binary structures formed under the presence of relatively high electric field can have potential applications in the field of electrorheological fluids. As was shown by Jun et al.<sup>152</sup>, binary mixtures of polymer particles with a size ratio of 0.35 having an excess of the large species ( $\phi_S/\phi_{\text{total}}$  up to 0.25) exhibit shear yield stress and viscoelasticity higher than that of the individual components under the presence of an electric field. They concluded that this effect is due to 'a close packing and a peculiar structural ordering at an optimum size ratio and mixing fraction'. A possible binary structure consisting of a bcc lattice of the large ones and the small filling the holes between them was suggested, although no observations were done to confirm this hypothesis. We speculate that possibly a NaCl-type structure was formed in their system similar to the one observed by us at similar size ratio and a relatively high electric field strength. For the bcc lattice of the large spheres proposed by the authors, the smaller particles should have a smaller size to fit in the available holes ( $\gamma$  should be  $\leq 0.32$ ).

Binary crystals with LS stoichiometry have been reported recently in several other papers. Such crystals have been grown with PMMA particles<sup>31, 34, 86</sup> (see also Chapter 5), nanocrystals<sup>45</sup>, mixtures of poly(4-vinylpyridine) and polystyrene spheres<sup>40</sup>, poly(styrene-methyl methacrylate)<sup>57</sup> and with silica particles<sup>113, 153</sup> (see Chapter 3) but only the methods described in Chapter 5 and Ref. [86, 31] present fast and well controlled ways to grow NaCl-type binary crystals. Therefore, the procedure that we propose in this chapter for making large domains with a good quality of NaCl-crystal of silica particles is important as such crystals can have many applications. The possibility to make the crystal structures more permanent by drying followed by sintering will give the opportunity to further infiltrate the crystals with silicon<sup>80</sup> and to obtain inverse NaCl-type silicon crystals. Finally, we mention again that our results have not yet been optimized. Based on our preliminary results, it can already be concluded that the general notion that it is very difficult to grow binary colloidal crystals by self-organization needs updating.

*ACKNOWLEDGEMENTS*

We thank Michiel Hermes for the experimental work and the characterization of the crystals formed at low-strength electric field, Jacob Hoogenboom and Christina Graf for particle synthesis, Job Thijssen for assistance with the electric field set-up, critical reading of the manuscript and useful discussions, Mirjam Leunissen and Hans Wisman for help with the experimental setup.

# 5

## Ionic colloidal crystals of oppositely charged particles

Spherically symmetric, long-range attractive interactions were found till now to lead only to non-equilibrium phases - aggregates. In this chapter, we show with confocal microscopy that oppositely charged colloids actually can readily form large crystals even with particles of different materials. In contrast with atomic systems, the stoichiometry of these colloidal analogues of the ionic crystals is not dictated by charge neutrality, which creates a remarkable diversity of crystal structures. Among the experimentally observed ones, such as CsCl-,  $LS_6$ -,  $LS_8$ -, NaCl- and NiAs-type, are several that were not seen before. An external electric field can melt the crystals and drives the system to a first order out-of-equilibrium phase transition. Control over opposite-charge interactions allows for a new range of condensed matter problems, such as those involving ionic crystals, to be studied with colloids and it greatly facilitates the fabrication of binary crystals of large particles for advanced materials, like photonic crystals.

### 5.1. INTRODUCTION

Suspensions of nano- to micrometer sized particles ('colloids') are important condensed matter model systems because, due to their well-defined thermodynamic temperature, they display the same phase behavior as atoms or molecules, but are easier to investigate quantitatively in three dimensions. This means that problems regarding melting, freezing<sup>8, 13, 66, 76, 154</sup> and the glass transition<sup>71, 155</sup> can be investigated quantitatively with microscopy. Improved chemical synthesis continues to expand the variety of feasible colloidal interactions. Interactions for which equilibrium colloidal phases have been observed for dispersions of one type colloid include long-range repulsive<sup>8, 76</sup>, short-range attractive<sup>154, 155</sup>, hard-sphere like<sup>13, 66, 71</sup>, dipolar<sup>76, 144</sup> and combinations of these. For binary systems, consisting of particles with different sizes or properties, less work is reported and almost exclusively for long-range repulsive<sup>6, 41</sup> and hard-sphere like systems<sup>30, 33, 34</sup> only. However, several researchers recently observed binary crystals of nanometer-sized colloids that probably formed in the presence of attractions<sup>45, 48</sup>. It is extremely difficult to grow binary crystals of particles in the micrometer range due to slow growth, large sedimentation rates and differences therein. Here we show that by creating conditions under which oppositely charged colloids form equilibrium phases these problems are overcome. Such crystals have potential photonic applications, as bandgaps in the important region of near-infrared require a dense, regular packing of micrometer-sized spheres<sup>142</sup>. Large particles also facilitate the quantitative real-space analysis of binary structures<sup>30, 34</sup>.

We recently developed a versatile model system using sterically stabilized polymethylmethacrylate (PMMA) spheres dispersed in a nearly density and index matching mixture of the apolar solvents cyclohexyl bromide (CHB) and cis-decalin<sup>70, 76</sup>. The matched refractive indices of the particles and the solvent reduce the Van der Waals forces to negligible strength<sup>156</sup>. With this suspension it is possible to achieve both, the hard-sphere-like limit and extremely long-ranged repulsive interactions that exceed the size of the particle, even for spheres of several micrometers. The range of the interactions can be tuned by adding the salt tetrabutylammonium bromide (TBAB) and is characterized by the Debye screening length,  $\kappa^{-1}$ , which for monovalent cations and anions with a number density  $2c_s$  reads:

$$\kappa^{-1} = \left(8\pi\lambda_B c_s\right)^{-\frac{1}{2}}. \quad (1)$$

Here, the Bjerrum length,  $\lambda_B$ , is defined as:

$$\lambda_B = \frac{e^2}{4\pi\epsilon\epsilon_0 k_B T} \quad (2)$$

with  $\epsilon$  the relative dielectric constant of the solvent mixture,  $\epsilon_0$  the dielectric permittivity of vacuum,  $e$  the elementary charge,  $k_B$  Boltzmann's constant and  $T$  the absolute temperature. For water  $\kappa^{-1}$  is limited to about 300 nm, but in our much less polar solvent mixture it can exceed 10  $\mu\text{m}$  because the ionic strength is orders of magnitude lower.

Nevertheless, from the experimental 3D radial distribution function, we found that the interactions in these suspensions are well-described by a pair-wise screened Coulomb potential  $V_{ij}(r)$ <sup>70</sup>:

$$\frac{V_{ij}(r)}{k_B T} = Z_i Z_j \lambda_B \frac{e^{\kappa(a_i + a_j)}}{(1 + \kappa a_i)(1 + \kappa a_j)} \frac{e^{-\kappa r}}{r}, \quad (3)$$

where  $r$  is the distance between two particles,  $a_i/a_j$  are the particle radii and  $Z_i/a_j$  their charges.

We considered binary suspensions that consist of two types of colloids with opposite, dissimilar charges  $Z_1$  and  $Z_2$  and different radii  $a_1$  and  $a_2$ . For such systems of oppositely charged colloids it was until now generally believed that they only form out-of-equilibrium structures – aggregates (Fig. 5.1). This is because contact energies resulting from Coulombic interactions easily exceed ten times the thermal energy at room temperature, even for micrometer-sized particles carrying just a few hundreds of elementary charges. Manifold particle contacts then quickly bring the system out of equilibrium, by a process known as ‘hetero-aggregation’<sup>156, 157</sup>. However, we found a way to keep the charges sufficiently low to prevent this scenario and get equilibrium behaviour instead.

We discovered that in our less polar suspensions of PMMA-particles the addition of TBAB salt not only regulates the screening length but also offers control over the particle charge which even reverses from positive to negative at moderate salt concentrations<sup>70</sup>. Given the many components involved in the synthesis of the colloids<sup>87</sup>, it is hardly surprising that we obtain a slightly different charge reversal point for each batch of particles. Exploiting this, we prepared salt-containing mixtures of differently labeled fluorescent spheres; thereby establishing binary systems of colloids that carry

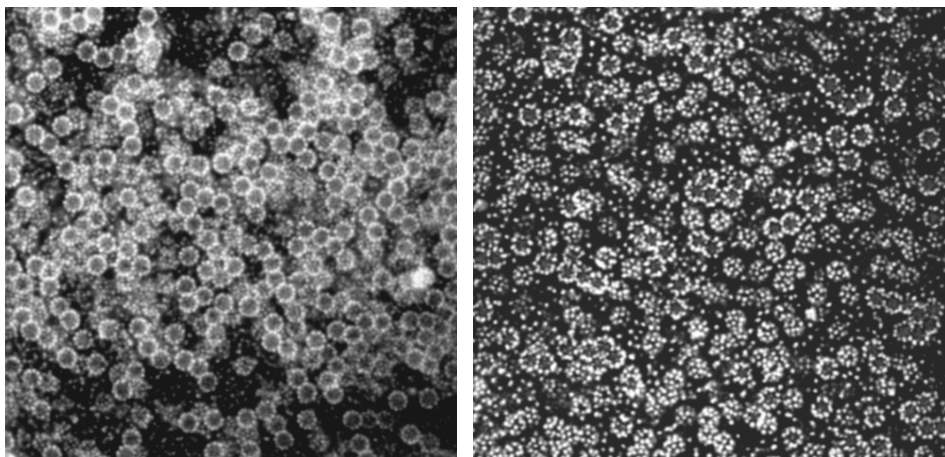


**Figure 5.1.** Aggregates of oppositely charged PMMA spheres (size ratio 0.31) in CHB-decaline solvent mixture.

small, opposite charges and that are distinguishable by confocal microscopy. In this chapter we present our experimental observations on systems that either consisted of equal-sized spheres or of spheres with a considerable size difference and we compare some of the observed phases and crystal structures with Madelung energy calculations and computer simulations.

## 5.2. EXPERIMENTAL PART

### *Particle synthesis*

We used polymethylmethacrylate (PMMA) and silica particles. The PMMA particles were made by dispersion polymerisation, covalently labelled with the fluorophore 7-nitrobenzo-2-oxa-1,3-diazol (NBD) or rhodamine isothiocyanate (RITC) and sterically stabilised with poly-12-hydroxystearic acid (PHSA)<sup>87</sup>. The NBD-PMMA spheres had radii of 0.99, 0.36 and 0.58  $\mu\text{m}$  and the RITC-PMMA - 1.08 and 1.16  $\mu\text{m}$ , the size polydispersity was 3-5%. The silica particles were prepared using a modified Stöber-synthesis<sup>63, 146</sup> and a continuous-feed seeded-growth method<sup>115</sup>, resulting in an RITC-labelled core of 200 nm radius and a 300 nm thick unlabeled shell. They were coated with 3-Methacryloxypropyltrimethoxysilane (TPM)<sup>158</sup>, stabilized with PHSA and redispersed in cis-decalin. The total radius was 0.52 micrometers with 4% polydispersity. The sizes and the polydispersity of the particles were measured by static light scattering and electron microscopy.

Unless indicated otherwise, the colloids were dispersed in a mixture of cyclohexyl bromide (CHB) (Fluka) and 27.2 wt% cis-decalin (Sigma-Aldrich) that nearly matches the density and the refractive index of PMMA. We purified the CHB as described before<sup>70</sup>, but skipped the distillation step. The particle charge and the range of the electrostatic interactions were tuned by adding the salt tetrabutylammonium bromide (TBAB, Sigma-Aldrich)<sup>70</sup>.

### *Confocal microscopy*

Separate dispersions of the individual particle species were left to equilibrate for several hours before being mixed together. The dispersions then were confined to glass capillaries (VitroCom) and studied by means of confocal laser scanning microscopy<sup>65, 70</sup>. The positive and negative particles could be imaged simultaneously on separate channels, due to their different fluorescent labels. Afterwards, we extracted the 3D particle coordinates with an adapted version of Crocker and Grier's particle tracking method<sup>70, 159</sup>. Gradient samples served to explore the phase behaviour as a function of the salt concentration. We made these by filling a capillary partly with a salt-free suspension and partly with a TBAB-solution and allowing it to form macroscopic gradients in a few days' time (at a constant particle volume fraction).

### *Electrical conductivity measurements*

We estimated the Debye screening length of our dispersions by measuring the conductivity of the particle-free solvent mixtures with a Scientifica 627 conductivity meter and then applying Walden's rule<sup>70</sup>. We used literature values for the limiting equivalent

conductance of TBAB in water and a viscosity of 2.217 centipoise at 25 °C (measured with a Schott ViscoSystem) for the solvent mixture.

#### *Electrophoretic mobility measurements*

Particle charges were quantified by means of electrophoresis (using a Coulter Delsa 440SX) on dilute suspensions (volume fraction 0.0015) in the CHB-decalin mixture<sup>70</sup>. The run parameters were: 25 Volts, 2.0/0.5 seconds on/off-time and a total run time of 60 seconds. We identified the stationary layers by Komagata linearization<sup>160</sup> and related the electrophoretic mobility to the zeta potential via the O'Brien & White scheme<sup>161</sup>. From dielectric spectroscopy (with an HP 4294A impedance analyser) the dielectric constant of the solvent mixture was found to be 5.59.

We also estimated the charges in the denser microscopy samples. The sample cell consisted of a 0.1 x 1 mm capillary with two 50  $\mu\text{m}$  diameter nickel-alloy wires (Goodfellow) threaded through along the sidewalls. We applied a dc-field (up to 25 V/mm) and captured the electrophoretic motion of individual particles shortly after they left the binary crystals (scan speed 1-3 frames/second). We determined the particles' mobility from their displacements between subsequent frames.

#### *Light scattering*

We determined the lattice parameter of the CsCl-type PMMA crystals by laser light powder diffraction. A crystalline sample inside a 0.1 x 2 mm capillary was illuminated with a 543.5 nm HeNe laser (Melles Griot) and the diffraction rings were recorded as digital pictures of a white screen behind the sample. We extracted the particle size from static light scattering measurements on dilute suspensions of the individual particle species in hexane and the CHB-decalin mixture. The refractive index of this mixture was measured with an Abbe refractometer and was 1.48928 at 22.2 °C.

### 5.3. RESULTS

#### 5.3.1. Equal-sized spheres

For a relatively broad and easily accessible range of parameters, mixtures of positively charged PMMA particles with a radius  $a_1 = 1.08 \mu\text{m}$  and charge  $Z_1 \sim +110e$  and negatively charged PMMA spheres having a radius  $a_2 = 0.99 \mu\text{m}$  and charge  $Z_2 \sim -75e$  were found to exhibit complete freezing into large, cesium chloride-type (CsCl) single crystals, that consist of several tens of particle layers measuring up to 300 x 300  $\mu\text{m}$  (Fig. 5.2). Typical suspensions with a 1:1 particle number ratio had an overall volume fraction  $\varphi \sim 0.12$  and contained  $\sim 60 \mu\text{M}$  TBAB, corresponding to  $\kappa^l = 285 \text{ nm}$ . As expected, for significantly higher charges only irreversible aggregation occurred.

The CsCl character of the lattice, i.e. two interlaced simple cubic lattices for each particle species forming together a body-centered cubic superlattice, was confirmed by quantitative real-space confocal microscopy and by measuring the Bragg angles with light scattering. We found 2.36  $\mu\text{m}$  for the lattice parameter, which translates into a packing

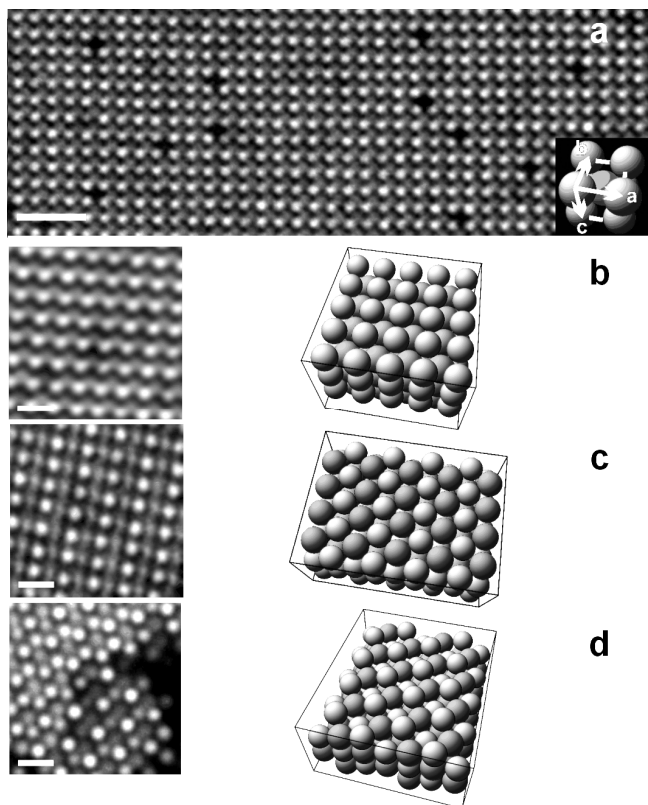


**Figure 5.2.** CsCl-type binary colloidal crystals of positively (red, radius  $1.08 \mu\text{m}$ ) and negatively (green, radius  $0.99 \mu\text{m}$ ) charged PMMA-spheres. (a), Confocal micrograph; inset: the cubic CsCl-type unit cell. (b), (c), (d), Close ups of the (100), (110) and (111) planes and the corresponding models. All particles were dispersed in TBAB-containing CHB-decalin. Scale bars are (a)  $10 \mu\text{m}$ , (b)-(d)  $4 \mu\text{m}$ . (See page 86 for color version).

fraction of 0.71. Within the experimental error this is the closest CsCl-type packing possible for spheres with this size ratio (0.92).

The first crystallites were observed within  $\sim 35$  hours after sample preparation and had a random orientation indicating homogeneous nucleation. It is remarkable that without fine-tuning the conditions the nucleation time we found for our binary mixtures

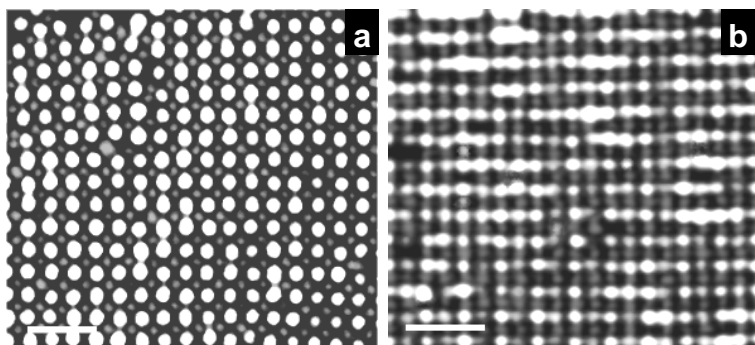


**Figure 5.3.** Confocal images of the (100) (a) and (110) (b) planes of a CsCl-type crystal of positively charged PMMA (green, radius  $0.52 \mu\text{m}$ ) and negatively charged silica (red, radius  $0.58 \mu\text{m}$ ) particles in CHB-decalin mixture with added TBAB. Scale bars are  $4 \mu\text{m}$ . (See page 86 for color version).

of large (2  $\mu\text{m}$ ) spheres was significantly shorter than, for instance, the four days reported for certain optimised hard-sphere systems of much smaller particles<sup>30, 34</sup>.

#### *Particles of different materials*

To explore further the use of oppositely charged colloids for applications, we also investigated the possibility to grow ‘ionic’ crystals from particles of different materials. We used positively charged PMMA ( $a_1 = 0.58 \mu\text{m}$ ) and negatively charged silica ( $a_2 = 0.52 \mu\text{m}$ ) particles in a 53/47 volume ratio mixture of CHB and decalin. The total particle volume fraction was  $\varphi \sim 0.13\text{-}0.20$  and the concentration of TBAB was approximately 160  $\mu\text{M}$ . Despite the very different densities ( $\sim 1.2 \text{ g/cm}^3$  for PMMA versus  $2.0 \text{ g/cm}^3$  for silica), resulting in large difference in sedimentation rates, a mixture of these oppositely charged spheres was found quickly to form binary CsCl-type crystals as well (Fig. 5.3). Here again the reason for the fast crystallization is related to the fact that the electrostatic attraction causes the positive and negative particles to stay together contrary to the behavior in the case of repulsive interactions. The composite crystals shown in Fig. 5.3 are important for several reasons. First, they demonstrate that ‘ionic’ crystals can be grown from oppositely charged silica spheres as well and such crystals of silica particles only are important for the production of inverse photonic crystals requiring a high temperature reaction to produce the ‘inverse’ index contrast<sup>142</sup>. Second, earlier work by us has shown that the latex can be burned away leaving the silica particles behind<sup>113</sup> (see also Chapter 3). This procedure would turn the CsCl-type crystal into a simple cubic structure of touching spheres. Until now, such simple cubic lattices have not yet been realized by self-organization of colloids. Alternatively, one could make a similar simple cubic PMMA-lattice by selectively etching away the silica component with hydrofluoric acid. Moreover, if a disordered face-centered-cubic (fcc) crystal could be realized with a mixture of two materials, this would be in fact a fcc lattice homogeneously doped with another dielectric material.

#### *External electric field*

We confirmed that the particles inside the binary crystals were still oppositely charged by applying an external, static electric field (on the order of several V/mm). The CsCl-type crystal melts as the differently labelled particles move towards opposite electrodes. This also demonstrates that electric fields are a powerful way to manipulate these soft colloidal

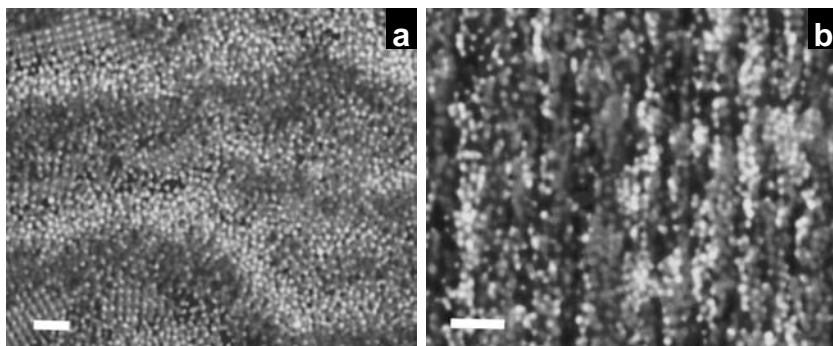


**Figure 5.4.** (a) Electric field induced jammed ‘band’ formation in a dense sample. (b), Dynamic lane formation at lower density and 80 V/mm. Scale bars are 10  $\mu\text{m}$ . (See page 86 for color version).

crystals. For atomic CsCl crystals one would need unrealistically high electric fields to achieve this kind of melting, but here no more than  $\sim 7,100$  V/m was sufficient. It is likely that the field can anneal out defects, e.g. when applied in oscillatory fashion. Furthermore, it is noteworthy that this system is very similar to a certain electronic ink ('e-ink')<sup>162</sup>, although the latter aggregates.

In some cases the electric field induced interesting novel pattern formation. Dense suspensions ( $\varphi > 0.40$ ) in fairly high fields ( $\sim 20$  V/mm) form 'bands' perpendicular to the field direction (Fig. 5.4a). The different particles initially move in opposite directions, but soon form a glassy state, which does not show any diffusion or field induced drift anymore. This process is reversible: the system 'unjams' when the field is switched off. In relatively dilute suspensions ( $\varphi \sim 0.20$ - $0.30$ ) the colloids remain mobile and another pattern appears, with the oppositely driven particles segregated into 'lanes' along the field direction (Fig. 5.4b). This so-called 'lane formation' is a first-order out-of-equilibrium phase transition<sup>163, 164</sup>. It can now be studied in a controlled way and quantitatively at the single particle level.

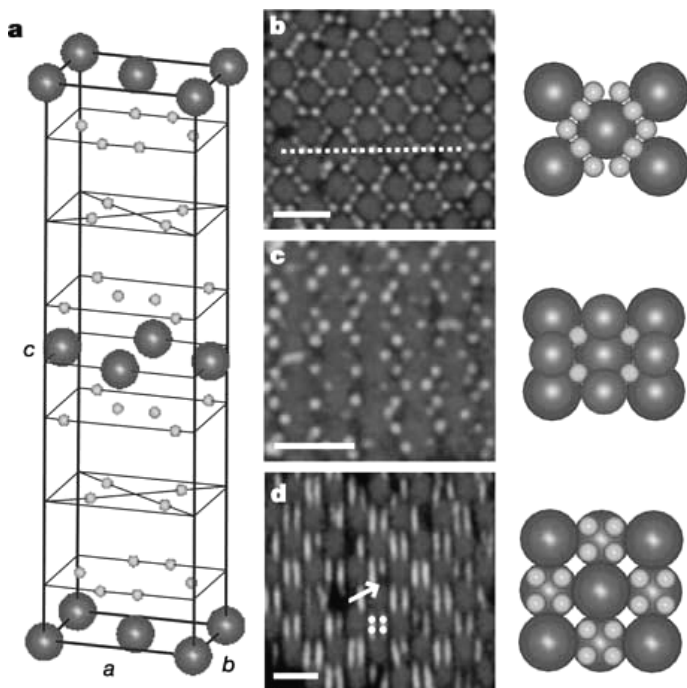


**Figure 5.5.**

*LS<sub>6</sub>-type binary crystals formed with positively (green, radius  $0.36 \mu\text{m}$ ) and negatively (red,  $1.16 \mu\text{m}$ ) charged PMMA-particles in TBAB-containing CHB-decalin solvent mixture. (a), Unit cell with observed lattice spacings  $a = 4.00$ ,  $b = 2.84$  and  $c = 4.7 \mu\text{m}$  (not to scale for clarity). (b)-(c), Confocal images and models of different  $ab$ -projections, showing (b) a layer of large and several layers of small particles and (c) a plane with only small particles. (d),  $ac$ -cut along the line in (b). As the microscope could not completely resolve the four small particles in each octahedral hole, we indicated their positions with dots. The arrow indicates a missing particle. All scale bars are  $4 \mu\text{m}$ . (See page 87 for color version).*

### 5.3.2. Spheres with a size ratio of 0.31

We expanded the parameter space for binary crystallization a bit further by studying mixtures of large ( $L$ ) and small ( $S$ ) spheres with a considerable size difference ( $a_2/a_1 = 0.31$ ). Using a suspension of negatively charged large particles ( $a_1 = 1.16 \mu\text{m}$ ) and positively charged small spheres ( $a_2 = 0.36 \mu\text{m}$ ) with a number ratio  $N_L:N_S = 1:8$ , total particles volume fraction  $\varphi \sim 0.11$  and estimated TBAB-concentration  $\sim 120 \mu\text{M}$ , we observed beautiful and complex binary crystals of  $LS_6$  stoichiometry (Fig. 5.5). In this new structure the large particles are arranged in a face-centred orthorhombic lattice. One small sphere occupies each of the tetrahedral holes, whilst four small spheres are found in each of the octahedral holes (two slightly above and two slightly below each  $ab$ -plane of large particles in Fig. 5.5a and d). The remaining small spheres are expelled from the crystal. This colloidal structure resembles the crystals with a stoichiometry  $LS_6$  formed by the fullerene molecule  $C_{60}$  and certain alkali metal ions<sup>165</sup>. In these compounds the constituent ions have a large size difference as well.

At slightly lower ionic strength we found other new structures, with a stoichiometry  $LS_8$ , for which no atomic or molecular analogues have been identified yet. Detailed description of these structures together with computer simulations results are presented in Chapter 6.

#### *Charged and uncharged particles*

Experimentally, it also proved possible to establish conditions at which the small spheres hardly carried any charge, while the large spheres were still slightly charged, as judged by the lattice spacing in crystals of the individual particle species and their electrophoretic mobility. In a binary mixture with particle volume fraction  $\varphi \sim 0.23$ , number ratio  $N_L:N_S = 1:4$  and no added salt ( $\kappa' = 1.57 \mu\text{m}$ ) we found binary crystals with  $LS$  stoichiometry and two different crystal structures - sodium chloride type (NaCl) and nickel arsenide type (NiAs) (Fig. 5.6). We believe that this is the first time that crystals of charged and uncharged spheres are observed. In the NaCl-type structure the large spheres are arranged in a face centered cubic (fcc) lattice and the small spheres fill all the octahedral interstitial sites, generating a second, interpenetrating fcc lattice. In the NiAs-type crystal the large particles form a hexagonal close packed (hcp) structure and the small spheres occupy again all the octahedral interstices but now they form a simple hexagonal sublattice.

An  $LS$  structure was formed by controlled-drying layer-by-layer method<sup>113</sup> and reported in Chapter 3. There, the stacking of the layers of large and small particles was found to be ambiguous. Colloidal  $LS$  crystals were observed for hard-sphere mixtures as well but the exact type of the crystal structure was not known<sup>34</sup>. Recently, a NaCl-type crystal made of two kinds of nano-crystals was reported, with attractions likely present between the particles<sup>45</sup>.

Electrostatic attraction between oppositely charged silica particles with modified surfaces and a size ratio of 0.5 was used by Masuda et al.<sup>153</sup> to induce the self assembly of the particles upon solvent evaporation into small 2D areas with local arrangements resembling the (100) plane of a NaCl-type crystal but it was not clear if this ordering was due to the electrostatic attraction between the particles or to the capillary forces upon

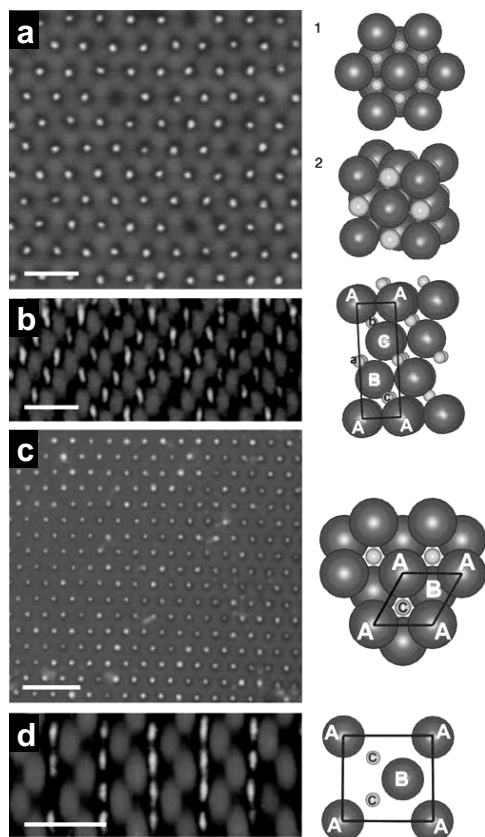


**Figure 5.6.**

*LS-type binary crystals form charged (red, radius  $1.16 \mu\text{m}$ ) and uncharged (green, radius  $0.36 \mu\text{m}$ ) PMMA-particles in CHB-decalin. (a) and (b) NaCl-type crystal. (a), Confocal image of the hexagonal plane and the unit cell in an hexagonal (1) and a cubic (2) representation (small spheres enlarged for clarity). (b), Confocal image and a model of a plane perpendicular to the hexagonal close packed layers, showing the ABC-stacking of both the large and small particles. (c) and (d) NiAs-type crystal. (c), Superposition of confocal images of 10 layers and the corresponding model. (d), Confocal image and a model of a plane perpendicular to the hexagonal close packed layers, showing the ABA-stacking of the large and the ccc-stacking of the small particles (spheres not to scale). All scale bars are  $8 \mu\text{m}$ . (See page 87 for color version).*

drying, as such local NaCl-type order of the two species was obtained by the authors with mixtures of same-charge particles as well.

Binary colloidal crystals (NaCl-type for a size ratio of 0.43 and MgCu<sub>2</sub>-type for a size ratio of 0.73) formed during solvent evaporation from mixtures of particles with different composition and surface properties were reported by Ma et al.<sup>40</sup>. They considered the presence of a weak attraction between the two dissimilar species as an important factor for the formation of the binary crystals upon drying. The authors were not definitive what type of attraction existed between the particles but we think that the formation of the binary crystals observed was likely caused by an electrostatic attraction between the protonated pyridine rings on the surface of one of the species and the OH<sup>-</sup> groups on the surface of the other species.

### 5.3.3. Madelung energy calculations and computer simulations

We explored theoretically the stability of different crystal structures for the size ratios studied experimentally ( $\sim 1$  and 0.31), as a function of the charge ratio  $Q = -Z_1/Z_2$  and the reduced screening constant  $\kappa a_1$ . In this chapter we will present the results for the systems of particles with almost equal sizes, while in the next chapter (Chapter 6) the theoretical

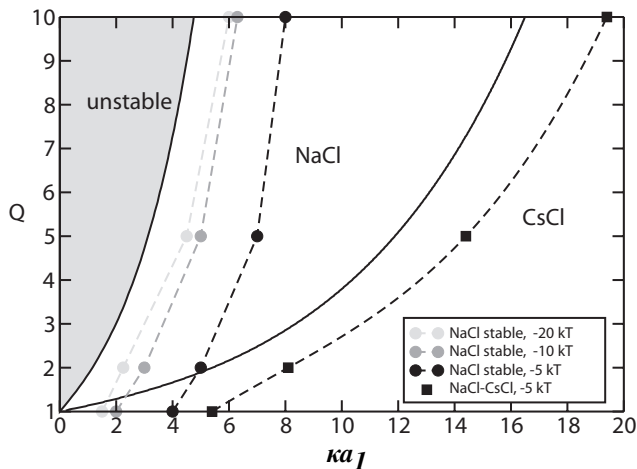


**Figure 5.7.**

Theoretical phase diagrams based on screened-Coulomb pair-interactions for different screening constants,  $\kappa a_1$ , and charge ratio  $Q = -Z_1/Z_2$  at a size ratio  $a_2/a_1$  of 1. Solid black lines indicate crystal-crystal transitions from Madelung energy calculations at zero-temperature. In the grey area the NaCl structure is unstable. The circles and squares present the results of finite-temperature, zero-pressure MC-simulations at contact energies given in the legend. The dashed lines are guide to the eye.

and computer simulation results for the particles with a size ratio of 0.31 will be shown. For long screening lengths (Eq. 1) our oppositely charged particles resemble ionic systems, but with differences. Most importantly, colloids *with* their surrounding ‘diffuse layer’ of counterions are charge-neutral objects. Therefore, the stoichiometry is not dictated by charge neutrality: even with a considerable charge asymmetry colloids can form crystals with  $LS$  (or some other) stoichiometry, as in Fig. 5.2 and 5.3. The equilibrium structure of a crystal is determined by geometric requirements, stemming from short-ranged repulsions, together with the potential energy of the lattice and the entropy associated with thermal vibrations (phonons). For ionic systems, the potential energy strongly depends on the Coulomb interactions. The difference between interacting pairs of either like or unlike charged particles is of special importance. For instance, even at a size ratio close to optimal packing *hard* spheres form only small, *metastable* CsCl-type crystallites in experiments<sup>30</sup>, whereas simulations and theory are still ambiguous about their stability<sup>27, 38, 39, 166</sup>. We used the pair-potential of Eq. 2 for the colloidal interactions. This probably is a good approximation for the like charge repulsions<sup>70</sup>, whereas its accuracy for the plus-minus attractions is not well known. We further assume a vanishingly small osmotic pressure, such that the crystals are self-supported by their cohesive energy and coexist with a zero-density colloidal vapour. Under these assumptions we estimated the stability of the crystal structures and the melting lines by performing so-called ‘constant-NPT’ Monte Carlo simulations, thus keeping the number of particles  $N$ , the pressure  $P$  and the temperature  $T$  fixed.

The phase diagram in Fig. 5.7 display structures with minimal Madelung energy (potential energy per particle in the perfect crystal; we assume touching neighbours), in which we neglect entropy. In this zero-temperature limit the phase diagram depends on

the change ratio and not on the absolute contact energies  $V_{ij}$  (Eq. 2 evaluated at  $r = a_i + a_j$ ). The absolute charges only become relevant in the Monte Carlo simulations that we performed in order to assess the importance of entropy at ambient temperature. We calculated the free energies from ‘constant-NVT’ Monte Carlo simulations (fixing the number of particles  $N$ , the volume  $V$  and the temperature  $T$ ) using the Frenkel-Ladd method<sup>167</sup>. We did all the simulations in a cubic box with periodic boundary conditions, taking 216 and 250 particles for the NaCl- and CsCl-crystals respectively.

The experimentally determined charges (of the particles in Fig. 5.2) give a contact energy  $V_{12}$  of  $\sim -2 k_B T$  for the plus-minus interactions. However, one should bear in mind that the electric field gradient becomes very steep near contact. It is neither known whether the Poisson-Boltzmann approach underlying Eq. 2 is valid in this case, nor what is the correct boundary condition; i.e. constant surface charge versus potential or something in between. Therefore, we chose several contact energies and looked how this affected the stability lines.

Figure 5.7 shows that the NaCl- and CsCl-structures dominate for same-size colloids. If we include entropic effects, both the NaCl-CsCl phase boundary and the NaCl melting line shift to higher  $\kappa a_1$  (more screening). In our experiments, the clear particle motion around the lattice positions indicates that entropy indeed is important. The observed CsCl-type crystals (Fig. 5.2) lie inside the predicted CsCl-regime. Their Madelung energy was calculated to be  $\sim -6 k_B T$  (per particle).

#### 5.4 DISCUSSION AND CONCLUSIONS

We showed in this chapter that suspensions of micrometer-sized, oppositely charged particles do not necessarily aggregate, but can form equilibrium phases instead, if one keeps the charges sufficiently low. This makes it for the first time possible to grow structures that resemble ionic crystals. As these suspensions have a well-defined thermodynamic temperature, they are different from *granular* systems of oppositely charged particles, as in the work reported recently<sup>168</sup>. Experimentally, we identified several binary crystal structures, e.g. CsCl-,  $LS_{\sigma}$ -,  $LS_g$ -, NaCl- and NiAs-type. Some of these ( $LS_{\sigma}$ -,  $LS_g$ - and NiAs-crystals) have not been observed before for colloidal systems, but are indeed stable according to our calculations of Madelung energies and computer simulations.

Our present experiments<sup>86, 169</sup>, but also those of others<sup>31</sup>, demonstrate that equilibrium phase behaviour of oppositely charged colloids occurs for a fairly broad and easily accessible range of parameters. Bartlett and Campbell saw evidence of crystallising oppositely charged spheres under different conditions than those used here<sup>31</sup>. We also suspect that Underwood *et al.*<sup>29</sup> may have ruled out the presence of opposite charges too quickly as the origin of the attractions that caused their CsCl-type crystals. All of these studies involved organic solvents, but we expect that ionic crystals can also be obtained in more polar solvents, such as water. Although it is more difficult to keep the van der Waals forces sufficiently small in water, this was recently achieved for a suspension with attractive interactions mediated through complementary strands of DNA on the

particles<sup>170</sup>. A mixture with different complementary sequences for different particles would actually mimic our system for short screening lengths.

We discovered that ionic colloidal crystals grow relatively fast compared to hard-sphere systems. This holds even for significantly bigger particles and larger differences in the sedimentation rates of the individual components than have been studied before. These features are important for the production of advanced materials, such as photonic crystals. Although suspensions with long-range repulsive interactions can also give fast binary crystallisation<sup>6, 41</sup>, these are less practical because they do not form dense packed structures. With respect to applications, it is also noteworthy that our large sphere system in the external electric field is very similar to a certain electronic ink ('e-ink')<sup>162</sup>, although the latter aggregates. It would be interesting to try and make a colour display by aligning ionic colloidal crystals with the electric field.

Our findings (see also Chapters 6 and 7) also open up a whole new range of condensed matter model studies, such as the freezing, melting and glass transition of ionic solids. In addition, the higher cohesive energy of the ionic structures offers the possibility to investigate certain material properties, like fracture, in a realistic way with colloids, for instance by applying optical tweezers<sup>171</sup>. Moreover, an external electric field introduces a controlled way to drive colloidal suspensions far from equilibrium and to study pattern formation like the laning transition at the single particle level.

#### ACKNOWLEDGMENTS

M.E. Leunissen is thanked for performing the experiments with equal-size PMMA spheres, A.P. Hynninen and M. Dijkstra for computer simulations, A.P. Hynninen and R. van Roij for calculating the Madelung energies, P. Royal for his work on the lane formation, A. Imhof for the Bragg scattering measurements, R.P.A. Dullens, D. Derks, N.A.M. Verhaegh, P. Vergeer and C.M. van Kats for particle synthesis, A.D. Hollingsworth for solvent characterization, and both P.N. Pusey and A.B. Schofield for pointing out the resemblance between our LS<sub>6</sub>-structure and certain fullerene compounds.



# 6

## Binary crystal structures in mixtures of oppositely charged colloids with a size ratio of 0.31

We present a study on the crystal structures in binary mixtures of large and small oppositely charged colloidal particles with a size ratio of 0.31 using confocal microscopy and Monte Carlo simulations. The stability of the experimentally observed binary crystal structures named  $LS_6^{bcc}$ ,  $LS_8^{fcc}$  and  $LS_8^{hcp}$  are confirmed by computer simulations which also predicted new stable binary structures. The constructed ground-state phase diagram shows a remarkably rich variety of binary structures in systems of oppositely charged colloids. Some of the structures have an atomic or molecular analogue while many of the most dominating structures in the phase diagrams do not.

## 6.1. INTRODUCTION

Colloids (nanometer to micrometer sized particles) are important model systems for atoms and molecules, as they exhibit similar phase behavior, but are easier to investigate and to manipulate. The possibility to tune colloidal interactions chemically or by an external field has led to a great variety of model systems<sup>8, 13, 71, 76, 155</sup>. Recently, we presented a new model system, consisting of oppositely charged colloids that form equilibrium crystals<sup>86</sup> (see Chapter 5). A major difference with atomic systems is that the stoichiometry of the ionic colloidal crystal structures is not dictated by charge neutrality as the charge balance is covered by the presence of counterions. This severs the link between charge ratio and stoichiometry, and enlarges the number of possible crystal structures. In our previous work<sup>86</sup> we reported the observation of several binary crystals with size ratio 0.31, some of which were not seen before. These observations triggered our interest to search for new structures using both experiments and computer simulations. Experimentally, we varied the parameters that influence the formation of binary crystals – number ratio between large and small particles, particles total volume fraction, salt concentration. Theoretically, we developed a novel interactive simulation method to predict a whole variety of binary crystal structures of oppositely charged colloids with different stoichiometries, which we used in Madelung energy calculations to map out the ground-state phase diagram. The joint theoretical and experimental approach helped to identify and locate the stability range of different binary crystal structures and to predict new ones.

## 6.2. EXPERIMENTAL RESULTS

Our experimental system consisted of spherical, monodisperse, sterically stabilized polymethylmethacrylate (PMMA) particles<sup>87</sup>, dispersed in an apolar solvent mixture. The negatively charged larger particles (*L*) had a radius  $a_L = 1.16 \mu\text{m}$  (polydispersity 3%), and the positively charged smaller particles (*S*) had a radius  $a_S = 0.36 \mu\text{m}$  (polydispersity 5%), thus the size ratio was  $a_S / a_L = 0.31$ . The two types of particles had two different fluorescent dyes incorporated in their volume. The large spheres were labeled with rhodamine isothiocyanate (RITC) and the small ones with 7-nitrobenzo-2-oxa-1,3-diazol (NBD), which made it possible to distinguish them using fluorescence microscopy. The colloids were dispersed in an almost density and refractive index matching mixture of cyclohexylbromide (CHB) – decalin (80/20 volume ratio) in which the Van der Waals interactions between the particles are strongly minimized. In this solvent mixture the particles acquire some small charge whose sign and magnitude was changed by adding the salt tetrabutylammoniumbromide (TBAB)<sup>70</sup>.

Stock salt-free dispersions of the two types of particles were prepared with different volume fractions ( $\varphi = 0.2 - 0.4$ ) and after allowing at least several hours for equilibration, mixtures of the two components were made with certain particle number ratio  $N_S / N_L$  and total volume fraction ( $\varphi = \varphi_S + \varphi_L$ ). In some cases salt-solution was added to these mixtures to adjust the interaction between the particles. The dispersions were loaded into glass capillaries in two manners: homogeneous samples were made by simply filling the capillary with the dispersion and concentration-gradient samples were

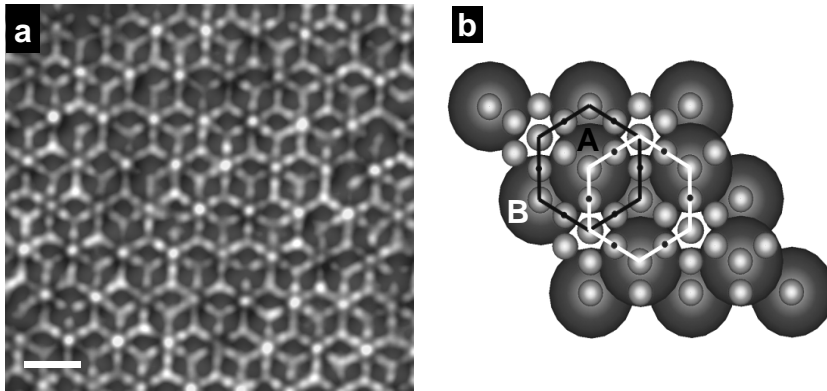


**Figure 6.1.**

$LS_8^{hcp}$  binary crystal formed with positive (green, radius  $0.36\ \mu\text{m}$ ) and negative (red, radius  $1.16\ \mu\text{m}$ ) PMMA-particles in TBAB-containing CHB-decalin mixture. (a) Superposition of confocal images of 5 layers of large colloids and approximately 15 layers of small one. Scale bar is  $3\ \mu\text{m}$ . (b) Schematic representation of the projection of two hexagonal layers (A and B) of large spheres and 6 layers of small particles. The hexagons show the small particles around a large sphere from layer A (black) and layer B (white), the dots on these hexagons represent the 2 planes with a kagomé-type arrangement above and below each of these layers. (See page 87 for color version).

prepared by filling part of the capillary with the dispersion and an other part with only salt-containing solvent mixture (in this way it was possible to scan the phase behavior as a function of the salt concentration). The structures formed were observed with a confocal laser scanning microscope in fluorescence mode and by collecting XYZ data stacks, and using suitable image analysis<sup>70, 159</sup>, the structures were studied in real space.

In samples containing particles with total volume fraction 0.2 and salt concentration  $15\text{--}35\ \mu\text{M}$  two types of crystal structures with stoichiometry  $LS_8$ , for which no atomic or molecular analogues have been identified yet, were found to coexist. The first crystal nuclei appeared within 24h after preparation of the samples (the earliest ones were observed after 4–5 h) and had different orientations, which suggests a homogeneous nucleation. With time the crystal domains grew larger and reached a size of about  $50\ \mu\text{m}$  in 120h. More details on the crystallization of these structures are given in Chapter 7. In the  $LS_8$  structure, called  $LS_8^{hcp}$  and shown on Fig. 6.1, the large colloids form hexagonal layers stacked in ABAB fashion. In these layers, each large colloid is surrounded by a ring of 6 small ones occupying the trigonal interstices. Above and below each layer, there are two planes only of small colloids ordered in a kagomé-type arrangement (see Fig. 6.1b). Fig. 6.1a shows the  $LS_8^{hcp}$  structure as a superimposition of 5 layers of large colloids and approximately 15 layers of small ones. The closest distance between two large spheres in a hexagonal layer was  $2.73 \pm 0.05\ \mu\text{m}$  and the interlayer distance was  $2.55 \pm 0.05\ \mu\text{m}$ , which gives a total packing fraction of 0.48.

In the other binary structure with stoichiometry 8, the  $LS_8^{fcc}$  crystal, the large colloids were ordered in a face-centered-cubic lattice and in every octahedral hole there were 8 small colloids forming a cube, see Fig. 6.2d. Fig. 6.2a shows the (100) plane of the  $LS_8^{fcc}$  unit cell and in Fig. 6.2b the (110) plane is shown. The insets in Figs. 6.2a and 6.2b

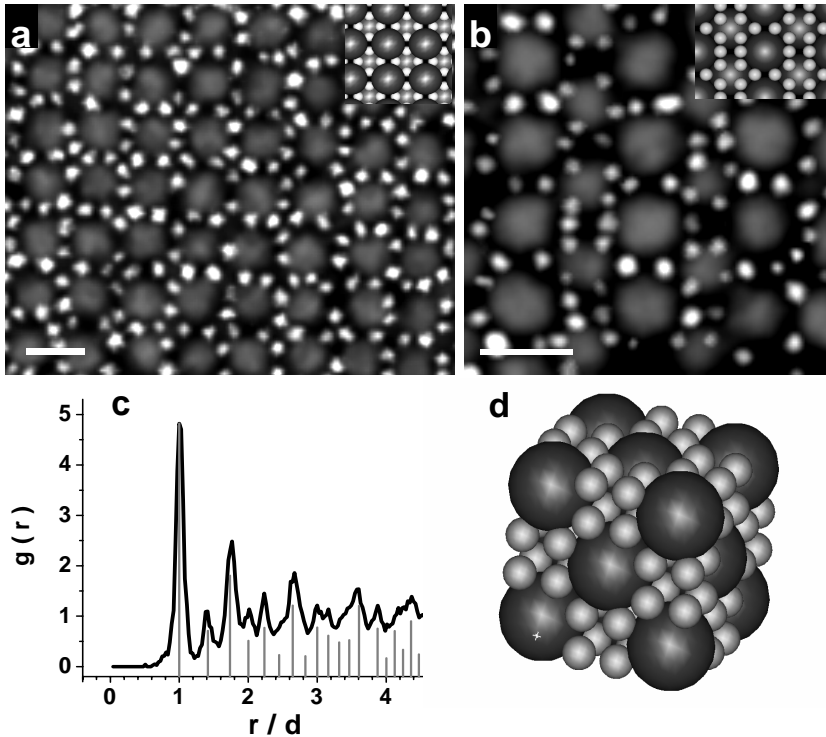


**Figure 6.2.**

$LS_8^{fcc}$  binary crystal from oppositely charged PMMA-particles with size-ratio 0.31. (a), (b) Confocal images of the (100) (a) and the (110) (b) planes; the insets show the corresponding planes from the models generated by computer simulations. Scale bars are 3  $\mu\text{m}$ . (c) 3D radial distribution function of the large particles in the crystal; the vertical lines denote the calculated peak positions. (d) Unit cell of the structure. (See page 87 for color version).

show the corresponding planes of this structure that was also predicted by computer simulations (see below). The distance between two nearest neighbors in the fcc-lattice of the large particles was also 2.73  $\mu\text{m}$  (estimated from the position of the first peak in the 3D radial distribution function- Fig. 6.2c), thus the size of the cubic unit cell was found to be 3.86  $\mu\text{m}$  and the total packing fraction of this crystal structure was 0.55, slightly higher than that of the  $LS_8^{hcp}$  crystal.

Some of the crystallites had a random stacking of the hexagonal layers of the large spheres, which gives a structure where the 3-layer unit of large and small spheres (one mixed layer and two layers only of small colloids above and below it) repeats in a random way (i.e., ABACB...). To the best of our knowledge, the  $LS_8$  structures don't have atomic or molecular analogues.

Besides  $LS_8$ -structures, a binary crystal with stoichiometry  $LS_6$ , called  $LS_6^{bcc}$ , was observed under similar conditions. It consisted of a body-centered-cubic (bcc) lattice of the large colloids and of 4 small colloids in a square situated in the plane between every large next nearest neighbours, see Fig. 6.3c. Figs. 6.3a and 6.3b show, respectively, the (100) and (110) planes of the  $LS_6^{bcc}$  structure unit cell together with the corresponding

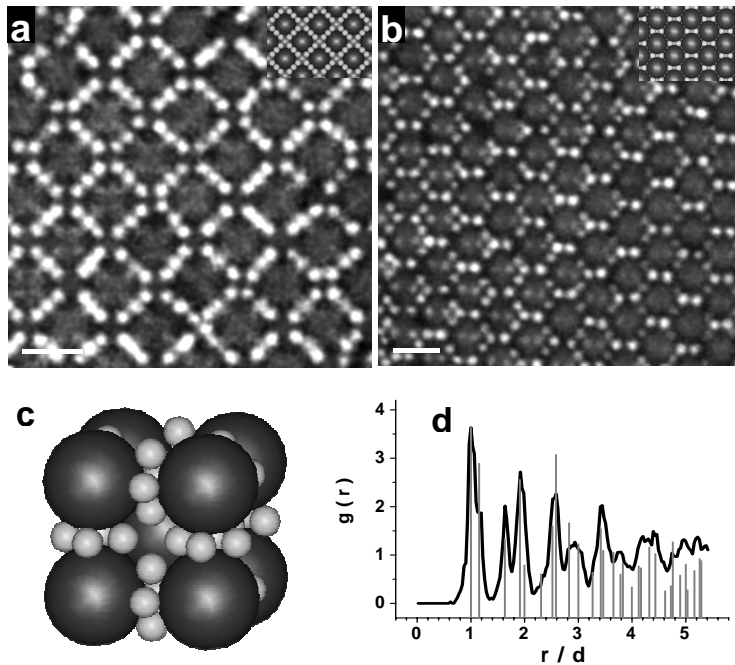


**Figure 6.3.**

$LS_6^{bcc}$  binary crystal from oppositely charged PMMA-particles with size-ratio 0.31. (a), (b) Confocal images of the (100) (a) and the (110) (b) planes; the insets show the corresponding planes from the models generated by computer simulations. Scale bars are  $3\ \mu\text{m}$ . (c) unit cell of the structure. (d) 3D radial distribution function of the large particles in the crystal; the vertical lines denote the calculated peak positions. (See page 87 for color version).

computer-generated models. The size of the unit cell was measured from the peak positions in the 3D radial distribution function of the large particles to be  $2.84\ \mu\text{m}$ , which makes the packing fraction of the crystal 0.66. The  $LS_6^{bcc}$  binary crystal is a colloidal analog of the body-centered-cubic fullerene structure  $A_6C_{60}$  where the large particles correspond to the  $C_{60}$  molecule and the small ones to A (=K, Rb or Cs ions)<sup>172</sup>. This is not surprising as the size ratios in the doped with alkali metals fullerene structures are very similar to ours, e.g.  $a_{\text{Rb}} / a_{C_{60}} = 0.3$ .  $LS_6$ -type binary crystals were previously reported by us<sup>86</sup> (see also Chapter 5) but they had a different symmetry of the large colloids lattice - face-centered-orthorhombic. In both  $LS_6$  and  $LS_6^{bcc}$ , the small colloids are at the same positions with respect to the large colloids. But because of the different experimental conditions under which the two structures were observed, the unit cells of the large colloids have different shapes. Pusey et al<sup>173</sup> have observed colloidal crystals with an  $LS_6^{bcc}$  structure, however, this was reported to be a binary hard-sphere crystal and no further details were given. It is quite possible, though, that these binary structures were grown from oppositely charged colloids.

### 6.3. THEORY AND COMPUTER SIMULATIONS

We modeled our experimental system as  $N_L$  large colloids in a volume  $V$  with a radius  $a_L$  carrying a negative charge  $Z_L e$  (where  $Z_L < 0$  and  $e$  the proton charge) and  $N_S$  small colloids with a radius  $a_S$  carrying a positive charge  $Z_S e$  ( $Z_S < |Z_L|$ ). We assumed that the pair potential  $u_{ij}(r)$ , between colloid  $i$  and  $j$  at inter-particle separation  $r$ , is given by an approximate solution of the Poisson-Boltzmann theory<sup>174, 175</sup>

$$\frac{u_{ij}(r)}{k_B T} = \begin{cases} \frac{Z_i Z_j \lambda_B e^{\kappa(a_i + a_j)}}{(1 + \kappa a_i)(1 + \kappa a_j)} \frac{e^{-\kappa r}}{r}, & r \geq a_i + a_j, \\ \infty, & r < a_i + a_j \end{cases}, \quad (1)$$

where  $Z_i$  ( $Z_j$ ) and  $a_i$  ( $a_j$ ) are the charge number and radius of colloid  $i$  ( $j$ ),  $\lambda_B = e^2 / \epsilon_S k_B T$  is the Bjerrum length,  $\kappa = (8\pi\lambda_B \rho_{\text{salt}})^{1/2}$  is the inverse Debye screening length,  $\epsilon_S$  is the dielectric constant of the solvent, and  $\rho_{\text{salt}}$  is the salt concentration. We denoted the composition by  $x = N_S / (N_L + N_S)$ , the packing fraction of large colloids by  $\eta_L = 4\pi a_L^3 N_L / 3V$ , the dimensionless large-small colloid contact potential by  $\Gamma = |u_{LS}(a_L + a_S)| / k_B T$ , and the charge ratio by  $Q = |Z_L / Z_S|$ . We fixed the size ratio to the experimental value  $a_S / a_L = 0.31$ , and determined the phase diagram of this system for varying  $Q$  and  $\kappa$  as these parameters turned out to be hard to measure under crystallization conditions and were likely to vary for different experiments.

Binary crystal structure candidates were predicted using an interactive Monte Carlo (MC) simulation program. Predicting such structures is a computational challenge, not only because of the overwhelming number of possible structures and system parameters (charge, size, solvent, salinity, composition, etc.) but also because of the intricate interplay between attractive and repulsive interactions, entropy, and packing effects. The simulations were performed using periodic boundary conditions. The program had real-time visualization, and allowed to change various parameters ( $\Gamma$ ,  $Q$ ,  $\kappa$ , stoichiometry) during the simulation, to switch between constant pressure ( $NPT$ ) and canonical ( $NVT$ ) ensembles<sup>176</sup>, and to turn on (or off) large-colloid displacement moves.

The simulations were started in the  $NVT$ -ensemble with the large colloids in a face-centered-cubic (fcc), body-centered-cubic (bcc), hexagonal-close-packed (hcp), simple-cubic (sc), simple hexagonal (sh) or base-centered (bc) crystal, and the small colloids at random (non-overlapping) positions. Next, we used simulated annealing to increase  $\Gamma$  slowly from 0 (high temperatures) to  $\Gamma \approx 10$ -20 (which gives us the ground-state structure), while only the small colloids were allowed to move. At the final  $\Gamma$  we switched to the  $NPT$ -ensemble, where volume moves were performed separately for each axis in order to equilibrate the small-colloid positions and the box shape. Finally, the large-colloid moves were turned on and the ideal crystal structures were constructed from snapshots of the final colloid configuration.

The search for new stable binary structures was performed by trying all the above mentioned large-colloid crystals as starting configurations, at packing fractions around  $\eta_L = 0.3 - 0.56$  and at various initial shapes of the simulation box. This was repeated for

$LS_n$	FCC	BCC	SC	SH	HCP	BC
1	Zinc blende	Zinc blende	-	-	<b>Wurtzite</b>	-
2	<b>CaF<sub>2</sub></b>	<b>CaF<sub>2</sub></b>	-	-	-	<b>CaF<sub>2</sub></b>
3	<u>LS<sub>3</sub><sup>fcc</sup></u>	<b>Cr<sub>3</sub>Si</b>	<b>ReO<sub>3</sub></b>	<b>Li<sub>3</sub>N</b>	LS <sub>3</sub> <sup>hcp</sup>	<b>ReO<sub>3</sub></b>
4	<b>A<sub>4</sub>C<sub>60</sub>, LS<sub>4</sub><sup>bct</sup></b>	<b>A<sub>4</sub>C<sub>60</sub>, SiF<sub>4</sub></b>	-	-	LS <sub>4</sub> <sup>hcp</sup>	-
6	<u>LS<sub>6</sub><sup>bcc</sup>, LS<sub>6</sub><sup>fcc</sup></u>	<u>LS<sub>6</sub><sup>bcc</sup></u>	-	-	<b>LS<sub>6</sub><sup>hcp+hp</sup></b>	-
8	<u>LS<sub>8</sub><sup>fcc</sup></u>	<u>LS<sub>8</sub><sup>fcc</sup></u>	-	<u>LS<sub>8</sub><sup>hcp</sup></u>	<u>LS<sub>8</sub><sup>hcp</sup></u>	-

**Table 6.1.**

The crystal structures found with simulated annealing for each large colloid starting configuration and stoichiometry  $n$ .  $C_{60}$  stands for the fullerene molecule and line (-) indicates absence of crystal structure. The structures presented in bold-style were found more stable than the others and the underlined have been observed experimentally.

small-large stoichiometries  $n = 1 - 8$  (denoted by  $LS_n$ ), where  $n$  is related to the composition by  $x = n/(n + 1)$ . The simulations were performed in a box with 4 to 16 large colloids. Such a small simulation box with periodic boundaries facilitates finding structures with crystalline order, as it reduces the probability of stacking faults. Table 6.1 lists the crystal structures found for each stoichiometry and large-colloid starting configuration, for  $\kappa_{AL} = 2$  and  $Q = n$ . Structures which had no atomic or molecular analog were named  $LS_n^{lat}$ , where "lat" is the lattice symmetry of the large colloids. We have not (yet) considered primitive unit cells with more than two large colloids, and have hence excluded  $n = 5$  and 7, as well as some other structures (e.g. a colloidal analog of the face-centered-cubic  $A_6C_{60}$  structure<sup>177</sup>). This does not mean, of course, that these structures could not form in experiments.

Predicting the phase diagram of a binary mixture often involves a calculation of the Gibbs free energy per particle, since its  $x$ -dependence at fixed  $P$  and  $T$  allows for common tangent constructions. It reduces, however, to the enthalpy for the ground state properties of interest here, where entropic effects are ignored. Moreover, since many of our experiments show crystals that are self-supported by their cohesive energy, we restricted our attention to the zero-pressure limit. The present phase diagram follows therefore from the internal energy, which for a crystal with all particles at their ideal lattice positions is the composition dependent Madelung energy  $U(x)$ <sup>86, 178</sup>. Including entropy and pressure complicates the theoretical studies considerably, and will be the subject of future research. In the zero-pressure ground-state approximation phase stability depends only on the charge ratio  $Q$  and the screening parameter  $\kappa$ , and *not* on the absolute values of  $Z_L$ ,  $Z_S$ , and  $\lambda_B$  separately. We calculated  $U(x)$  with the MC code (relative error smaller than  $10^{-7}$ ) for the structures listed in Table 6.1 and for many known structures: NaCl, CsCl, NiAs, CuAu, AlB<sub>2</sub>, Cu<sub>3</sub>Au, Al<sub>3</sub>Ti, CaCu<sub>5</sub>, and CaB<sub>6</sub><sup>179</sup>. The lowest  $U(x)$  per colloidal particle was

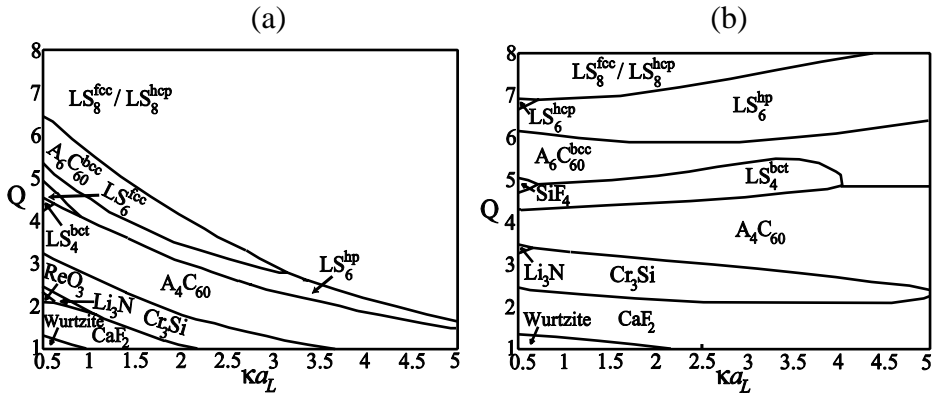


**Figure 6.4.**

The ground-state phase diagram of a mixture of large and small oppositely charged colloids with size ratio 0.31 as a function of the Debye screening parameter  $\kappa$  and the charge ratio  $Q$ . In (a) the structures coexist with a gas of only small colloids, and in (b) with gas of large colloids only.

found for given  $Q$  and  $\kappa$  by optimizing each possible structure with respect to  $\eta_L$  and the shape of the unit cell. The structures that were found more stable than the others are presented in bold-style in Table 6.1 and those that were observed experimentally are underlined. We then performed, for fixed  $Q$  and  $\kappa$ , the common tangent construction. Fig. 6.4 shows the resulting phase diagram for two extreme cases, where the crystal coexists with an infinitely dilute gas of (a) pure small colloids ( $x = 1$ ), and (b) pure large colloids ( $x = 0$ ). Note that  $U(0) = U(1) = 0$  because of the repulsive character of like species. Other overall compositions yielded crystal-crystal phase coexistence<sup>180</sup>.

Figure 4 shows an increasing stoichiometry with increasing  $Q$  at low  $\kappa a_L$ . In addition, one observes that an excess of small colloids favors structures with high stoichiometry. Moreover, we see that  $\text{ReO}_3$ ,  $\text{Li}_3\text{N}$ ,  $\text{SiF}_4$ ,  $\text{LS}_6^{\text{fcc}}$ , and  $\text{LS}_6^{\text{hcp}}$  are only stable for relatively long-ranged interactions with  $\kappa a_L \gg 0.5$ . In these structures, the small colloids are in between pairs of neighboring large colloids in these structures. Although such structures are electrostatically favorable, they pack inefficiently and thus destabilize at stronger screening.

The  $\text{LS}_6^{\text{bcc}}$ ,  $\text{LS}_8^{\text{fcc}}$  and  $\text{LS}_8^{\text{hcp}}$  structures dominate the phase diagrams in Figs. 6.4a and 6.4b at high  $Q$  and high  $\kappa a_L$ . Interestingly, these are the structures that were found experimentally as well; see Figs. 6.1 - 6.3 (the computer-generated models of the different planes of the predicted structures shown as insets reveal excellent agreement with the observed ones). The  $\text{LS}_8^{\text{hcp}}$  and  $\text{LS}_8^{\text{fcc}}$  structures were found in the experiments to coexist. This is also in agreement with our calculations, which predicted essentially equal Madelung energies (although  $\text{LS}_8^{\text{fcc}}$  is more stable, but only by 0.005-0.1%).

According to the Madelung energy calculations,  $\text{LS}_6^{\text{bcc}}$  (which we had not yet considered in Ref. [86]) is more stable than  $\text{LS}_6$  structure reported in Chapter 5. It is possible, though, that entropy and pressure can change the relative stability of these two structures.

#### 6.4. CONCLUSIONS

We observed experimentally several new binary crystal structures formed from oppositely charged particles with a size ratio 0.31 –  $LS_8^{\text{fcc}}$ ,  $LS_8^{\text{hcp}}$ ,  $LS_6^{\text{bcc}}$ . For the first two crystals we didn't find an atomic or molecular analogue, while the  $LS_6^{\text{bcc}}$  structure is a colloidal analogue of the doped with alkali metals fullerene compound  $A_6C_{60}$ . The stability of these binary crystals was confirmed by computer simulations using a screened Coulomb potential to describe the interparticle interactions. We developed an interactive method based on simulated-annealing to predict binary crystal structures of oppositely charged colloids, from which we constructed a ground-state phase diagram for a size ratio of 0.31 displaying a variety of novel crystal structures. As computer simulations are easier and quicker to perform than experiments, they can be used as a very powerful tool to locate the range of parameters where a given structure could be observed experimentally. In experiments, it is not easy to control the charge ratio  $Q$ , the screening length  $\kappa$  and the stoichiometry independently. This means that structures with a small area of stability will be difficult to observe. We have so far restricted our attention to stoichiometries up to  $n = 8$ , but we expect more structures for larger  $n$ , e.g., for  $n = 10$  and  $Q \approx 10$ , we can expect a colloidal analog of the  $Na_{10}C_{60}$  structure<sup>181, 182</sup>. Of course, it is possible that other structures exist that make the current ones metastable. However, introduction of a new structure typically reduces the stability area of the prior ones, but does not completely replace them. The experimentally observed Brownian motion of the particles in the crystals suggests that entropy should not be ignored, thus detailed studies involving free energy calculations should be performed. Finally, it is reasonable to expect even more and different structures for other size ratios, the exploration of which is not only of fundamental but also of practical interest, e.g., for photonic applications.

#### ACKNOWLEDGEMENTS

We thank A.P. Hynninen and M. Dijkstra for performing the computer simulations and R.van Roij for the theoretical input.



# 7

## Preliminary observations on crystallization in binary mixtures of oppositely charged PMMA particles

In this Chapter we discuss preliminary results on the crystallization mechanism of binary crystals with stoichiometry  $LS_8$  formed by oppositely charged particles with size ratio 0.31, and on a crystal-crystal transition between two binary structures with widely different stoichiometries in the same system. A scenario where the two species crystallize together forming small ordered nuclei that grow larger is proposed for the formation of the  $LS_8$ -type binary structure. The continuous transformation from the crystal with the lower stoichiometry to the one with the higher stoichiometry under the influence of gradient in the small particles concentration is followed in a qualitative way.

## 7.1. INTRODUCTION

In the course of our study on the crystallization of binary mixtures of oppositely charged PMMA particles with a size ratio of 0.31<sup>86, 169</sup> (Chapters 5 and 6) we encountered several interesting phenomena which are described here qualitatively as preliminary observations. These include the nucleation and growth of the binary crystals with stoichiometry of LS<sub>8</sub> (reported in Chapter 6) and coexistence of binary crystals with different stoichiometries. While a significant number of studies, both experimental<sup>63, 73-75, 183-188</sup> and theoretical<sup>189-194</sup> are dedicated on the growth of crystals of single-sized colloidal particles, there is a limited amount of studies on the crystallization mechanism of binary colloidal crystals<sup>35, 143, 195, 196</sup>. Due to the large differences in sizes, leading to large differences in the sedimentation rates as well, binary mixtures of spheres are found to crystallize much slower than one-component dispersions. Under the conditions of negligible gravity the crystallization of mixtures of particles with similar sizes (size ratio  $\sim 0.8$ ) was found to accelerate significantly<sup>143</sup> implying that indeed growth is impeding binary crystallization. Without the effect of gravity, Eldridge et al<sup>35</sup> concluded that for binary hard-sphere systems maximizing the packing density is a strong driving force for binary crystallization. These authors performed computer simulations on a mixture of hard spheres crystallizing into a binary crystal of stoichiometry LS<sub>13</sub> and found that the stability of these crystals can be explained by entropy alone. The nucleation mechanism of random substitutional crystals from charged spheres with small size differences (size ratio = 0.75-0.90) was found to be similar to that of a single-species case<sup>196</sup>. The presence of electrostatic attractions between the small and large spheres (as is the case in our oppositely charged mixtures described in Chapters 5 and 6 and Ref. [86, 169]) can have a significant effect on the crystallization mechanism in such systems which are found to form binary crystals much faster than mixtures of hard spheres. The first section in this Chapter gives some insights into the growth mechanism of binary crystal structures with stoichiometry LS<sub>8</sub> formed by oppositely charged particles with size ratio 0.31.

The second part of the Chapter describes the coexistence of binary crystals with a significant difference in the stoichiometry and the continuous transition from one of these structures to the other. Coexisting binary crystals with LS<sub>2</sub> and LS<sub>13</sub> stoichiometries were found by Murray and Sanders<sup>5</sup> in Brazilian opal containing mixtures of silica spheres with a size ratio of 0.58. The authors attributed this coexistence to the fact that a mixture of the two structures will have the maximum packing density possible within a certain range of size ratios and relative concentrations of the two species. Bartlett et al.<sup>33</sup> also studied hard-sphere mixtures with a size ratio of 0.58. They didn't observe coexistence between two different binary structures but predicted compositions at which such coexistence can be found for this size ratio and at certain total particle volume fraction. Computer simulations<sup>35</sup> and cell theory calculations<sup>39</sup> confirmed the presence in the phase diagrams of hard-sphere mixtures of regions of coexisting LS<sub>2</sub> and LS<sub>13</sub> binary crystals. Yoshimura and Hachisu<sup>7</sup> observed a coexistence of LS<sub>2</sub> and LS<sub>13</sub> structures in mixtures of polystyrene particles with a size ratio of 0.45 and found that the preference for any of the two structures to form didn't depend on the particle number ratio but was mostly influenced by the 'mode of packing' of the two species.

*Experimental*

Our experimental system is the same as reported in Chapter 6 – mixtures of polymethylmethacrylate (PMMA) particles<sup>87</sup> with a size ratio  $a_S / a_L = 0.31$ , where  $a_S = 0.36 \mu\text{m}$  is the radius of the small species and  $a_L = 1.16 \mu\text{m}$  is that of the large ones. The large colloids were labeled with rhodamine isothiocyanate (RITC) and the small ones with 7-nitrobenzo-2-oxa-1,3-diazol (NBD). Stock dispersions of the two types of particles in a density and refractive index matching mixture of cyclohexylbromide (CHB) and decalin (80/20 volume ratio) were prepared and mixtures with certain particle volume fractions and proportions were made. The particles acquired small charge and by adding the salt tetrabutylammoniumbromide (TBAB)<sup>70</sup> to the mixtures a control over the sign and the magnitude of the charge was achieved.

The dispersions were sealed into glass capillaries as described in Chapter 6 and left flat during the time of observation. A fluorescence confocal laser scanning microscope was used to observe the structures obtained.

7.2. NUCLEATION AND GROWTH OF  $LS_8$ -BINARY CRYSTALS

The crystallization mechanism of the binary structures of oppositely charged PMMA particles with size ratio 0.31,  $LS_8^{fcc}$  and  $LS_8^{hcp}$  (Fig. 7.1), described in Chapter 6 and Ref. [169] was investigated with confocal microscopy. Samples containing binary mixtures of large (L) and small (S) particles in CHB-decalin with a total particle volume fraction  $\phi = \phi_L + \phi_S = 0.2$ , a particle number ratio  $N_S / N_L = 8$  and a salt concentration of 15-25  $\mu\text{M}$  were followed in time from their preparation until several weeks later. The structures observed in the course of time are described qualitatively in this section.

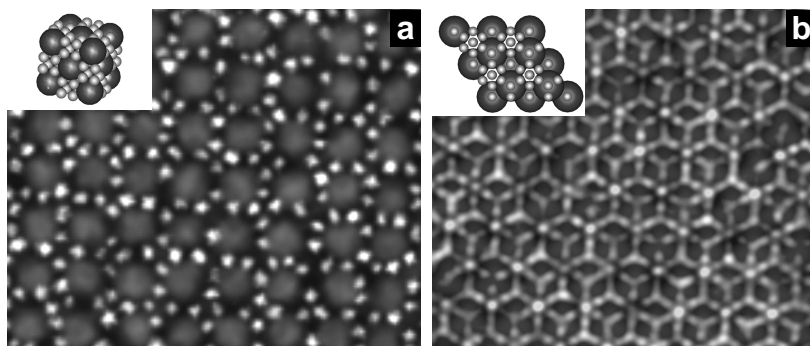


**Figure 7. 1.**

$LS_8^{fcc}$  (a) and  $LS_8^{hcp}$  (b) binary crystals observed with oppositely charged PMMA particles with size ratio 0.31 in CHB/decalin. The insets show schematic representations of these structures. (See page 87 for color version).

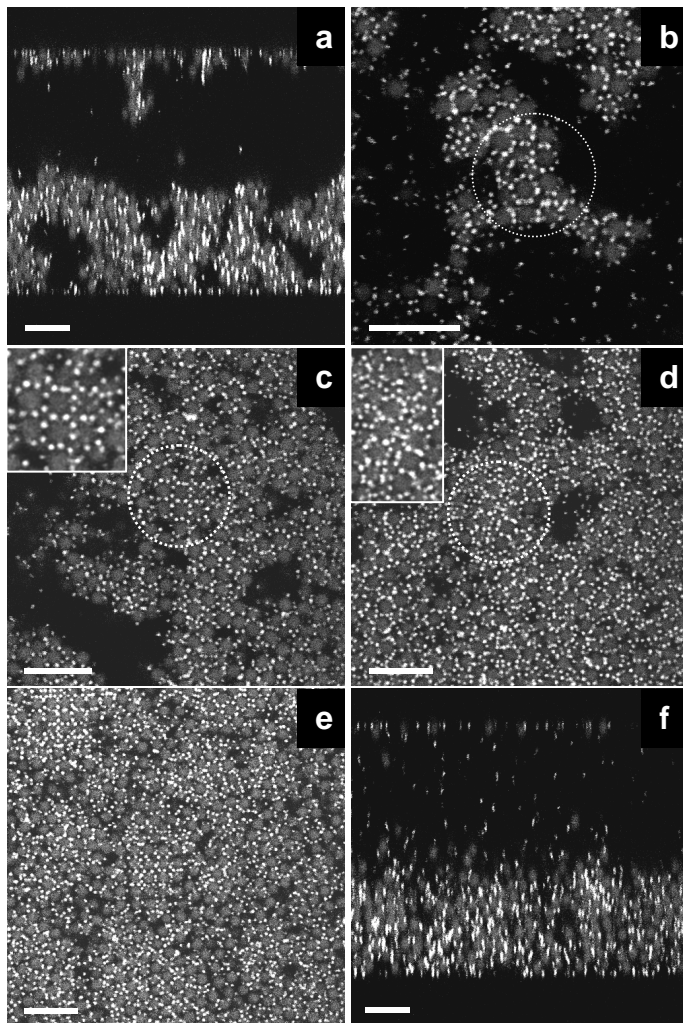
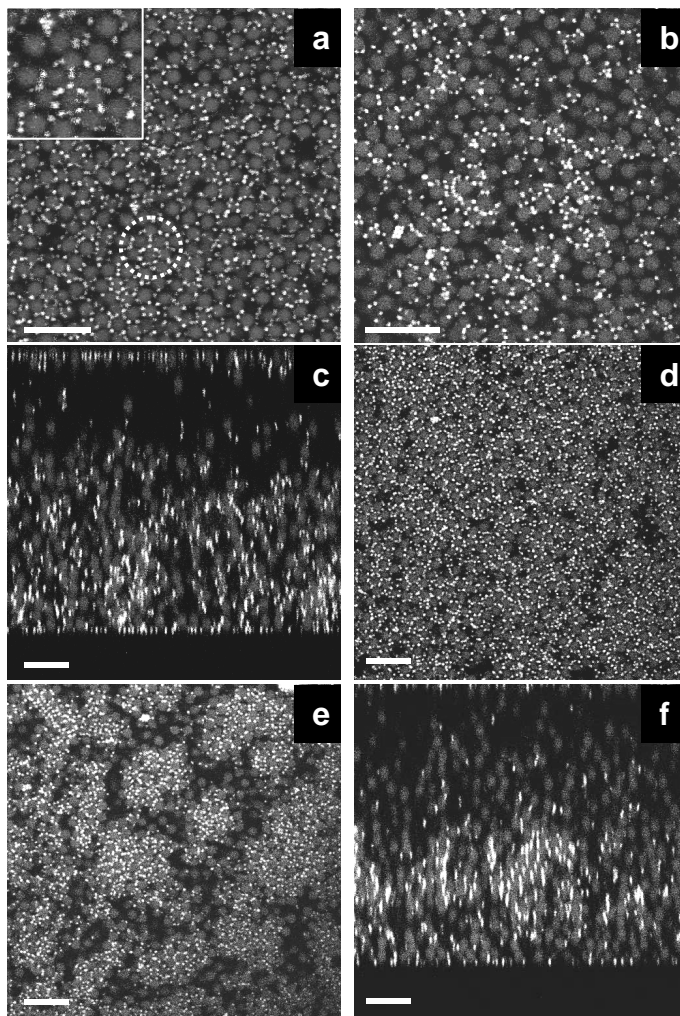


**Figure 7.2.** Time evolution of structures formed by oppositely charged particles with a size ratio of 0.31 in regions of strong interparticle attraction. Confocal images presenting the structures: 2 hours (a), (b), 20 hours (c), (d), and 30 hours (e),(f) after sample preparation. The circles show ordered areas some of which are magnified in the insets. Scale bars are  $10\ \mu\text{m}$ .

Although the samples had a constant particle and salt concentration, regions with different local densities were found within the samples (probably due to the slight tilt of the samples). Local variation of the particle concentration and number ratio induced also a change in the strength and type of interaction between the large and small particles. This finding is also supported by observations that binary mixtures prepared with different total particle volume fraction and different number ratio exhibit different large-small interactions even without salt present. For example, mixtures with  $\phi = 0.12$  and  $N_s / N_L = 8$  have strong electrostatic attraction between the large and the small spheres, while for  $\phi = 0.12$  and  $N_s / N_L = 15$  the two species repel each other.

Figure 7.2 presents structures formed in regions with a slight excess of small spheres and stronger large-small attraction during the first 30h after sample preparation. Fig. 7.3 shows the initial time evolution in areas with a slight excess of large colloids and weaker attraction between the two species. In the first case, open aggregates of large and

**Figure 7.3.**  
*Time evolution of structures formed by oppositely charged particles with size ratio 0.31 in regions with weaker interparticle attraction. Confocal images presenting the structures: 2 hours (a), (b), (c), 20 hours (d), and 30 hours (e),(f) after sample preparation. Scale bars are 10  $\mu\text{m}$ .*



small particles, with a branched shape, were formed immediately after sample preparation. They were in coexistence with a very dilute gas of mostly small spheres (see Fig. 7.2a,b). Time series show that the aggregates are dynamic structures, the particles inside are not immobilized but still move locally and those that are in contact with the gas phase detach and attach. The individual large spheres that were seen to jump between different parts of the aggregates were surrounded by an “atmosphere” of 6 to 10 small particles which were not stuck onto the particle surface but were moving round the large colloid. Inside the aggregates there were small areas ( $\sim 3 \times 3 \mu\text{m}^2$ ) with local order of both, large and small spheres (e.g., as shown in the circle in Fig. 7.2b) with the square and the hexagonal pattern typical for the  $\text{LS}_8^{\text{fcc}}$  and  $\text{LS}_8^{\text{hcp}}$  structures, respectively. The small colloids in between the large ones in these ordered areas were localized and didn’t escape from their positions (although they were still mobile). These small ordered regions were the earliest observed nuclei of the  $\text{LS}_8$ -crystals although they were only 2D-like and didn’t extend yet in the

vertical direction. The aggregates sedimented to the bottom wall of the sample and formed a sharp interface with the dilute gas of small spheres on top. Upon sedimentation they densified and became more compact, with less voids. Together with this increase in volume fraction, the initial small ordered regions became larger and extended also in 3D. After about 20h their size was about  $10 \times 10 \times 10 \mu\text{m}^3$  and the patterns seen most often consisted of the (100) and (110) planes of the  $\text{LS}_8^{\text{fcc}}$  structure; see Figs. 7.2c and 2d. In these nuclei the large spheres were less mobile than the particles from the surrounding solid and the stoichiometry was already defined by the fixed number of small colloids between the large ones.

About 25-30 h after sample preparation a change in the appearance of the structures was observed. Individual crystallites had formed with different crystal planes from both  $\text{LS}_8$ -type structures displayed parallel to the bottom wall. In contrast to the ordered crystalline regions described above which had grown within the solid aggregates, the separate crystallites were surrounded by a dense binary fluid. The crystallites had an average size of about  $20 \times 20 \times 15 \mu\text{m}^3$  but didn't have well defined shapes as the particles at their borders were shared between the neighboring crystallites (Fig 7.2e). On top of the crystallites was the very dilute gas of predominantly small spheres. These binary crystallites most likely had formed from the many small locally ordered domains which expanded and separated from the disordered solid which 'melted' into a fluid.

In the regions with a weaker attraction between the large and small spheres no aggregates were formed immediately after sample preparation but rather a dense binary fluid phase close to the bottom wall and a more dilute binary fluid on top without a sharp interface between them – Fig. 7.3a,c. In the dense phase the particles were mobile and generally disordered, only at some places small, more ordered areas were observed like the one shown within the circle in Fig. 7.3a. Some of the large spheres at the border between the dense and the dilute fluid phases were like "glued" by the small ones in between them

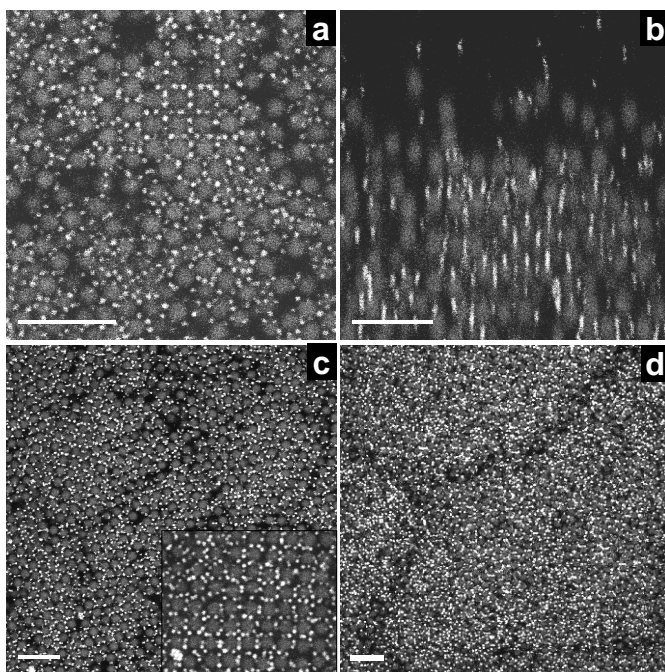


**Figure 7.4.**  
Time evolution of structures formed by oppositely charged particles with size ratio 0.31. Confocal images presenting the structures: 52 hours (a), (b), 125 hours (c), and 16 days (d) after sample preparation. Scale bars are  $10 \mu\text{m}$ .

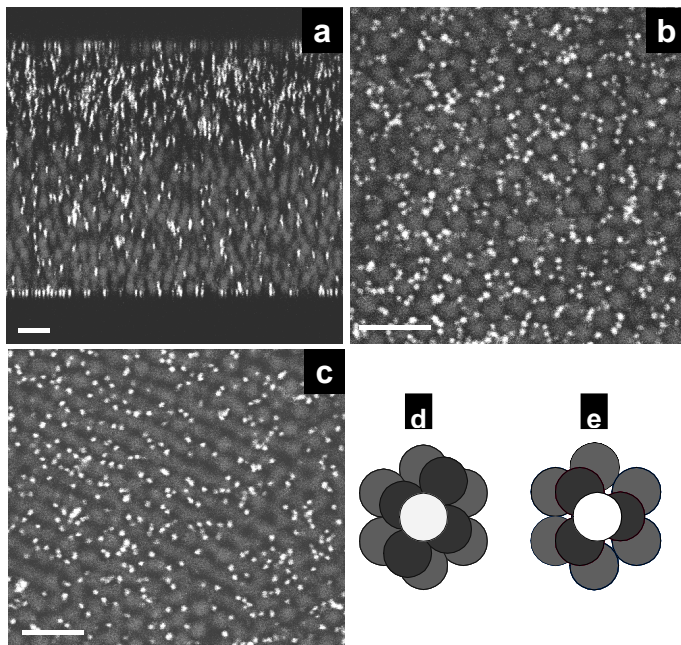


**Figure 7.5.**  
 (a)-(c) Confocal images of a mixture of large and small particles (size ratio 0.31) a few hours after sample preparation. Scale bars are  $7\ \mu\text{m}$ .  
 (d), (e) Schematic representations of bridge-site stacked (d) and hollow-site stacked (e) hexagonal layers producing body-centered tetragonal and hexagonal close packed structures, respectively.

and performed a collective motion (Fig. 7.3b). For the next 20 hours the dense fluid phase became more compact (Fig. 7.3d) and layering was observed but without correlations of the particles positions in vertical direction.

About 10 hours later again separate differently oriented binary crystallites were observed, as in the former case, but here they were more compact and had clear borders separating them from the surrounding gas of mostly large spheres (Fig. 7.3e). Probably they formed from the small clusters of large and small particle formed on top of the dense phase as they were observed to “float” on top of the sedimented liquid (Fig 7.3f).

After another 24 hours both types of  $LS_8$ -crystallites became larger in vertical direction (Fig. 7.4b), with a well-defined structure (Fig. 7.4a). With time the domains grew larger but while the large spheres retained their order, the small ones became more mobile and didn't have permanent lattice positions anymore, as shown in Fig. 7.4c,d. Probably the

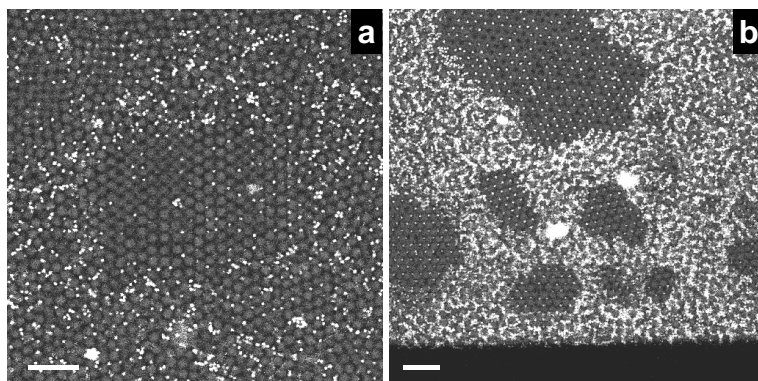


**Figure 7.6.**  
 Crystallites of large (a) and large and small (b) colloids formed 1 day (a) and 5 days (b) after sample preparation. Scale bars are  $10\ \mu\text{m}$ .

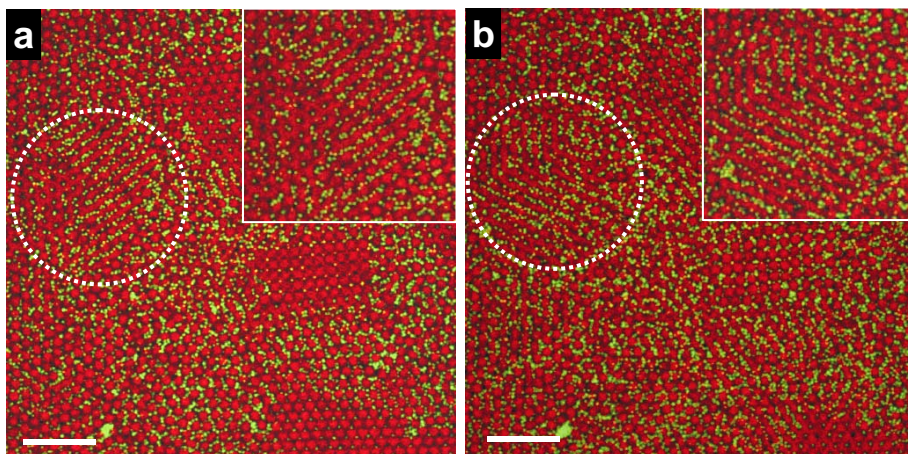


**Figure 7.7.**

Two successive images of binary structures with line-like patterns (shown in the circled area and in the insets) having different orientation. Images are taken at distances of  $12\ \mu\text{m}$  (a) and  $14.5\ \mu\text{m}$  (b) from the bottom wall, 5 days after sample preparation. Scale bars are  $15\ \mu\text{m}$ .

charge on the particles changed and the electrostatic attractions between them became weaker.

From these observations on the formation of the LS<sub>8</sub>-crystals we can arrive at the following conclusions. When the attraction between the two oppositely charged species is strong enough the first small nuclei appear already several hours after sample preparation, either within solid aggregates or as forming and dissolving on top and in a dense fluid phase. They consisted of ordered arrangements with different orientations of both, large and small spheres, which suggest that they homogeneously nucleate together, driven by minimization of their free energy. With time, the local order is transferred to the neighboring particles and the crystalline domains grew larger with a high positional order in 3D. It is unlikely that a mechanism in which the large spheres order first and the small ones then start to occupy certain positions, occurs with these binary crystals because no ordered domains of only large colloids were observed

These preliminary insights into the crystallization mechanism of binary ‘ionic’

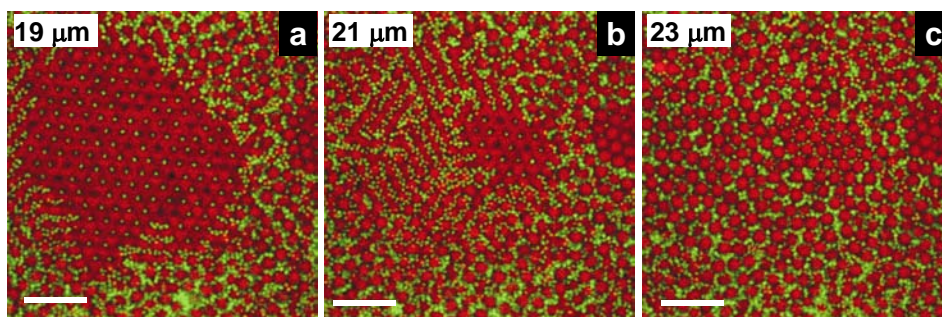


**Figure 7.8.**

Successive images at different distances from the bottom wall, showing coexistence of LS crystal (a) and binary structures with line-like patterns (b). Images are taken 5 days after sample preparation. Scale bars are  $10\ \mu\text{m}$ .

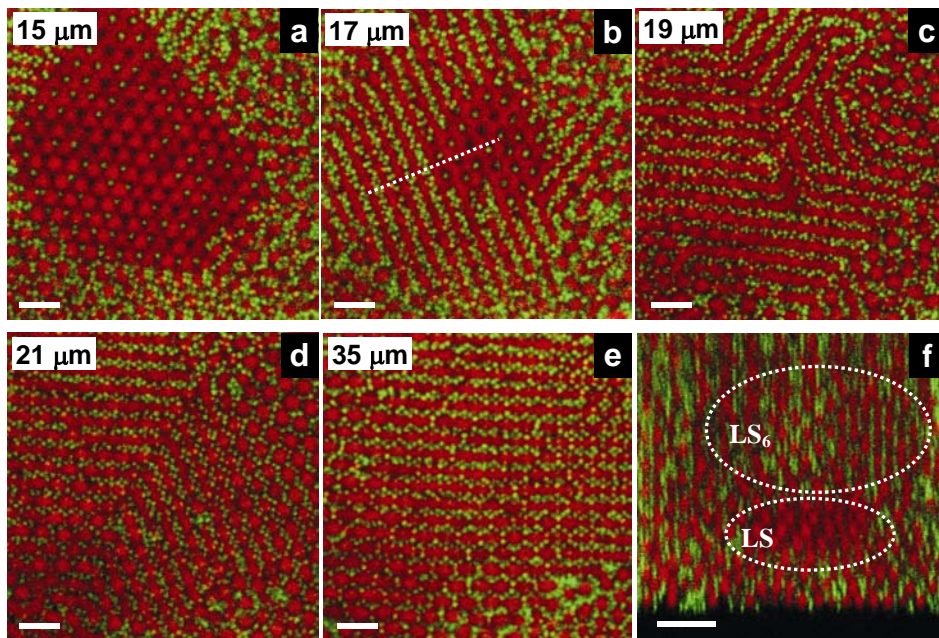


**Figure 7.9.**

Successive images at different distances from the bottom wall where coexistence of LS (a) and  $LS_6$  (b-e) structures are seen. (f) is an  $xz$  image taken through the line shown in (b). Images are taken 7 days after sample preparation. Scale bars (a)-(e) are  $5\ \mu\text{m}$ , (f)  $10\ \mu\text{m}$ .

colloidal crystals should be confirmed by more detailed and quantitative investigations and should include a measurement of the interparticle distances, mean-square-root-displacements and order parameters as a function of time.

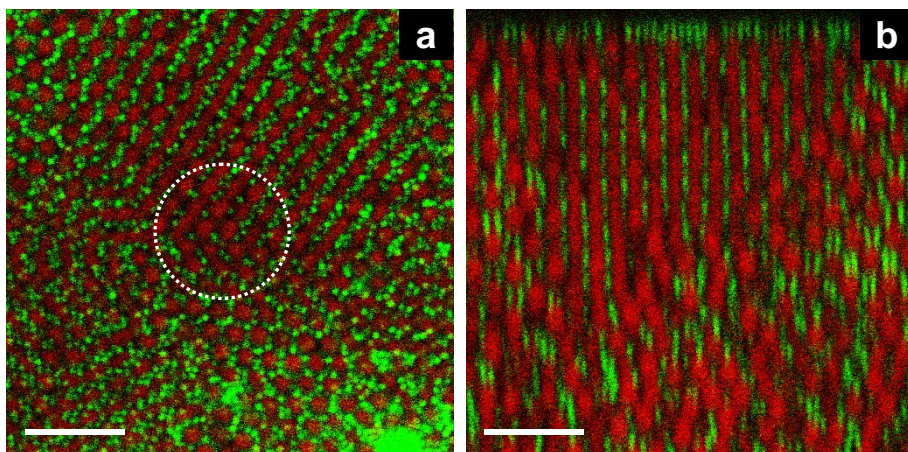


**Figure 7.10.**

Confocal images showing a very small area with LS-crystal left 8 days after sample preparation at a distance of  $13\ \mu\text{m}$  from the bottom wall (a) and large domains with  $LS_6$  crystals observed 4 more days later (b). Scale bars  $10\ \mu\text{m}$ .

### 7.3. COEXISTENCE OF BINARY CRYSTALS WITH DIFFERENT STOICHIOMETRIES

In this section observations will be presented on the coexistence of binary structures with stoichiometries LS and LS<sub>6</sub> that were found in a sample with a mixture of small and large particles (size ratio 0.31) in CHB/decalin. The total particle volume fraction was  $\phi = 0.23$ , the number ratio  $N_S / N_L = 8$  and the salt (TBAB) concentration 15-25  $\mu\text{M}$ .

As discussed in the previous section, inside a sample with a constant particle volume fraction, number ratio and salt concentration regions with different structure and behavior were observed, most likely due to a slight tilt of the sample. A similar situation was found in the sample under investigation in this section. Close to the interface between the dispersion and air the two species were observed to repel each other. Several hours after sample preparation a sedimented dense phase of both, small and large particles was observed here and a fluid of small spheres formed on top of it (Fig. 7.5a). In the dense phase the large colloids were tightly packed without long-ranged order and the small ones were moving locally between them (Fig. 7.5b).

On the other side of the sample, the large spheres were ordered in hexagonal planes which were stacked on top of each other either in a close-packed or in bridge-site stacked fashion (producing lines-pattern when observed between two layers – Fig. 7.5c,d). The large spheres were very mobile and had an average inter-particle distance of about 2.8  $\mu\text{m}$ . The small spheres moved freely in the holes and “channels” between the large particles.

We will focus our observations on the time evolution of the structures in the part of the sample closer to the air-meniscus. One day after sample preparation the large particles there crystallized in domains with different structures (fcc, hcp or rhcp), orientation and sizes (the largest ones measured about  $70 \times 70 \times 30 \mu\text{m}^3$ ) (Fig. 7.6a) with a mean inter-particle distance of about 2.45  $\mu\text{m}$ . The small spheres occupied some of the octahedral interstices in the crystals of the large particles. They moved in the holes but very rarely hopped from hole to hole.

After 4 more days interesting structures were observed still at the side of the air meniscus where the particle concentration in the mean time had become even higher. Binary, well defined crystallites appeared with different orientations (Fig. 7.6b). They were surrounded by a dense disordered mixture of large and small spheres in which the large particles were highly localized and the small ones were still able to move between them. The structure of the crystallites was found to be of NaCl- and NiAs-type (described in Ref. [86] and Chapter 5), or a mixture of the two. Next to these binary LS-crystals, different patterns were observed consisting of lines of large particles with the small ones filling the space in between them (Figs. 7.7, 7.8). These lines reflect bridge-site stacked hexagonal layers of the large colloids and are a typical pattern of the LS<sub>6</sub>-structures described in Ref [86, 169] and Chapters 5 and 6, see also Fig. 7.5d. A closer look at this new structure (Fig. 7.7, insets) reveals that it consists of much more small particles than the LS-crystals. The small colloids were situated mostly in channels formed by the strings of large spheres and they moved freely in there but rarely jumped to neighboring channels.

This means that they are partially localized but are not yet confined to lattice positions. The line-pattern formed by the bridge-site stacked layers of large particles had different orientations at different heights ( $Z$ ) in the sample. Fig. 7.7 presents two 2D slices through an area with binary crystallites taken at a distance  $2.42\ \mu\text{m}$  from each other (corresponding roughly to the distance between two hexagonal layers of large colloids), which show how successive layers of large particles are stacked in a bridge-site fashion but without any preferred orientation. The line-patterns were observed mostly at the upper part of some binary LS crystallites where the concentration of the small spheres is higher. In Fig. 7.8 successive xy-images are shown, taken from an xyz-stack of a crystal domain with two different binary structures – one with stoichiometry LS (Fig. 7.8a) and the other with a bct structure of the large spheres having a much higher stoichiometry (Fig. 7.8b).

After 2 more days the LS-crystallites almost disappeared and large areas with a structure resembling that of the  $\text{LS}_6$ -crystals was found instead. This structure was formed from the bridge-stacked hexagonal layers of the large particles and the small spheres situated in between them. The latter became now more localized and, although they were still mobile, they showed the arrangement typical for the  $\text{LS}_6$ -crystals (Fig. 7.9e). Close to the bottom of the sample a  $\text{LS}_6$ -like structure was in coexistence with a small LS-crystal (Fig. 7.9a,b).  $\text{LS}_6$ -like, because this structure was not yet completely defined as successive hexagonal layers of large spheres had different orientations (Fig. 7.9b,c,d). At the top the  $\text{LS}_6$  crystal was well-defined as can be seen in the xz-cut (Fig. 7.9f) through a plane denoted by a dashed line in Fig. 7.9b. With time the LS-crystal disappeared completely (Fig. 7.10a) and the whole volume in this part of the sample became filled with  $\text{LS}_6$ -crystals (Fig. 7.10b).

We can speculate that the mechanism involved in the observed coexistence of the two binary structures with different stoichiometries includes as an important driving force the increased concentration of the small particles (pressure) due to a small tilt of the sample causing the colloids to accumulate more at one of the sample ends. It is very interesting to see how the small particles seemed able to first change the stacking of the close packed hexagonal layers to a bct structure in which the small particles were not yet crystalline. In the course of time this structure became more defined and resembled the  $\text{LS}_6$  structures described in Ref. [86, 169]. The distance between the hexagonal layers of large particles in the coexisting LS and in the  $\text{LS}_6$  crystals was the same ( $\sim 2.18\ \mu\text{m}$ ). The hexagonal layers of large spheres in the LS structure were perfectly hexagonal (as judged from the similar interparticle distances ( $\sim 2.36\ \mu\text{m}$ ) along each of the three main directions in the layers) while the ‘hexagonal’ layers of the  $\text{LS}_6$  structure were found to be slightly stretched in one of the directions.

It will be very interesting to confirm this fascinating crystal transition more quantitatively and, through computer simulations, see if it represents an equilibrium path. It should also be investigated further if this type of crystal-crystal transition has molecular analogs or whether it is specific to ionic colloidal crystals.

#### ACKNOWLEDGEMENTS

We thank A.P. Hynninen for helpful discussions.

COLOR FIGURES

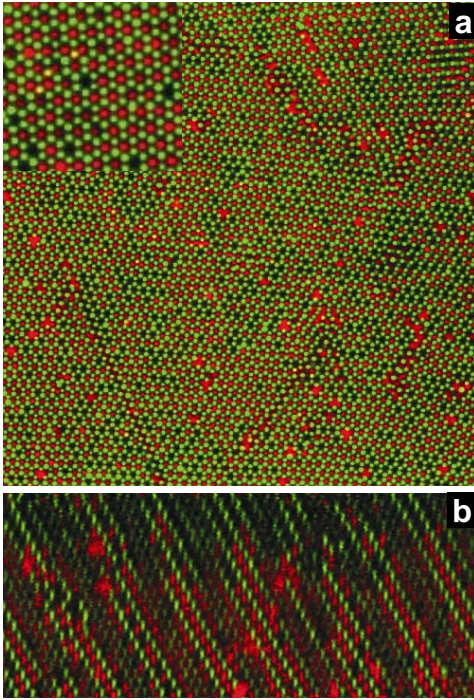


Figure 4.4.

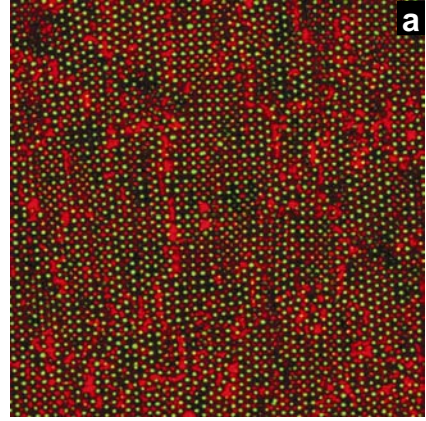


Figure 4.11.

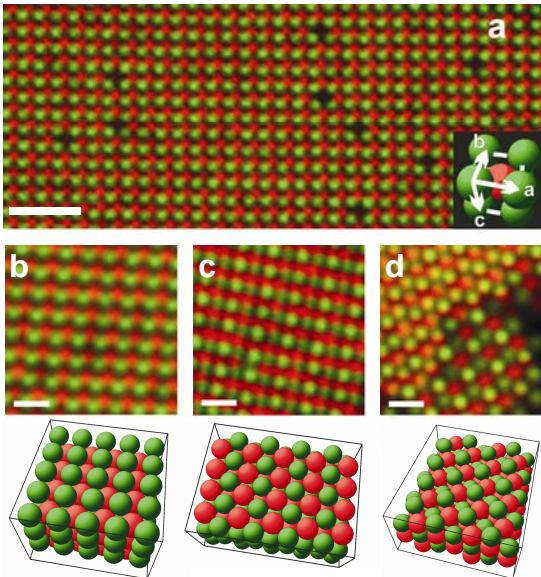


Figure 5.2.

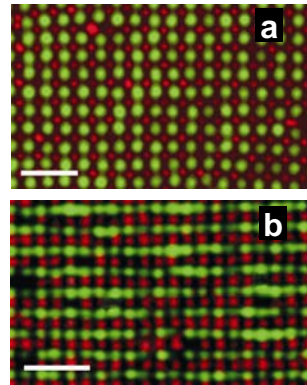


Figure 5.3.

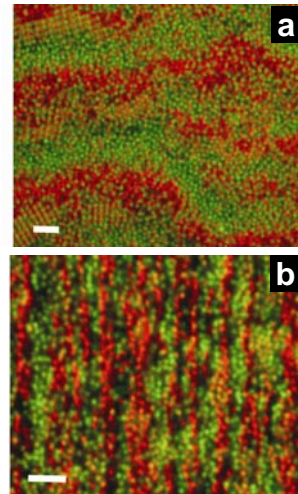


Figure 5.4.

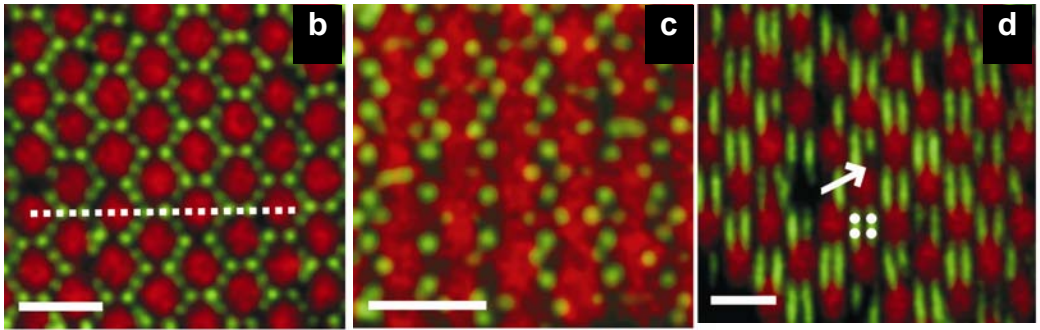


Figure 5.5.

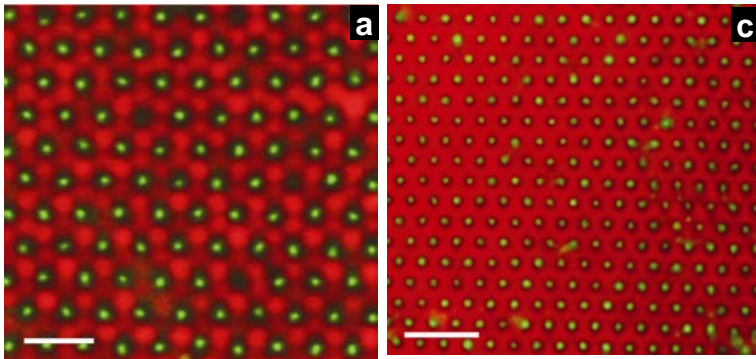


Figure 5.6.

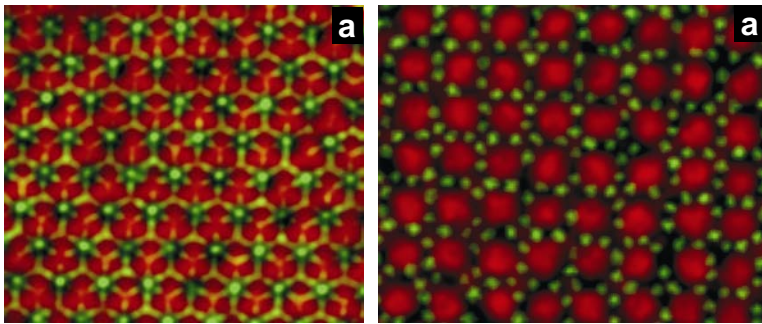


Figure 6.1.

Figure 6.2.

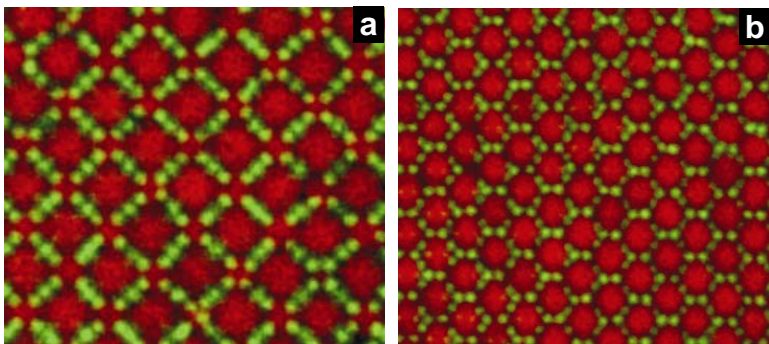


Figure 6.3.



## REFERENCES

- [1] Sanders, J.V., *Colour of precious opal*, Nature, no. 4964, p. 1151, (1964).
- [2] Sanders, J.V. and Murray, M.J., *Ordered arrangements of spheres of two different sizes in opal*, Nature, 275, p. 201, (1978).
- [3] Sanders, J.V., *Close-packed structures of spheres of two different sizes. I. Observations on natural opal*, Philosophical Magazine A, 42(6), p. 705, (1980).
- [4] Sanders, J.V., Lapidary Journal, 29, p. 1986, (1976).
- [5] Murray, M.J. and Sanders, J.V., *Close-packed structures of spheres of two different sizes. Ii. The packing densities of likely arrangements*, Philosophical Magazine A, 42(6), p. 721, (1980).
- [6] Hachisu, S. and Yoshimura, S., *Optical demonstration of crystalline superstructures in binary mixtures of latex globules*, Nature, 283, p. 188, (1980).
- [7] Yoshimura, S. and Hachisu, S., *Order formation in binary mixtures of monodisperse lattices. I. Observation of ordered structures*, Progress in Colloid & Polymer Science, 68, p. 59, (1983).
- [8] Hachisu, S., Kobayashi, Y., and Kose, A., *Phase separation in monodisperse latexes*, J. Colloid Interface Sci., 42(2), p. 342, (1973).
- [9] Alder, B.J., Hoover, W.G., and Young, D.A., *Studies in molecular dynamics. V. High-density equation of state and entropy for hard disks and spheres*, The Journal of Chemical Physics, 49(8), p. 3688, (1968).
- [10] Alder, B.J. and Wainwright, T.E., *Phase transition in elastic disks*, Physical Review, 127(2), p. 359, (1962).
- [11] Nowick, A.S. and Mader, S.R., *A hard-sphere model to simulate alloy thin films*, IBM Journal, September-November, p. 358, (1965).
- [12] Hachisu, S., Kose, A., Kobayashi, Y., and Takano, K., *Segregation phenomena in monodisperse colloids*, J. Colloid Interface Sci., 55(3), p. 499, (1976).
- [13] Pusey, P.N. and van Meegen, W., *Phase behaviour of concentrated suspensions of nearly hard colloidal spheres*, Nature, 320, p. 340, (1986).
- [14] Lebowitz, J.L., *Exact solution of generalized percus-yevick equation for a mixture of hard spheres*, Physical Review, 133(4A), p. A895, (1964).
- [15] Biben, T. and Hansen, J.P., *Phase separation of asymmetric binary hard-sphere fluids*, Phys. Rev. Lett., 66(17), p. 2215, (1991).
- [16] Sanyal, S., Easwar, N., Ramaswamy, S., and Sood, A.K., *Phase-separation in binary nearly-hard-sphere colloids - evidence for the depletion force*, Europhys. Lett., 18(2BIS), p. 107, (1992).
- [17] Kaplan, P.D., Rouke, J.L., Yodh, A.G., and Pine, D.J., *Entropically driven surface phase-separation in binary colloidal mixtures*, Phys. Rev. Lett., 72(4), p. 582, (1994).
- [18] Bartlett, P. and Ottewill, R.H., *A neutron-scattering study of the structure of a bimodal colloidal crystal*, Journal of Chemical Physics, 96(4), p. 3306, (1992).
- [19] Bartlett, P. and Ottewill, R.H., *Geometric interactions in binary colloidal dispersions*, Langmuir, 8(8), p. 1919, (1992).

- [20] Imhof, A. and Dhont, J.K.G., *Experimental phase-diagram of a binary colloidal hard-sphere mixture with a large-size ratio*, Phys. Rev. Lett., 75(8), p. 1662, (1995).
- [21] Dinsmore, A.D., Yodh, A.G., and Pine, D.J., *Phase-diagrams of nearly hard-sphere binary colloids*, Phys. Rev. E, 52(4), p. 4045, (1995).
- [22] Frenkel, D. and Louis, A.A., *Phase separation in binary hard-core mixtures: An exact result*, Phys. Rev. Lett., 68(22), p. 3363, (1992).
- [23] Xiao, C.M., Jin, G.J., Shi, X.D., and Ma, Y.Q., *Entropy-driven phase transition in binary mixtures*, Phys. Rev. E, 6401(1), p. art. no., (2001).
- [24] Dijkstra, M., van Roij, R., and Evans, R., *Direct simulation of the phase behavior of binary hard-sphere mixtures: Test of the depletion potential description*, Phys. Rev. Lett., 82(1), p. 117, (1999).
- [25] Barrat, J.L., Baus, M., and Hansen, J.P., *Density-functional theory of freezing of hard-sphere mixtures into substitutional solid solutions*, Phys. Rev. Lett., 56(10), p. 1063, (1986).
- [26] Cottin, X. and Monson, P.A., *A cell theory for solid-solutions - application to hard-sphere mixtures*, Journal of Chemical Physics, 99(11), p. 8914, (1993).
- [27] Denton, A.R. and Ashcroft, N.W., *Weighted-density-functional theory of nonuniform fluid mixtures: Application to freezing of binary hard-sphere mixtures*, Physical Review A, 42(12), p. 7312, (1990).
- [28] Kranendonk, W.G.T. and Frenkel, D., *Computer simulation of solid-liquid coexistence in binary hard-sphere mixtures*, Journal of Physics: Condensed Matter, 1(41), p. 7735, (1989).
- [29] Underwood, S.M., Vanmegen, W., and Pusey, P.N., *Observation of colloidal crystals with the cesium-chloride structure*, Physica A, 221(4), p. 438, (1995).
- [30] Schofield, A.B., *Binary hard-sphere crystals with the cesium chloride structure*, Phys. Rev. E, 6405(5), p. art. no., (2001).
- [31] Bartlett, P. and Campbell, A.I., *Three-dimensional binary superlattices of oppositely charged colloids*, Phys. Rev. Lett., 95, p. 128302, (2005).
- [32] Bartlett, P., Ottewill, R.H., and Pusey, P., *Freezing of binary mixtures of colloidal hard spheres*, Journal of Chemical Physics, 93(2), p. 1299, (1990).
- [33] Bartlett, P., Ottewill, R.H., and Pusey, P.N., *Superlattice formation in binary-mixtures of hard-sphere colloids*, Phys. Rev. Lett., 68(25), p. 3801, (1992).
- [34] Hunt, N., Jardine, R., and Bartlett, P., *Superlattice formation in mixtures of hard-sphere colloids*, Phys. Rev. E, 62(1), p. 900, (2000).
- [35] Eldridge, M.D., Madden, P.A., and Frenkel, D., *Entropy-driven formation of a superlattice in a hard-sphere binary mixture*, Nature, 365(6441), p. 35, (1993).
- [36] Eldridge, M.D., Madden, P.A., and Frenkel, D., *A computer-simulation investigation into the stability of the  $ab2$  superlattice in a binary hard-sphere system*, Mol. Phys., 80(4), p. 987, (1993).
- [37] Eldridge, M.D., Madden, P.A., and Frenkel, D., *The stability of the  $ab13$  crystal in a binary hard-sphere system*, Mol. Phys., 79(1), p. 105, (1993).
- [38] Eldridge, M.D., Madden, P.A., Pusey, P.N., and Bartlett, P., *Binary hard-sphere mixtures - a comparison between computer-simulation and experiment*, Mol. Phys., 84(2), p. 395, (1995).
- [39] Cottin, X. and Monson, P.A., *Substitutionally ordered solid-solutions of hard-spheres*, Journal of Chemical Physics, 102(8), p. 3354, (1995).

- [40] Ma, G.H., Fukutomi, T., and Morone, N., *Preparation and analysis of ordered structure of binary- mixtures composed of poly(4-vinylpyridine) and polystyrene microgels*, J. Colloid Interface Sci., 168(2), p. 393, (1994).
- [41] Hachisu, S. and Yoshimura, S., in *Physics of complex and supermolecular fluids*, S.A. Safran and N.A. Clark, Editors. 1987, Wiley: New York. p. 221.
- [42] Trizac, E., Eldridge, M.D., and Malghan, S.G., *Stability of the ab crystal for asymmetric binary hard sphere mixtures*, Mol. Phys., 90(4), p. 675, (1997).
- [43] Hachisu, S., *Nacl structure in a mixture of silica and gold sols*, Phase Transit., 21(2-4), p. 243, (1990).
- [44] Korgel, B.A., Fullam, S., Connolly, S., and Fitzmaurice, D., *Assembly and self-organization of silver nanocrystal superlattices: Ordered "soft spheres"*, J. Phys. Chem. B, 102(43), p. 8379, (1998).
- [45] Saunders, A.E. and Korgel, B.A., *Observation of an ab phase in bidisperse nanocrystal superlattices*, ChemPhysChem, 6(1), p. 61, (2005).
- [46] Shevchenko, E.V., Talapin, D.V., O'Brien, S., and Murray, C.B., *Polymorphism in ab(13) nanoparticle superlattices: An example of semiconductor-metal metamaterials*, J. Am. Chem. Soc., 127(24), p. 8741, (2005).
- [47] Kiely, C.J., Fink, J., Brust, M., Bethell, D., and Schiffrin, D.J., *Spontaneous ordering of bimodal ensembles of nanoscopic gold clusters*, Nature, 396(6710), p. 444, (1998).
- [48] Redl, F.X., Cho, K.-S., Murray, C.B., and O'Brien, S., *Three-dimensional binary superlattices of magnetic nanocrystals and semiconductor quantum dots*, Nature, 423(6943), p. 968, (2003).
- [49] Rogach, A.L., *Binary superlattices of nanoparticles: Self-assembly leads to "metamaterials"*, Angew. Chem.-Int. Edit., 43(2), p. 148, (2004).
- [50] Rogach, A.L., Talapin, D.V., Shevchenko, E.V., Kornowski, A., Haase, M., and Weller, H., *Organization of matter on different size scales: Monodisperse nanocrystals and their superstructures*, Adv. Funct. Mater., 12(10), p. 653, (2002).
- [51] Hanley, H.J.M., Straty, G.C., and Lindner, P., *Order in a simple colloidal mixture suspension*, Physica A, 174(1), p. 60, (1991).
- [52] Hanley, H.J.M., Straty, G.C., and Lindner, P., *Partial scattered intensities from a binary suspension of polystyrene and silica*, Langmuir, 10(1), p. 72, (1994).
- [53] Rugge, A. and Tolbert, S.H., *Effect of electrostatic interactions on crystallization in binary colloidal films*, Langmuir, 18(18), p. 7057, (2002).
- [54] GaribayAlonso, R., MendezAlcaraz, J.M., and Klein, R., *Phase separation of binary liquid mixtures of hard spheres and yukava particles*, Physica A, 235(1-2), p. 159, (1997).
- [55] Mendez-Alcaraz, J.M., Aguanno, B.D., and Klein, R., *Structure of binary colloidal mixtures of charged and uncharged spherical particles*, Langmuir, 8(12), p. 2913, (1992).
- [56] Mendez-Alcaraz, J.M., Chavezpaez, M., Daguanno, B., and Klein, R., *Structural-properties of colloidal suspensions*, Physica A, 220(1-2), p. 173, (1995).
- [57] Cong, H.L. and Cao, W.X., *Array patterns of binary colloidal crystals*, Journal of Physical Chemistry B, 109(5), p. 1695, (2005).
- [58] Bartlett, P. and Pusey, P.N., *Freezing of binary-mixtures of hard-sphere colloids*, Physica A, 194(1-4), p. 415, (1993).

- [59] Lutterbach, N., Versmold, H., Reus, V., Belloni, L., and Zemb, T., *Charge-stabilized liquidlike ordered binary colloidal suspensions. 1. Ultra-small-angle x-ray scattering characterization*, Langmuir, 15(2), p. 337, (1999).
- [60] Harada, T., Matsuoka, H., Yamamoto, T., Yamaoka, H., Lin, J.S., Agamalian, M.M., and Wignall, G.D., *The structure of colloidal alloy crystals revealed by ultra-small-angle neutron scattering*, Colloid Surf. A-Physicochem. Eng. Asp., 190(1-2), p. 17, (2001).
- [61] Lutterbach, N., Versmold, H., Reus, V., Belloni, L., Zemb, T., and Lindner, P., *Charge-stabilized liquidlike ordered binary colloidal suspensions. 2. Partial structure factors determined by small-angle neutron scattering*, Langmuir, 15(2), p. 345, (1999).
- [62] Ottewill, R.H., Hanley, H.J.M., Rennie, A.R., and Straty, G.C., *Small-angle neutron scattering studies on binary mixtures of charged particles*, Langmuir, 11(10), p. 3757, (1995).
- [63] Verhaegh, N.A.M. and Van Blaaderen, A., *Dispersions of rhodamine-labeled silica spheres - synthesis, characterization, and fluorescence confocal scanning laser microscopy*, Langmuir, 10(5), p. 1427, (1994).
- [64] van Blaaderen, A., *Quantitative real-space analysis of colloidal structures and dynamics with confocal scanning light microscopy*, Progress in Colloid & Polymer Science, 104, p. 59, (1997).
- [65] van Blaaderen, A. and Wiltzius, P., *Real-space structure of colloidal hard-sphere glasses*, Science, 270(5239), p. 1177, (1995).
- [66] Van Blaaderen, A., Ruel, R., and Wiltzius, P., *Template-directed colloidal crystallization*, Nature, 385(6614), p. 321, (1997).
- [67] Chestnut, M.H., *Confocal microscopy of colloids*, Curr. Opin. Colloid Interface Sci., 2(2), p. 158, (1997).
- [68] Dinsmore, A.D., Weeks, E.R., Prasad, V., Levitt, A.C., and Weitz, D.A., *Three-dimensional confocal microscopy of colloids*, Appl. Optics, 40(24), p. 4152, (2001).
- [69] Weeks, E.R., Crocker, J.C., Levitt, A.C., Schofield, A., and Weitz, D.A., *Three-dimensional direct imaging of structural relaxation near the colloidal glass transition*, Science, 287(5453), p. 627, (2000).
- [70] Royall, C.P., Leunissen, M.E., and van Blaaderen, A., *A new colloidal model system to study long-range interactions quantitatively in real space*, J. Phys.-Condes. Matter, 15(48), p. S3581, (2003).
- [71] Kegel, W.K. and van Blaaderen, A., *Direct observation of dynamical heterogeneities in colloidal hard-sphere suspensions*, Science, 287(5451), p. 290, (2000).
- [72] Jardine, R. and Bartlett, P., *Probing the structure of colloidal systems using fluorescence confocal microscopy*, Abstr. Pap. Am. Chem. Soc., 216, p. 204, (1998).
- [73] Hoogenboom, J.P., Vergeer, P., and van Blaaderen, A., *A real-space analysis of colloidal crystallization in a gravitational field at a flat bottom wall*, Journal of Chemical Physics, 119(6), p. 3371, (2003).
- [74] Gasser, U., Weeks, E.R., Schofield, A., Pusey, P.N., and Weitz, D.A., *Real-space imaging of nucleation and growth in colloidal crystallization*, Science, 292(5515), p. 258, (2001).
- [75] Yoshida, H., Yamanaka, J., Koga, T., Ise, N., and Hashimoto, T., *Novel crystallization process in dilute ionic colloids*, Langmuir, 14(3), p. 569, (1998).
- [76] Yethiraj, A. and van Blaaderen, A., *A colloidal model system with an interaction tunable from hard sphere to soft and dipolar*, Nature, 421, p. 513, (2003).

- [77] Dullens, R.P.A. and Kegel, W.K., *Reentrant surface melting of colloidal hard spheres*, Phys. Rev. Lett., 92(19), p. 195702, (2004).
- [78] Gasser, U., Schofield, A., and Weitz, D.A., *Local order in a supercooled colloidal fluid observed by confocal microscopy*, J. Phys.-Condes. Matter, 15(1), p. S375, (2003).
- [79] Varadan, P. and Solomon, M.J., *Direct visualization of long-range heterogeneous structure in dense colloidal gels*, Langmuir, 19(3), p. 509, (2003).
- [80] Yethiraj, A., Thijssen, J.H.J., Wouterse, A., and van Blaaderen, A., *Large-area electric-field-induced colloidal single crystals for photonic applications*, Adv. Mater., 16(7), p. 596, (2004).
- [81] Yagi, Y., Matsushita, S.I., Tryk, D.A., Koda, T., and Fujishima, A., *Observation of light propagation in single layers of composite two-dimensional arrays*, Langmuir, 16(3), p. 1180, (2000).
- [82] Imhof, A., in *Nanoscale materials*, L.M. Liz-Marzan and P.V. Kamat, Editors. 2003, Kluwer Academic: Boston. p. 423.
- [83] Muller, M., Zentel, R., Maka, T., Romanov, S.G., and Torres, C.M.S., *Dye-containing polymer beads as photonic crystals*, Chem. Mat., 12, p. 2508, (2000).
- [84] Imhof, A., Megens, M., Engelberts, J.J., de Lang, D.T.N., Sprik, R., and Vos, W.L., *Spectroscopy of fluorescein (fitc) dyed colloidal silica spheres*, J. Phys. Chem. B, 103, p. 1408, (1999).
- [85] Hoogenboom, J.P., Yethiraj, A., van Langen-Suurling, A.K., Romijn, J., and van Blaaderen, A., *Epitaxial crystal growth of charged colloids*, Phys. Rev. Lett., 89(25), p. 256104, (2002).
- [86] Leunissen, M.E., Christova, C.G., Hynninen, A.-P., Royall, C.P., Campbell, A.I., Imhof, A., Dijkstra, M., van Roij, R., and van Blaaderen, A., *Ionic colloidal crystals of oppositely charged particles*, Nature, 437(7056), p. 235, (2005).
- [87] Bosma, G., Pathmamanoharan, C., de Hoog, E.H.A., Kegel, W.K., van Blaaderen, A., and Lekkerkerker, H.N.W., *Preparation of monodisperse, fluorescent pmma-latex colloids by dispersion polymerization*, J. Colloid Interface Sci., 245(2), p. 292, (2002).
- [88] Dullens, R.P.A., Claesson, E.M., and Kegel, W.K., *Preparation and properties of cross-linked fluorescent poly(methyl methacrylate) latex colloids*, Langmuir, 20(3), p. 658, (2004).
- [89] Li, L., Sosnowski, S., Kumacheva, E., Winnik, M.A., Rajaram, S., Balke, S.T., and Chaffey, C.E., *Coalescence at the surface of a polymer blend as studied by laser confocal fluorescence microscopy*, Langmuir, 12(9), p. 2141, (1996).
- [90] Kumacheva, E., Kalinina, O., and Lilge, L., *Three-dimensional arrays in polymer nanocomposites*, Adv. Mater., 11(3), p. 231, (1999).
- [91] Muller, M., Zentel, R., Maka, T., Romanov, S.G., and Torres, C.M.S., *Dye-containing polymer beads as photonic crystals*, Abstr. Pap. Am. Chem. Soc., 219, p. U451, (2000).
- [92] Campbell, A.I. and Bartlett, P., *Fluorescent hard-sphere polymer colloids for confocal microscopy*, J. Colloid Interface Sci., 256(2), p. 325, (2002).
- [93] Bohren, C.F. and Huffman, D.R., *Absorption and scattering of light by small particles*. 1983, New York: John Wiley & Sons.
- [94] Lakowicz, J.R., *Principles of fluorescence spectroscopy*. 1983, New York: Plenum Press.
- [95] Murray, M.J. and Sanders, J.V., *Ordered arrangements of spheres of two different sizes in opal*, Nature, 275, p. 201, (1978).

- [96] Murray, M.J. and Sanders, J.V., *Closed-packed structures of spheres of two different sizes. Ii the packing densities of likely arrangements*, Philosophical Magazine, 43(6), p. 721, (1980).
- [97] Hachisu, S. and Yoshimura, S., *Optical demonstration of crystalline superstructures in binary mixtures of latex globules*, Nature, 283(10), p. 188, (1980).
- [98] Joannopoulos, J.D., Villeneuve, P.R., and Fan, S.H., *Photonic crystals: Putting a new twist on light*, Nature, 386(6621), p. 143, (1997).
- [99] Pan, G.S., Kesavamoorthy, R., and Asher, S.A., *Optically nonlinear bragg diffracting nanosecond optical switches*, Physical Review Letters, 78(20), p. 3860, (1997).
- [100] Holtz, J.H., Holtz, J.S.W., Munro, C.H., and Asher, S.A., *Intelligent polymerized crystalline colloidal arrays: Novel chemical sensor materials*, Analytical Chemistry, 70(4), p. 780, (1998).
- [101] Hulteen, J.C., Treichel, D.A., Smith, M.T., Duval, M.L., Jensen, T.R., and Van Duyne, R.P., *Nanosphere lithography: Size-tunable silver nanoparticle and surface cluster arrays*, Journal of Physical Chemistry B, 103(19), p. 3854, (1999).
- [102] Tessier, P.M., Velev, O.D., Kalambur, A.T., Rabolt, J.F., Lenhoff, A.M., and Kaler, E.W., *Assembly of gold nanostructured films templated by colloidal crystals and use in surface-enhanced raman spectroscopy*, Journal of the American Chemical Society, 122(39), p. 9554, (2000).
- [103] Holland, B.T., Blanford, C.F., Do, T., and Stein, A., *Synthesis of highly ordered, 3-dimensional, macroporous structures of amorphous or crystalline inorganic oxides, phosphates, and hybrid composites*, CHEMISTRY OF MATERIALS, 11(3), p. 795, (1999).
- [104] Velev, O.D. and Lenhoff, A.M., *Colloidal crystals as templates for porous materials*, Current Opinion in Colloid & Interface Science, 5(1-2), p. 56, (2000).
- [105] Yang, P.D., Rizvi, A.H., Messer, B., Chmelka, B.F., Whitesides, G.M., and Stucky, G.D., *Patterning porous oxides within microchannel networks*, Advanced Materials, 13(6), p. 427, (2001).
- [106] Jiang, P., Bertone, J.F., and Colvin, V.L., *A lost-wax approach to monodisperse colloids and their crystals*, Science, 291(5503), p. 453, (2001).
- [107] Heni, M. and Lowen, H., *Surface freezing on patterned substrates*, Physical Review Letters, 85(17), p. 3668, (2000).
- [108] Denkov, N.D., Velev, O.D., Kralchevsky, P.A., Ivanov, I.B., Yoshimura, H., and Nagayama, K., *2-dimensional crystallization*, Nature, 361(6407), p. 26, (1993).
- [109] Jiang, P., Bertone, J.F., Hwang, K.S., and Colvin, V.L., *Single-crystal colloidal multilayers of controlled thickness*, Chemistry of Materials, 11(8), p. 2132, (1999).
- [110] Kralchevsky, P.A. and Denkov, N.D., *Capillary forces and structuring in layers of colloid particles*, Current Opinion in Colloid & Interface Science, 6(4), p. 383, (2001).
- [111] Denkov, N.D., Velev, O.D., Kralchevsky, P.A., Ivanov, I.B., Yoshimura, H., and Nagayama, K., *Mechanism of formation of 2-dimensional crystals from latex-particles on substrates*, LANGMUIR, 8(12), p. 3183, (1992).
- [112] Dimitrov, A.S. and Nagayama, K., *Continuous convective assembling of fine particles into 2-dimensional arrays on solid-surfaces*, LANGMUIR, 12(5), p. 1303, (1996).
- [113] Velikov, K.P., Christova, C.G., Dullens, R.P.A., and van Blaaderen, A., *Layer-by-layer growth of binary colloidal crystals*, Science, 296(5565), p. 106, (2002).

- [114] Osseasare, K. and Arriagada, F.J., *Preparation of  $\text{SiO}_2$  nanoparticles in a nonionic reverse micellar system*, Colloids and Surfaces, 50, p. 321, (1990).
- [115] Giesche, H., *Synthesis of monodispersed silica powders .2. Controlled growth reaction and continuous production process*, J. European Ceram. Soc., 14(3), p. 205, (1994).
- [116] Smith, J.V., *Geometrical and structural crystallography*. 1982, New York: Wiley.
- [117] Lin, S.Y., Fleming, J.G., Hetherington, D.L., Smith, B.K., Biswas, R., Ho, K.M., Sigalas, M.M., Zubrzycki, W., Kurtz, S.R., and Bur, J., *A three-dimensional photonic crystal operating at infrared wavelengths*, Nature, 394(6690), p. 251, (1998).
- [118] Denton, A.R. and Ashcroft, N.W., *Weighted-density-functional theory of nonuniform fluid mixtures - application to freezing of binary hard-sphere mixtures*, Physical Review A, 42(12), p. 7312, (1990).
- [119] Prevo, B.G., Hwang, Y., and Velev, O.D., *Convective assembly of antireflective silica coatings with controlled thickness and refractive index*, Chemistry of Materials, 17(14), p. 3642, (2005).
- [120] Yamaki, M., Higo, J., and Nagayama, K., *Size-dependent separation of colloidal particles in 2-dimensional convective self-assembly*, Langmuir, 11(8), p. 2975, (1995).
- [121] Kitaev, V. and Ozin, G.A., *Self-assembled surface patterns of binary colloidal crystals*, Advanced Materials, 15(1), p. 75, (2003).
- [122] van Blaaderen, A. and Wiltzius, P., *Growing large, well-oriented colloidal crystals*, Advanced Materials, 9(10), p. 833, (1997).
- [123] Wostyn, K., Zhao, Y.X., Yee, B., Clays, K., Persoons, A., de Schaezen, G., and Hellemans, L., *Optical properties and orientation of arrays of polystyrene spheres deposited using convective self-assembly*, Journal of Chemical Physics, 118(23), p. 10752, (2003).
- [124] Xia, Y.N., Yin, Y.D., Lu, Y., and McLellan, J., *Template-assisted self-assembly of spherical colloids into complex and controllable structures*, Adv. Funct. Mater., 13(12), p. 907, (2003).
- [125] Thijssen, J.H.J., *Private communications*,
- [126] Norris, D.J., Arlinghaus, E.G., Meng, L.L., Heiny, R., and Scriven, L.E., *Opaline photonic crystals: How does self-assembly work?*, Adv. Mater., 16(16), p. 1393, (2004).
- [127] Manoharan, V.N., Elsesser, M.T., and Pine, D.J., *Dense packing and symmetry in small clusters of microspheres*, Science, 301(5632), p. 483, (2003).
- [128] Lauga, E. and Brenner, M.P., *Evaporation-driven assembly of colloidal particles*, Phys. Rev. Lett., 93(23), p. 238301, (2004).
- [129] van Blaaderen, A., *Colloidal molecules and beyond*, Science, 301(5632), p. 470, (2003).
- [130] Hoogenboom, J.P., Retif, C., de Bres, E., de Boer, M.V., van Langen-Suurling, A.K., Romijn, J., and van Blaaderen, A., *Template-induced growth of close-packed and non-close-packed colloidal crystals during solvent evaporation*, Nano Lett., 4(2), p. 205, (2004).
- [131] Cong, H. and Cao, W.X., *Colloidal crystallization induced by capillary force*, Langmuir, 19(20), p. 8177, (2003).
- [132] Wang, D.Y. and Mohwald, H., *Rapid fabrication of binary colloidal crystals by stepwise spin-coating*, Advanced Materials, 16(3), p. 244, (2004).
- [133] Kim, M.H., Im, S.H., and Park, O.O., *Rapid fabrication of two- and three-dimensional colloidal crystal films via confined convective assembly*, Adv. Funct. Mater., 15(8), p. 1329, (2005).

- [134] Schaak, R.E., Cable, R.E., Leonard, B.M., and Norris, B.C., *Colloidal crystal microarrays and two-dimensional superstructures: A versatile approach for patterned surface assembly*, Langmuir, 20(17), p. 7293, (2004).
- [135] Choi, D.G., Yu, H.K., Jang, S.G., and Yang, S.M., *Colloidal lithographic nanopatterning via reactive ion etching*, Journal of the American Chemical Society, 126(22), p. 7019, (2004).
- [136] Tan, B.J.Y., Sow, C.H., Lim, K.Y., Cheong, F.C., Chong, G.L., Wee, A.T.S., and Ong, C.K., *Fabrication of a two-dimensional periodic non-close-packed array of polystyrene particles*, Journal of Physical Chemistry B, 108(48), p. 18575, (2004).
- [137] Reculosa, S., Masse, P., and Ravaine, S., *Three-dimensional colloidal crystals with a well-defined architecture*, Journal of Colloid and Interface Science, 279(2), p. 471, (2004).
- [138] Jiang, P., Ostojic, G.N., Narat, R., Mittleman, D.M., and Colvin, V.L., *The fabrication and bandgap engineering of photonic multilayers*, Adv. Mater., 13(6), p. 389, (2001).
- [139] Zhao, Y.X., Wostyn, K., de Schaezen, G., Clays, K., Hellemans, L., Persoons, A., Szekeres, M., and Schoonheydt, R.A., *The fabrication of photonic band gap materials with a two-dimensional defect*, Applied Physics Letters, 82(21), p. 3764, (2003).
- [140] Li, H.L. and Marlow, F., *Controlled arrangement of colloidal crystal strips*, Chemistry of Materials, 17(15), p. 3809, (2005).
- [141] Nykypanchuk, D., Strey, H.H., and Hoagland, D.A., *Brownian motion of DNA confined within a two-dimensional array*, Science, 297(5583), p. 987, (2002).
- [142] Vlasov, Y.A., Bo, X.-Z., Sturm, J.C., and Norris, D.J., *On-chip natural assembly of silicon photonic bandgap crystals*, Nature, 414(6861), p. 289, (2001).
- [143] Okubo, T., Tsuchida, A., Takahashi, S., Taguchi, K., and Ishikawa, M., *Kinetics of colloidal alloy crystallization of binary mixtures of monodispersed polystyrene and/or colloidal silica spheres having different sizes and densities in microgravity using aircraft*, Colloid Polym. Sci., 278(3), p. 202, (2000).
- [144] Dassanayake, U., Fraden, S., and van Blaaderen, A., *Structure of electrorheological fluids*, Journal of Chemical Physics, 112(8), p. 3851, (2000).
- [145] Yethiraj, A., Wouterse, A., Groh, B., and van Blaaderen, A., *Nature of an electric-field-induced colloidal martensitic transition*, Phys. Rev. Lett., 92(5), p. 058301, (2004).
- [146] Vanblaaderen, A. and Vrij, A., *Synthesis and characterization of colloidal dispersions of fluorescent, monodisperse silica spheres*, Langmuir, 8(12), p. 2921, (1992).
- [147] Hoogenboom, J.P., Derks, D., Vergeer, P., and van Blaaderen, A., *Stacking faults in colloidal crystals grown by sedimentation*, Journal of Chemical Physics, 117(24), p. 11320, (2002).
- [148] Griffiths, D.J., *Introduction to electrodynamics*. second ed. 1989, Upper Saddle City (New Jersey): Prentice-Hall, Inc.532.
- [149] Steinhardt, P.J., Nelson, D.R., and Ronchetti, M., *Bond-orientational order in liquids and glasses*, Phys. Rev. B, 28(2), p. 784, (1983).
- [150] Wang, Z. and Holm, C., *Structure and magnetic properties of polydisperse ferrofluids: A molecular dynamics study*, Physical Review E (Statistical, Nonlinear, and Soft Matter Physics), 68(4), p. 041401, (2003).
- [151] Hynninen, A.P. and Dijkstra, M., *Phase diagram of dipolar hard and soft spheres: Manipulation of colloidal crystal structures by an external field*, Phys. Rev. Lett., 94(13), (2005).

- [152] Jun, J.B., Uhm, S.Y., Cho, S.H., and Suh, K.D., *Bidisperse electrorheological fluids using hydrolyzed styrene-acrylonitrile copolymer particles: Synergistic effect of mixed particle size*, Langmuir, 20(6), p. 2429, (2004).
- [153] Masuda, Y., Itoh, T., Itoh, M., and Koumoto, K., *Self-assembly patterning of colloidal crystals constructed from opal structure or nacl structure*, Langmuir, 20(13), p. 5588, (2004).
- [154] Kose, A. and Hachisu, S., *Ordered structure in weakly flocculated monodisperse latex*, J. Colloid Interface Sci., 55(3), p. 487, (1976).
- [155] Pham, K.N., Puertas, A.M., Bergenholtz, J., Egelhaaf, S.U., Moussaid, A., Pusey, P.N., Schofield, A.B., Cates, M.E., Fuchs, M., and Poon, W.C.K., *Multiple glassy states in a simple model system*, Science, 296(5565), p. 104, (2002).
- [156] Russel, W.B., Saville, D.A., and Schowalter, W.B., *Colloidal dispersions*. 1999, Cambridge: Cambridge Univ. Press.
- [157] Islam, A.M., Chowdhry, B.Z., and Snowden, M.J., *Heteroaggregation in colloidal dispersions*, Adv. Colloid Interface Sci., 62(2-3), p. 109, (1995).
- [158] Philipse, A.P. and Vrij, A., *Preparation and properties of nonaqueous model dispersions of chemically modified, charged silica spheres*, J. Colloid Interface Sci., 128(1), p. 121, (1989).
- [159] Crocker, J.C. and Grier, D.J., *Methods of digital video microscopy for colloidal studies*, J. Colloid Interface Sci., 179(1), p. 298, (1996).
- [160] Hunter, R.J., *Zeta potential in colloid science*. Vol. chapter 4. 1981, London: Academic Press Inc.
- [161] O'Brien, R.W. and White, L.R., *Electrophoretic mobility of a spherical colloidal particle.*, J. Chem. Soc. Faraday Trans. II, 74, p. 1607, (1978).
- [162] Gelinck, G.H., Huitema, H.E.A., Van Veenendaal, E., Cantatore, E., Schrijnemakers, L., Van der Putten, J., Geuns, T.C.T., Beenhakkers, M., Giesbers, J.B., Huisman, B.H., Meijer, E.J., Benito, E.M., Touwslager, F.J., Marsman, A.W., Van Rens, B.J.E., and De Leeuw, D.M., *Flexible active-matrix displays and shift registers based on solution-processed organic transistors*, Nat. Mater., 3(2), p. 106, (2004).
- [163] Dzubiella, J., Hoffmann, G.P., and Lowen, H., *Lane formation in colloidal mixtures driven by an external field*, Phys. Rev. E, 65(2), p. art. no., (2002).
- [164] Lowen, H. and Dzubiella, J., *Nonequilibrium pattern formation in strongly interacting driven colloids*, Faraday Discuss., 123, p. 99, (2003).
- [165] Dresselhaus, M.S., Dresselhaus, G., and Eklund, P.C., *Science of fullerenes and carbon nanotubes*. 1996, London: Academic.
- [166] Smithline, S.J. and Haymet, A.D.J., *Density functional theory for the freezing of 1:1 hard sphere mixtures*, Journal of Chemical Physics, 86, p. 6486, (1987).
- [167] Frenkel, D. and Smit, B., *Understanding molecular simulations*. Chapters 5, 10. 2002, London: Academic.
- [168] Grzybowski, B.A., Winkleman, A., Wiles, J.A., Brumer, Y., and Whitesides, G.M., *Electrostatic self-assembly of macroscopic crystals using contact electrification*, Nat. Mater., 2(4), p. 241, (2003).
- [169] Hynninen, A.P., Christova, C.G., van Roij, R., van Blaaderen, A., and Dijkstra, M., *Crystal structures in binary mixtures of oppositely charged colloids*, submitted to Physical Review Letters, (2005).

- [170] Biancaniello, P.L., Kim, A.J., and Crocker, J.C., *Colloidal interactions and self-assembly using DNA hybridization*, Phys. Rev. Lett., 94(5), (2005).
- [171] Vossen, D.L.J., van der Horst, A., Dogterom, M., and van Blaaderen, A., *Optical tweezers and confocal microscopy for simultaneous three-dimensional manipulation and imaging in concentrated colloidal dispersions*, Rev. Sci. Instrum., 75(9), p. 2960, (2004).
- [172] Zhou, O., Fischer, J.E., Coustel, N., Kycia, S., Zhu, Q., McGhie, A.R., Romanow, W.J., McCauley, J.P., Smith, A.B., and Cox, D.E., *Structure and bonding in alkali-metal-doped c60*, Nature, 351(6326), p. 462, (1991).
- [173] Pusey, P., *General discussions*, Faraday Discuss., 123, p. 177, (2003).
- [174] Derjaguin, B. and Landau, L., Acta Phys. Chem., 14, p. 633, (1941).
- [175] Verwey, E.J.W. and Overbeek, J.T.G., *Theory of the stability of lyotropic colloids*. 1948, Amsterdam: Elsevier.
- [176] Frenkel, D. and Smit, B., *Understanding molecular simulations*. second ed. 2002, New York: Academic.
- [177] Rosseinsky, M.J., Murphy, D.W., Fleming, R.M., Tycko, R., Ramirez, A.P., Siegrist, T., Dabbagh, G., and Barrett, S.E., *Structural and electronic-properties of sodium-intercalated c-60*, Nature, 356(6368), p. 416, (1992).
- [178] Maskaly, G.R., *Ph.D. Thesis*. 2005, MIT: Boston.
- [179] Pauling, L., *The nature of the chemical bond*. 3rd ed. 1960, Ithaca, New York: Cornell University Press.
- [180] Hynninen, A.P., *Ph.D. Thesis*. 2005, Utrecht University: Utrecht.
- [181] Yildirim, T., Zhou, O., Fischer, J.E., Bykovetz, N., Strongin, R.A., Cichy, M.A., Smith, A.B., Lin, C.L., and Jelinek, R., *Intercalation of sodium heteroclusters into the c-60 lattice*, Nature, 360(6404), p. 568, (1992).
- [182] Forro, L. and Mihaly, L., *Electronic properties of doped fullerenes*, Rep. Prog. Phys., 64(5), p. 649, (2001).
- [183] Aastuen, D.J.W., Clark, N.A., Cotter, L.K., and Ackerson, B.J., *Nucleation and growth of colloidal crystals*, Phys. Rev. Lett., 57(14), p. 1733, (1986).
- [184] Okubo, T., *Phase-diagram of ionic colloidal crystals*, in *Macro-ion characterization*. 1994, AMER CHEMICAL SOC: Washington. p. 364.
- [185] Harland, J.L. and van Megen, W., *Crystallization kinetics of suspensions of hard colloidal spheres*, Phys. Rev. E, 55(3), p. 3054, (1997).
- [186] Zhu, J., Li, M., Rogers, R., Meyer, W., Ottewill, R.H., Crew, S.-S.S., Russel, W.B., and Chaikin, P.M., *Crystallization of hard-sphere colloids in microgravity*, Nature, 387, p. 883, (1997).
- [187] Ackerson, B.J., Paulin, S.E., Johnson, B., van Megen, W., and Underwood, S., *Crystallization by settling in suspensions of hard spheres*, Phys. Rev. E, 59(6), p. 6903, (1999).
- [188] Ito, K. and Yoshida, H., *Inhomogeneous distribution of charged colloidal particles studied by confocal laser scanning microscopy*, Colloid Surf. A-Physicochem. Eng. Asp., 174(1-2), p. 55, (2000).
- [189] ten Wolde, P.R., Ruiz-Montero, M.J., and Frenkel, D., *Numerical calculation of the rate of crystal nucleation in a lennard-jones system at moderate undercooling*, Journal of Chemical Physics, 104(24), p. 9932, (1996).

- 
- [190] Tandon, S., Kesavamoorthy, R., and Asher, S.A., *Image charge effects on colloidal crystal ordering*, Journal of Chemical Physics, 109(15), p. 6490, (1998).
- [191] Auer, S. and Frenkel, D., *Suppression of crystal nucleation in polydisperse colloids due to increase of the surface free energy*, Nature, 413(6857), p. 711, (2001).
- [192] Auer, S. and Frenkel, D., *Prediction of absolute crystal-nucleation rate in hard-sphere colloids*, Nature, 409(6823), p. 1020, (2001).
- [193] Auer, S. and Frenkel, D., *Crystallization of weakly charged colloidal spheres: A numerical study*, J. Phys.-Condes. Matter, 14(33), p. 7667, (2002).
- [194] O'Malley, B. and Snook, I., *Crystal nucleation in the hard sphere system*, Phys. Rev. Lett., 90(8), (2003).
- [195] Henderson, S.I. and van Megen, W., *Metastability and crystallization in suspensions of mixtures of hard spheres*, Phys. Rev. Lett., 80(4), p. 877, (1998).
- [196] Wette, P., Schope, H.J., and Palberg, T., *Crystallization in charged two-component suspensions*, Journal of Chemical Physics, 122(14), p. 144901, (2005).



## SUMMARY

Binary crystals are crystals composed of two types of particles having different properties like size, mass density, charge etc. The first binary colloidal crystals were found in 1978 in samples from a gem stone (Brazilian opal) and consisted of silica particles with two different sizes organized in complex crystalline arrays. Before we started our work on binary colloidal crystals, there were several binary structures known to occur in mixtures of large (L) and small (S) particles. Most of them had atomic analogues:  $\text{AlB}_2$ -,  $\text{MgCu}_2$ -,  $\text{NaZn}_{13}$ -,  $\text{CaCu}_5$ -,  $\text{CsCl}$ - and  $\text{NaCl}$ -type colloidal crystals have been observed, and one structure with a stoichiometry of  $\text{LS}_4$  was found to have no atomic counterpart. For using binary crystals in different applications, like for photonic materials, compact crystals with a well defined symmetry and orientation are needed. Till now the procedures to grow such crystals required fine tuning of the composition and particle concentration of the mixtures they were grown from, and even then crystal growth proceeded relatively slowly. We report in this thesis several new approaches to make binary crystals of colloidal particles that differ in size, material and charge. We found a variety of crystal structures, amongst which five not seen before with colloids ( $\text{LS}_3$ ,  $\text{LS}_6$ -, two  $\text{LS}_8$ - and  $\text{NiAs}$ -type), and show that the general feeling that growing binary colloidal crystals is an arduous task needs to be revised.

Before presenting our methods and the crystals obtained, in Chapter 2 we report a characterization of the *spectroscopic properties* of fluorescently labeled PMMA spheres used in the fabrication of the binary crystals. Because the main technique we used to characterize the binary structure was confocal fluorescence microscopy, it is very relevant to know what kind of fluorophores can be used to label the two species in such a way as to be able to distinguish them in the microscope. For this purpose we measured the absorption, excitation and emission spectra of several fluorophores (RITC, NBD,  $\text{DiIC}_{18}$ , and Coumarin) before and after their incorporation in the particles. Furthermore, we investigated the photostability of the dyes in the colloids under continuous laser illumination and found that two of the RITC-labeled systems exhibit interesting anomalous ‘anti-bleaching’ behavior. Our results suggested that the combination of NBD- and RITC-labeled particles we used in growing some of the binary crystals reported in the thesis allows for a good distinction of the two types of spheres with the instrumental settings we used in the fluorescence microscopy technique.

The first approach for making binary colloidal crystals, reported in Chapter 3, utilized a combination of the method of controlled drying of a suspension on a substrate with a *layer-by-layer* procedure. By successively depositing single layers of each of the two species (silica particles with a size ratio  $\gamma = 0.50$ - $0.54$ ) we were able to create large areas of binary structures with different stoichiometries:  $\text{LS}$ ,  $\text{LS}_2$  and  $\text{LS}_3$ , the last one never seen before. In this method the orientation and the structure of the crystals is controlled on a layer level which allowed us to make binary crystals of particles having not only different sizes but also different composition (in this case silica and polystyrene). Moreover, by selectively removing one of these two components a non-closed packed crystal of the other species was obtained which is not possible to be grown by self-assembly. We show also in a separate section of this chapter that our approach opened new opportunities for

fabricating complex structures from colloids, as well as new directions for their applications.

In Chapter 4 we used an external field, in this case an *electric field* in addition to gravity, to grow binary crystals of NaCl-type from silica particles with a size ratio of 0.3. Without electric field the difference in the sedimentation rates of the two species, caused by the difference in their sizes, makes the formation of binary crystals a difficult task. But when we applied a high-frequency alternating electric field with a direction perpendicular to gravity the silica particles polarized and the dipole-dipole attraction between them acted as a main driving force in the crystallization process. We were able to control the strength of the dipolar interactions from low to high compared to  $k_B T$  by changing the strength of the electric field. We obtained large areas of NaCl-type crystals using both, low- and high-strength electric fields, with different mechanisms underlying their formation in the two cases. Our approach showed new ways to grow binary NaCl-type crystals from silica particles and it can be further modified and optimized to lead to some other structures as well, which can have potential applications as photonic materials and in the field of electrorheological fluids.

The next three Chapters, 5, 6 and 7, describe binary crystals we made from *oppositely charged* particles. Usually, electrostatic long-ranged attractions between colloids lead to formation of aggregates instead of ordered structures. But we showed that by controlling the amount and the sign of the charge on the particles we can obtain colloidal analogues of the ionic crystals with a variety of structures, whose stoichiometry is not dictated by charge neutrality. In Chapter 5 we outline our approach and describe some of the binary structures observed. We were able to create binary CsCl-type crystals not only from oppositely charged particles with the same material but also from mixtures of silica and PMMA spheres having large density differences. Furthermore, we present two binary structures obtained from mixtures of *charged* and *neutral* species. We show in this chapter also that an external electric field can be used to manipulate the crystals formed and to induce a phase transition to lane-like structures. Our novel approach to make crystals from oppositely charged particles allows for a quick formation of binary crystals of particles as large as 2  $\mu\text{m}$ , which can be important as photonic materials. Moreover, it opens up a new area of fundamental studies in the field of ionic crystals.

In Chapter 6 we focus on binary crystals from oppositely charged PMMA particles with a *size ratio of 0.31*. Three new binary structures found experimentally are described:  $\text{LS}_6^{\text{bcc}}$  (analogue to the fullerene compounds  $\text{A}_6\text{C}_{60}$ ),  $\text{LS}_8^{\text{fcc}}$  and  $\text{LS}_8^{\text{hcp}}$ , the last two with no atomic analogues and never seen before. Computer simulations confirmed the stability of these structures using a screened Coulomb potential to describe the interparticle interactions and a novel interactive simulation method predicted a variety of new structures from oppositely charged particles. Based on Madelung energy calculations a ground-state ( $T=0$ ,  $P=0$ ) phase diagram is presented for the size ratio studied.

Finally, Chapter 7 describes some *preliminary observations* in mixtures of oppositely charged PMMA particles with a size ratio of 0.31 concerning the *crystallization* mechanism of the  $\text{LS}_8$ -type binary crystals and the *coexistence* of binary structures with a large difference in their stoichiometries. We followed the formation of the  $\text{LS}_8$ -crystals in time in a qualitative way and showed that when the attraction between the two oppositely charged species was strong enough the first small ordered domains were observed a few hours after sample preparation and grew larger with time. The nucleation was found to be

---

homogeneous as different orientations of the nuclei were seen parallel to the bottom wall. The other phenomenon that we describe in this chapter is a continuous transformation from a binary crystal with a low stoichiometry (LS) to one with a higher stoichiometry (LS<sub>6</sub>). This transition was observed in a sample with a gradient in the concentration of the small particles and the phases it goes through were followed in a qualitative way. More detailed studies should reveal if this crystal-crystal transition is an equilibrium process and whether it has a molecular analog.



## SAMENVATTING

Kristallen die opgebouwd zijn uit twee soorten deeltjes worden binaire kristallen genoemd. Zo kunnen de deeltjes onderling verschillen in grootte, massadichtheid, elektrische lading, etc. De eerste binaire, colloïdale kristallen werden ontdekt in 1978 in monsters die onttrokken waren aan Braziliaans opaal. Deze edelsteen bestaat uit grote en kleine silica deeltjes die regelmatig gerangschikt zijn op ingewikkelde roosters. Voordat wij aan binaire, colloïdale kristallen begonnen te werken, was het reeds bekend dat zich binaire structuren voordoen in mengsels van grote (G) en kleine (K) colloïden. Afgezien van een structuur met een  $GK_4$  stoichiometrie komen de tot nu toe waargenomen structuren in binaire, colloïdale kristallen ook voor in atomaire of moleculaire stoffen:  $AlB_2$ ,  $MgCu_2$ ,  $NaZn_{13}$ ,  $CaCu_5$ ,  $CsCl$  en  $NaCl$ . Om binaire kristallen in de praktijk te kunnen toepassen, bijvoorbeeld voor de fabricatie van fotonische materialen, zijn dichtgepakte kristallen nodig waarvan zowel de symmetrie als de oriëntatie goed gedefinieerd zijn. Er bestaan reeds methodes om dit soort kristallen te groeien vanuit mengsels bestaande uit verschillende soorten deeltjes, maar daarbij luistert de precieze samenstelling van het mengsel nogal nauw. In dit proefschrift beschrijven we een aantal nieuwe manieren om binaire kristallen te maken van colloïdale deeltjes die onderling verschillen in grootte, samenstelling of elektrische lading. We zijn daarbij heel wat kristalstructuren tegengekomen. Vijf van die structuren, met een  $GK_3$ , een  $GK_6$ , een  $GK_8$  of een  $NiAs$  stoichiometrie, zijn nog niet eerder waargenomen in colloïdale systemen.

Voordat we de waargenomen kristallen en de bijbehorende productiemethodes presenteren, bekijken we in hoofdstuk 2 eerst een manier om de spectroscopische eigenschappen te karakteriseren van fluorescent gelabelde PMMA bollen. Dit soort bollen zijn gebruikt bij het maken van de binaire kristallen. Voor de karakterisatie van deze binaire structuren hebben we vooral gebruik gemaakt van confocale fluorescentiemicroscopie. Het is daarbij van groot belang om te weten welke kleurstoffen als labels gebruikt kunnen worden, opdat dat de twee verschillende soorten deeltjes onder de microscoop onderscheiden kunnen worden. Daartoe hebben we zowel voor als na hun koppeling aan de deeltjes de absorptie-, excitatie- en emissiespectra gemeten van verscheidene kleurstoffen (RITC, NBD, DiIC<sub>18</sub> en Coumarine). Daarnaast hebben we bestudeerd hoe stabiel deze kleurstoffen zijn als ze worden blootgesteld aan continue belichting met een laser. In tegenstelling tot wat verwacht werd, is er in twee van de RITC-gelabelde systemen waargenomen dat de fluorescentie niet monotoon daalt als functie van de belichtingstijd. Voor het groeien van binaire kristallen hebben we gebruik gemaakt van systemen waarin de twee verschillende soorten deeltjes gelabeld zijn met, respectievelijk, NBD en RITC. Onze resultaten tonen aan dat het gebruik van deze twee kleurstoffen het mogelijk maakt om de twee soorten deeltjes van elkaar te onderscheiden onder een fluorescentiemicroscoop.

De eerste methode om binaire, colloïdale kristallen te groeien, wordt besproken in hoofdstuk 3. Hierbij hebben we een kristalgroei methode die bekend staat als gecontroleerde verdamping laag-voor-laag toegepast. Bij gecontroleerde verdamping hechten colloïdale deeltjes in een dispersie zich onder invloed van het verdampende oplosmiddel aan een oppervlak en vormen daarop regelmatige patronen. Het bleek

mogelijk om op deze manier een kristallaag van kleine silica deeltjes op een kristallaag van grote silica deeltjes te groeien. In deze experimenten waren de grote deeltjes 1.85 tot 2 keer groter dan de kleine deeltjes. Door dit proces meerdere malen te herhalen, hebben we uitgestrekte, binaire structuren kunnen maken met GK, GK<sub>2</sub> en GK<sub>3</sub> stoichiometrieën. De GK<sub>3</sub> stoichiometrie is nog nooit eerder waargenomen. Bij deze methode kunnen we zelf, in beperkte mate, zowel de symmetrie als de oriëntatie van elke kristallaag bepalen. Hierdoor is het mogelijk om binaire kristallen te maken van deeltjes die niet alleen in grootte maar ook in samenstelling verschillen, zoals silica en polystyreen. Bovendien hebben we een open kristalstructuur gemaakt door één van de twee componenten te verwijderen. Zulke open structuren kunnen niet gemaakt worden met behulp van zelf-assemblage van één soort deeltjes. In een ander deel van dit hoofdstuk tonen we aan dat onze aanpak nieuwe mogelijkheden biedt voor het maken van ingewikkelde structuren met behulp van colloïden en voor het ontwikkelen van nieuwe praktische toepassingen.

In hoofdstuk 4 wordt een extern, elektrisch veld gebruikt in combinatie met het zwaartekrachtsveld om binaire kristallen te maken van grote en kleine silica deeltjes. De deeltjes hebben een onderlinge verhouding van 1:3.3 en zijn geordend in een structuur die dezelfde symmetrie heeft als keukenzout (NaCl). Als er geen elektrisch veld gebruikt wordt, dan is het moeilijk om binaire kristallen te vormen omdat de sedimentatiesnelheid van de grote en de kleine deeltjes behoorlijk verschilt. Echter, een elektrisch veld dat loodrecht staat op de zwaartekracht, en gegenereerd wordt met behulp van een wisselspanning met een hoge frequentie, induceert een dipoolmoment in elk silica deeltje. De onderlinge dipool-dipoolinteractie is dan de drijvende kracht achter de kristallisatie. De dipoolinteracties kunnen zowel kleiner als groter dan  $k_B T$  zijn, afhankelijk van de elektrische-veldsterkte. Zowel bij kleine als bij grote elektrische-veldsterktes werden uitgestrekte kristallen van het type NaCl gevormd. Bij kleine veldsterktes vormen de kristallen zich echter via een ander mechanisme dan bij grote veldsterktes. Onze aanpak heeft nieuwe manieren opgeleverd om met silica deeltjes binaire kristallen van het type NaCl te groeien. De methode kan nog aangepast of geoptimaliseerd worden. Dat zou kunnen resulteren in een aantal andere structuren die op zichzelf weer nieuwe praktische toepassingen kunnen opleveren op het gebied van fotonische materialen of elektro-rheologische vloeistoffen.

In de volgende drie hoofdstukken, hoofdstukken 5, 6 en 7 dus, wordt beschreven hoe binaire kristallen gemaakt kunnen worden van deeltjes die tegengesteld geladen zijn. Normaliter resulteren elektrostatische aantrekkingskrachten met een grote dracht in aggregaten van colloïden en niet in colloïdale kristallen. Wij tonen echter aan dat we genoeg controle hebben over de hoeveelheid lading op de deeltjes, en het teken daarvan, om een verscheidenheid aan colloïdale zouten te fabriceren. Deze colloïdale zouten zijn analoog aan ionische kristallen, maar ze kunnen meer verschillende stoichiometrieën hebben, omdat ze niet ladingsneutraal hoeven te zijn. In hoofdstuk 5 beschrijven we de experimentele methoden en beschrijven we enkele waargenomen binaire structuren. Zo hebben we met behulp van tegengesteld geladen deeltjes kristallen kunnen groeien van het type CsCl. We hebben zelfs aangetoond dat dit mogelijk is als de twee verschillende soorten deeltjes van twee verschillende materialen met een groot verschil in massadichtheid gemaakt zijn, silica en PMMA bijvoorbeeld. Daarnaast tonen we twee binaire structuren die gegroeid zijn uit mengsels van geladen en neutrale deeltjes. Verder tonen we in dit hoofdstuk aan dat een extern, elektrisch veld gebruikt kan worden om de gevormde kristallen te beïnvloeden en om een fase-overgang te induceren die resulteert in

gebaande structuren. De gepresenteerde aanpak maakt het zelfs mogelijk om van deeltjes met een diameter tot wel  $2\ \mu\text{m}$  relatief snel kristallen te groeien. Dit zou wel eens van groot belang kunnen zijn voor de fabricatie van fotonische materialen. Daarnaast opent het de deur naar een hele serie fundamentele experimenten met betrekking tot ionische kristallen.

In hoofdstuk 6 vestigen we de aandacht op binaire kristallen die bestaan uit grote en kleine, tegengesteld geladen PMMA deeltjes. De onderlinge verhouding van de diameter van de kleine en de grote deeltjes is 0.31. Drie nieuwe binaire structuren die we tegengekomen zijn in onze experimenten worden beschreven. Eén van de drie nieuwe structuren is de  $\text{GK}_6^{\text{bcc}}$  structuur. Het equivalent van deze structuur in de atomaire wereld ( $\text{A}_6\text{C}_{60}$ ) is een stof die lijkt op de bekende 'Bucky Balls'. De andere twee structuren,  $\text{GK}_8^{\text{fcc}}$  en  $\text{GK}_8^{\text{hcp}}$ , zijn nog nooit eerder waargenomen en hebben ook geen atomair equivalent. De stabiliteit van deze structuren is geverifieerd in computersimulaties waarin de onderlinge interactie tussen de deeltjes wordt beschreven door een afgeschermd Coulomb potentiaal. Daarnaast is er een nieuwe, interactieve simulatiemethode ontwikkeld waarmee vele nieuwe structuren van tegengesteld geladen deeltjes zijn voorspeld. Voor het experimenteel bestudeerde systeem wordt een fase-diagram ( $T = 0$ ,  $p = 0$ ) gepresenteerd dat gebaseerd is op berekende Madelung-energieën.

Tenslotte worden in hoofdstuk 7 enkele zeer recente metingen aan mengsels van grote en kleine (1:3.22), tegengesteld geladen PMMA deeltjes gepresenteerd. Er is vooral gekeken naar het mechanisme achter het ontstaan van  $\text{GK}_8$  binaire kristallen en naar de coëxistentie van binaire kristallen met een groot verschil in stoichiometrie. We hebben kwalitatief de vorming van  $\text{GK}_8$  kristallen in de tijd gevolgd. Als de aantrekkingskracht tussen de tegengesteld geladen deeltjes groot genoeg is, dan vormen zich een paar uur na de preparatie van een monster de eerste kleine, geordende domeinen, welke vervolgens groter worden naarmate de tijd verstrijkt. Aangezien de kristalkiemen verschillend georiënteerd zijn ten opzichte van de bodem van het monster, betreft het hier homogene kiemvorming. Een ander verschijnsel dat beschreven wordt in dit hoofdstuk is de overgang van een binair kristal met een  $\text{GK}$  stoichiometrie naar een kristal met een grote  $\text{GK}_6$  stoichiometrie. Deze overgang is waargenomen in een monster met een gradiënt in de concentratie aan kleine deeltjes. Door langs de concentratiegradiënt te bewegen hebben we de verschillende fases die het systeem doorloopt kwalitatief kunnen bestuderen. Een gedetailleerd onderzoek zal nodig zijn om vast te kunnen stellen of deze faseovergang van kristal naar kristal een evenwichtsproces is en of er een moleculair analogon bestaat.



## РЕЗЮМЕ

Бинарните кристали са кристали състоящи се от два вида частици, имащи различни свойства като например размер, плътност, заряд и др. Когато частиците са с размер от няколко нанометра до няколко микрометра те се наричат колоидни частици, а кристалите направени от тях – колоидни кристали. Колоидните частици могат да се разглеждат като модел на атомите и молекулите защото имат подобно фазово поведение, но имат предимството че са достатъчно големи по размер за да могат да бъдат наблюдавани директно с микроскоп и позволяват контрол върху свойствата им. Първите бинарни колоидни кристали са били открити през 1978 година в образци от скъпоценен камък (Бразилски опал) и са се състояли от силициеви частици с два различни размера, организирани в комплексни кристални структури. Преди да започнем нашите изследвания върху бинарните колоидни кристали, налице са били само няколко бинарни структури наблюдавани в смеси от големи (L) и малки (S) колоидни частици. Повечето от тях имат атомни аналози като например:  $\text{NaZn}_{13}$  и  $\text{NaCl}$ , а за една структура със стехиометрия  $\text{LS}_4$  е било установено че няма атомен двойник. За да се използват бинарните кристали в различни приложения, като например за фотонни материали, са необходими компактни кристали с добре определена симетрия и ориентация. Известните досега процедури за израстване на такива кристали изискват много прецизно определяне на композицията и на концентрацията на частиците в сместа от която кристалите са израствани. Дори и тогава, кристалния растеж се е извършвал относително бавно. В тази дисертация са описани няколко нови метода за направата на бинарни кристали от различни по размер, материал и заряд колоидни частици. Ние наблюдавахме различни видове кристални структури, 5 от които за първи път срещани с колоиди, и показахме че трябва да бъде преразгледано общото твърдение че израстване на бинарни колоидни кристали е трудна задача.

Преди да представим нашите методи и получените кристали, в глава 2 от дисертацията е представена характеристика на *спектроскопичните свойства* на полимерни (PMMA) колоидни частици маркирани с флуоресциращи молекули (флуорофори) които сме използвали за направата на бинарните кристали. За да наблюдаваме и характеризираме бинарните структури основно сме използвали специален тип микроскоп (конфокален лазерен микроскоп) който позволява флуоресциращите частици да се наблюдават триизмерно и точно да се определят координатите им. за този метод е особено важно да се знае какъв вид флуорофори могат да бъдат използвани за маркиране на двата вида частици така че да могат да бъдат различени с микроскопа. За тази цел ние измерихме спектрите на абсорбция, на възбуждане и на емисия на няколко флуорофори (RITC, NBD,  $\text{DiC}_{18}$ , и Coumarin) преди и след като те са инкорпорирани в частиците. Флуоресциращите молекули е известно че намаляват интензитета си на излъчване и постепенно деградира (обезцветяват се) когато се облъчват продължително със светлина. Ние изследвахме фотостабилността на използваните от нас флуорофори подложени на непрекъсната лазерна илюминация и открихме, че две от RITC-маркираните системи показват интересно, не наблюдавано досега, поведение – флуоресциращата

светлина която излъчват нараства с времето вместо да намалява. Резултатите ни показват че комбинацията от NBD- и RITC-оцветени частици, която използваме за израстването на някои бинарни кристали показани в дисертацията, позволява добра различимост на двата вида сфери при използваните инструментали параметри на микроскопа ни.

Първия опит за направа на бинарни колоидни кристали, представен в глава 3, използва метода на *контролирано изпаряване* на колоидна суспензия върху подложка, комбиниран с процедура при която орделни слоеве от двата вида частици (малки и големи) се нанасят *един след друг*. Размера на големите частици е около два пъти по-голям от този на малките и с тях успяхме да създадем големи области от бинарни структури с различни стехиометрии (стехиометрията отразява броя на малките частици падащи се на една голяма частица в кристала):  $LS$ ,  $LS_2$  и  $LS_3$ , като последната не е била виждана досега. Чрез този метод ориентацията и структурата на кристалите е контролирана на ниво слой, което ни позволява направата на бинарни кристали от частици не само с различни размери но също и направени от различен материал (в този случай силициеви и полистиренни). Освен това чрез селективно премахване на единия от тези два компонента ние получихме кристал от останалия вид частици, в който частиците не са така плътно подредени и който не може да бъде получен чрез спонтанно организиране на частиците. В отделна секция от тази глава ние показваме че нашия подход отваря нови възможности за направата на комплексни структури от колоиди, както и нови направления за тяхното приложение.

В глава 4 от дисертацията ние използвахме външно поле, в случая *електрично поле* като допълнение на гравитационното, за израстването на бинарни кристали от типа на  $NaCl$  (кухненската сол), използвайки силициеви частици такива по размер че големите са 3 пъти по-големи от малките. В отсъствието на електрично поле разликата в скоростите на седиментация на двата вида частици, причинена от разликата в техните размери, прави формирането на бинарни кристали много трудна задача. Но когато приложим високочестотно променящо се електрично поле в посока перпендикулярна на гравитацията, силициевите частици се поляризират и диполното привличане между тях действа като основна движеща сила за процеса на кристализация. Чрез промяна на силата на електричното поле ние имахме възможност да контролираме силата на диполните взаимодействия от слаба до силна в сравнение с топлинната енергия която те притежават. Използвайки както слабо така и силно електрично поле, ние получихме големи области от кристали от типа  $NaCl$ , като механизмите на формация на кристалите са различни в тези два случая. Нашия подход показва нови начини за израстване на бинарни кристали от  $NaCl$  – тип от силициеви частици, и може да бъде модифициран и оптимизиран за да доведе и до други структури с евенуално приложение като фотонни материали и в областта на електро-реологичните флуиди.

Следващите три глави от дисертацията, 5, 6 и 7, описват бинарните кристали които ние направихме от *противоположно заредени* частици. Електростатичното привличане между частици с противоположни заряди беше считано досега да води до формирането на агрегати вместо на подредени структури. Но ние показвахме че чрез контролиране на големината и знака на заряда върху частиците можем да получим колоидни аналози на йонните кристали с разнообразни структури. В глава 5 е очертан нашия новаторски подход и са описани някои от наблюдаваните

структури. Ние успяхме да създадем бинарни кристали не само от противоположно заредени частици от един и същ материал но също и от смеси от силициеви и полимерни (PMMA) сфери с голяма разлика в плътностите. Освен това са представени две бинарни структури (едната от които наблюдавана за първи път) получени от смеси на *заредени* и *неутрални* частици. В тази глава показваме още че външно електрично поле може да бъде използвано за манипулиране на формираните кристали. Нашия нов подход към използването на противоположно заредени частици позволява бързо образуване на бинарни кристали от частици големи почти 2 микрометра, които кристали могат да имат важни приложения, като например фотонни материали, 'електронно' мастило и др. Освен това отваряме ново поле за фундаментални изследвания в областта на йонните кристали.

В глава 6 сме се фокусирали върху бинарни кристали от противоположно заредени PMMA частици с разлика в размерите 1:3. Описани са три нови, екзотични бинарни структури открити експериментално и наречени  $LS_6^{bcc}$ ,  $LS_8^{fcc}$  и  $LS_8^{hcp}$ , като последните две структури нямат атомни аналози и не са виждани досега. Компютърните симулации потвърдиха стабилността на тези структури. Представен е и един нов интерактивен симулационен метод за предсказване на стабилни бинарни структури изградени от противоположно заредени частици и фазова диаграма показваща разнообразието от предсказани бинарни структури.

Най-накрая, глава 7 описва някои предварителни наблюдения върху смеси от противоположно заредени PMMA частици с разлика в размерите 1:3. Разгледан е механизма на кристализация на бинарни кристали от типа  $LS_8$  и съвместното съществуване на бинарни структури с голяма разлика в техните стехиометрии. Качествено е проследено формирането на  $LS_8$  – типа кристали с времето и е показано че когато привличането между двата вида противоположно заредени частици е достатъчно силно, първите подредени домени са наблюдават няколко часа след приготвянето на образците и с времето те нарастват по големина. Кристални зародиши с различна ориентация са наблюдавани което показва че нуклеацията протича хомогенно в обема. Другия феномен който е описан в тази глава е постепенната трансформация на бинарен кристал с ниска стехиометрия ( $LS$ ) към кристал с по-висока стехиометрия ( $LS_6$ ). Този преход е наблюдаван в образци с градиент на концентрацията на малките частици, като фазите през които минава са проследени качествено. По-детайлни изследвания са необходими за да разкрият дали този преход от един тип кристал към друг е равновесен процес и дали се наблюдава и при атомните и молекулни системи.



---

## *List of publications*

### **This thesis is based on the following publications**

- C.G. Christova et al., Spectroscopic characterization of fluorescently labeled polymethylmetacrylate (PMMA) particles, in preparation. (Chapter 2).
- K.P. Velikov, C.G. Christova, R.P.A. Dullens and A. van Blaaderen, *Layer-by-layer growth of binary colloidal crystals*, Science, 296(5565), p. 106, (2002). (Chapter 3).
- C.G. Christova, J.H.J. Thijssen, M. Hermes and A. van Blaaderen, *Binary colloidal crystals grown under an external electric field*, in preparation. (Chapter 4).
- M.E. Leunissen, C.G. Christova, A.-P. Hynninen, C.P. Royall, A.I. Campbell, A. Imhof, M. Dijkstra, R. van Roij and A. van Blaaderen, *Ionic colloidal crystals of oppositely charged particles*, Nature, 437(7056), p. 235, (2005). (Chapter 5)
- A.-P. Hynninen, C.G. Christova, R. van Roij, A. van Blaaderen and M. Dijkstra, *Crystal structures in binary mixtures of oppositely charged colloids*, submitted to Physical Review Letters, (2005). (Chapter 6).
- C.G. Christova, and A. van Blaaderen, *Crystallization mechanism of binary colloidal crystals of oppositely charged particles*, in preparation. (Chapter 7).

### **Other publications**

- N.D. Denkov, K.G. Marinova, C. Christova, A. Hadjiiski, and P. Cooper, *Mechanisms of action of mixed solid-liquid antifoams: Exhaustion and reactivation*, Langmuir, 16(6), p. 2515, (2000).



## *Acknowledgements*

My first thanks go certainly to my supervisor, Alfons van Blaaderen, for offering me the unique possibility and privilege to perform a high-level research, something I've been dreaming to do since I was at school. Alfons, I still remember how intrigued and impressed I was by your way of describing the fascinating world of colloids when I came in The Netherlands for an interview. Since then, you've always been a source of motivation and inspiration for me, making it easier for me to overcome the moments of hesitation when I felt lost or uncertain. Thank you for being very understanding, stimulating and helpful, always giving ideas and provoking my professional ambitions. Most of all, I want to thank you for your confidence in me which had a great impact on my development, not only as a scientist but also as a person.

Next I would like to express my acknowledgements to my colleagues with whom I've worked in a very close collaboration. Krassimir Velikov introduced me to the 'binary' world of the colloids and helped me to grow my first binary crystals. I want to thank Antti-Pekka Hynninen and Mirjam Leunissen for inspiring me in my quest for new binary crystal structures, for the many useful and pleasant discussions and for being always willing to help. The fruitful discussions and support from Marjolein Dijkstra, Rene van Roij and Arnout Imhof are very much appreciated. Job Thijssen, Didi Derks, Paddy Royall, Roel Dullens and Andrew Campbell receive my thanks for their help and for the very useful discussions and suggestions. My thanks also go to Hans Wisman for the great technical support I received from him. I want to acknowledge Dave van den Heuvel, Oleg Tovmachenko, Sasha Agronskaia and Hans Gerritsen for making the 'fluorescent' field more clear to me. My thanks go also to my student Michiel Hermes for his wonderful results and for the stimulating discussions we had. I would like to acknowledge Carlos van Kats and Didi Derks for teaching me how to synthesize particles, Andy Hollingsworth, Anand Yethiraj and Roel Dullens for sharing with me their knowledge. I am very grateful to all the people who provided particles and fluorescent dyes which I've used: Didi Derks, Krassimir Velikov, Jacob Hoogenboom, Christina Graf, Roel Dullens, Peter Vergeer and Nynke Verhaegh.

I want to thank also the people from the Van't Hoff group, especially Henk Lekkerkerker, Willem Kegel, Roel Dullens, Dirk Aarts, Andrei Petukhov, as well as my colleagues from the Molecular Biophysics group for being always friendly and willing to help and discuss. My thanks go to our remarkable secretary Maria Delgado Flores and also to Thea de Caes, Karijn Heling and Nina Matitaputty from the personal department for their willingness to help me in all kind of administrative problems.

My office mates, Carlos van Kats, Peter Vergeer, Arnout Imhof, Jacob Hoogenboom, Carmen Zoldesi and Job Thijssen (in 'order of appearance'), deserve special acknowledgements as their support and help during all these years was very encouraging. Carlos, thank you for helping me with everything when I came in the group. Carmen and Job, I hope you know how much I appreciate the incredible atmosphere that you created by your sense of humor, kindness and readiness to respond, advise or help in any situation. The unique supply of Carmen with fresh 'vitamins' and the persistent care of Job for not missing the lunches are unforgettable. Job, thank you also for being always willing to assist when my Dutch-speaking abilities were not good enough and for translating the summary of my thesis in Dutch in a very competent way. Next to them my sincere thanks go to Didi Derks and Christina Graf who were a source of support and enthusiasm for me and shared my good and bad moments.

I want to thank all the (ex-) members of Alfons' group for their help, for the number of useful discussions and the wonderful and stimulating atmosphere of team spirit and friendship: Andrea Fortini, Andrew Campbell, Antti-Pekka Hynninen, Arnout Imhof, Ahmet Demirors, Astrid van der Horst, Carlos van Kats, Carmen Zoldesi, Dannis 't Hart, Didi Derks, Esther Vermolen, Hans Wisman, Joan Penninkhof, Job Thijssen, Johan Keijzer, Maria Delgado Flores, Marjolein Dijkstra, Mirjam Leunissen, Svytoslav Savenko, Yu Ling Wu, Alexander Moroz, Anand Yethiraj, Catherine Quilliet, Christina Graf, Gerard van Lingen, Jacob Hoogenboom, Krassimir Velikov, Matthias Schmidt, Paddy Royall and Patrick Johnson. Thank you all, it was really a pleasure and an honor for me to work next to you.

I want to thank my first housemates in Utrecht, Jelena Petrovic, Carmelina Dipierrri, Dima Mazurenko and Bill van Megen, for their friendship and help. My thanks go also to Ani and Kiril, Emi and Ivan, Snezhka and Mitko, Maria and Kamen, Eli and Goro, Maya and Roman, Maya and Todor, Gaby and Alain, Adriana and Petyr, Nelly and Arjan, Hasha and Martin, Dragan and Milena, Maya and Voikan, Jelena and Thijs, Nadia and Krassi, Veronika and Hans, Nikoleta and Ivan, Sotir and Maria, Lubo and Liana, Villi, Sasho, Gosho, Samuil, Kire, Petio, Valia, Plamen, Lubo, Linda, Arminda for their support and the nice moments we shared. Snezhe, I'm very grateful to you for being so kind and helpful. My best friends Irina, Lili, Rosi, Nadia and Maria receive my special sincere thanks for being always there for me even from far away. Мили дружки, нашето приятелство е много старо и изпитано и искам да ви благодаря че ме дарихте с него. Вашата подкрепа, обич, ентузиазъм, съвети винаги са означавали много за мен, насърчавали са ме и са ми помагали в трудни моменти.

My deepest acknowledgements go now to my close relatives and family members whose endless support and love encouraged me most. Мили мамо и татко, от цялото си сърце искам да ви благодаря за безграничната обич с която ме дарявате, за това че винаги сте заставали зад мен и сте ме насърчавали, за това че вярвате в мен дори повече отколкото аз самата си вярвам и винаги успявате да ме накарате да намеря сили да се справям с проблемите дори когато на мен това ми изглежда почти невъзможно. Преведеното на български резюме на дисертацията ми е специално за вас. Искам да благодаря и на баба си от която винаги съм получавал топлина и грижи. Мамо Лозе, на теб дължа искрени благодарности за това че ме обичаш безрезервно и искрено, за търпението, добротата и помощта ти. Благодаря сърдечно и на Данчо и Вели за тяхната отзивчивост и добрина. Arjen, you were always understanding, willing to help and give advice. Thank you for the wonderful moments of fun and joy that you and my sister gave to us, and for your good suggestions on the cover design. My sister Denka is maybe the person I have to thank most, as her backing was very crucial for finishing this thesis. Deni, there are so many things I want to thank you for, that I don't know where to start from. Here are only several of them, the rest you know yourself. Thank you for being the greatest fan of my crystals, available to discuss, listen to and help in anything, at any time. Having such a positive, strong character as you near me was a comfort that I am greatly thankful for. Thank you for reading carefully, correcting and helping with formatting the manuscript, for translating the summary in Bulgarian in a very professional way.

My most warm gratitude I give to my two dearest people – my husband Alex and my son Max. Thank you for the indescribable atmosphere of love, joy, happiness and care you created around me. My words are not enough to thank you for your unreserved support, for your patience and firmness which gave me the strength to accomplish this book. I dedicate this thesis with all my love to both of you.

## *Curriculum Vitae*

The author of this thesis was born on 30<sup>th</sup> of August 1973 in Sliven, Bulgaria. In 1991 she finished the Physics class in the High School of Mathematics and Natural Sciences in Sliven, Bulgaria. The same year she continued her education at Sofia University “St. Kliment Ohridski”, Sofia, Bulgaria, in the Faculty of Physics. In July 1996 she obtained her Master of Science degree in Solid State Physics. Her thesis was done in cooperation with the Institute of Biophysics, Bulgarian Academy of Sciences. From 1996 until 2000 she was working at the Laboratory of Chemical Physics and Engineering, Faculty of Chemistry, Sofia University “St. Kliment Ohridski”, Sofia, Bulgaria. During this period she obtained her second Master of Science degree in Chemical Engineering (1998) within the program of a joint European TEMPUS project with a thesis on antifoams and also experienced a 5 months research practice (1997) in the Research centre of Rhone-Poulenc-Silicones company (currently Rhodia-Silicones), Lyon, France. In 2000 she started her PhD research in the Soft Condensed Matter group of prof. dr. Alfons van Blaaderen, Debye Institute, Utrecht University, The Netherlands. The results of this research are presented in this thesis and are published in high-impact factor journals.





